A theoretical basis for salinity intrusion in estuaries

Zhang, Zhilin

DOI
10.4233/uuid:d95a29ff-8865-4484-864a-74fd75028292

Publication date
2019

Document Version
Final published version

Citation (APA)
Zhang, Z. (2019). *A theoretical basis for salinity intrusion in estuaries*. [Dissertation (TU Delft), Delft University of Technology]. https://doi.org/10.4233/uuid:d95a29ff-8865-4484-864a-74fd75028292

A theoretical basis for salinity intrusion in estuaries

A theoretical basis for salinity intrusion in estuaries

Dissertation

for the purpose of obtaining the degree of doctor
at Delft University of Technology
by the authority of the Rector Magnificus prof.dr.ir. T.H.J.J. van der Hagen
chair of the Board for Doctorates
to be defended publicly on
Wednesday 23 January 2019 at 15:00 o'clock

by

Zhilin ZHANG

Master in Environmental Engineering, South China University of Technology, China
born in Pingxiang, China

This dissertation has been approved by the promotors.

Composition of the doctoral committee:

Rector Magnificus	chairperson
Prof.dr.ir. H.H.G. Savenije	Delft University of Technology, promotor
Prof.dr.ir. Z.B. Wang	Delft University of Technology, promotor
Independent members:	
Prof.dr.ir. N.C. van de Giesen	Delft University of Technology
Prof.dr.ir. S.N. Jonkman	Delft University of Technology
Dr. H.M. Schuttelaars	Delft University of Technology
Prof.dr. M.G. Kleinhans	Utrecht University
Dr. A. Kleidon	Max Planck Institute for Biogeochemistry
Prof.dr.ir. S.G.J. Aarninkhof	Delft University of Technology, reserve member

Keywords: Alluvial estuary, salinity intrusion, empirical model, predictive equations, maximum power concept

Printed by: IPSKAMP

Front & Back: Designed by Zhilin Zhang

ISBN 000-00-0000-000-0

An electronic version of this dissertation is available at
http://repository.tudelft.nl/.

To my family

Notation

Symbols used regularly are defined in the following and others are defined where they first appear. Numbers in parentheses indicate the equation where the symbol first appears.

a	Cross-sectional convergence length [L] (2.1)
a_0	a downstream of an inflection point [L] (2.1)
a_1	a upstream of an inflection point [L] (2.1)
A	Cross-sectional area [L^2] (1.1)
A_1	Cross-sectional area at inflection point [L^2] (2.1)
A_f	Cross-sectional area of the river [L^2] (2.4)
A_m	Cross-sectional area at estuary mouth [L^2] (2.1)
b	Width convergence length [L] (2.2)
b_0	b downstream of an inflection point [L] (2.2)
b_1	b upstream of an inflection point [L] (2.2)
B	Width [L] (2.2)
B_1	Width at inflection point [L] (2.2)
B_f	Bankfull stream Width [L] (2.5)
B_m	Width at estuary mouth [L] (2.2)
c_S	Saline expansivity [psu^{-1}] (2.11)
C	The coefficient of Chézy's [$L^{1/2}T^{-1}$] (2.19)
d	Length scale of the longitudinal variation of dispersion [L] (4.10)
D	Dispersion [L^2T^{-1}] (1.1)
D_{ef}	Dispersion due to residual circulation [L^2T^{-1}] (2.8)
D_g	Dispersion due to gravitational circulation [L^2T^{-1}] (2.8)
D_t	Dispersion due to tide [L^2T^{-1}]
E	Tidal excursion length [L] (2.11)
F	Force [MLT^{-2}] (5.2)
g	Gravitational acceleration [LT^{-2}] (2.10)
h	Depth [L] (2.3)
H	Tidal range [L]
i	Longitudinal exchange discharge [L^3T^{-1}] (3.14)

j	Lateral exchange discharge [L^3T^{-1}] (3.14)
K	Van der Burgh's coefficient [-] (1.1)
K_E	Eddy viscosity [L^2T^{-1}] (3.2)
K_H	Diffusion coefficient [L^2T^{-1}] (3.2)
K_M	Strickler's coefficient [$L^{1/3}T^{-1}$] (3.5)
l	Salinity intrusion length from the boundary [L] (3.7)
l_m	Dispersive distance [L] (5.2)
L	Salinity intrusion length [L]
M	Moment [ML^2T^{-2}] (5.1)
N_R	Estuarine Richardson number [-] (2.11)
O	Contact area [L^2] (5.3)
P	Power [ML^2T^{-3}] (5.5)
q	Laminar resistance [LT^{-1}] (5.4)
Q	Freshwater discharge [L^3T^{-1}] (1.1)
s	Length scale of the longitudinal salinity variation [L] (4.10)
S	Salinity [psu] (2.6)
S_f	Salinity of the fresh river water [psu] (2.7)
t	Time [T] (2.6)
T	Tidal period [T] (2.11)
u_f	Freshwater velocity [LT^{-1}] (3.2)
v	Residual flow velocity [LT^{-1}] (5.4)
V	Water volume [L^3] (3.14)
x	Distance [L] (1.1)
x_1	Location of the inflection point [L] (2.1)
z	Water level [L] (4.1)

α	Mixing coefficient [L^{-1}]
β	Dispersion reduction rate [-] (2.14)
δ_H	Tidal damping rate [L^{-1}] (2.19)
δ_v	Damping rate of tidal velocity amplitude [L^{-1}] (3.23)
ε	Phase lag [-]
η	Tidal amplitude [L]
λ	Length of the tidal wave [L] (2.20)
ρ	Density [ML^{-3}] (2.10)
σ	A shape factor [-] (4.10)
τ	Shear stress [$ML^{-1}T^{-2}$] (5.3)
v	Tidal velocity amplitude [LT^{-1}] (2.11)

Abbreviations:

HW	High water
HWS	High water slack
LW	Low water
LWS	Low water slack
TA	Tidal average
MP	Maximum power (in Chapter 5)
VDB	Van der Burgh (in Chapter 5)

Contents

Summary

Saltwater intrusion is a crucial issue in estuaries. The spread of salinity is described by the dispersion coefficient. A purely empirical equation which links the effective tidal average dispersion to the freshwater discharge was developed by Van der Burgh [1972]. Combining it with the salt balance equation, Savenije [1986] derived a one-dimensional model for salinity intrusion in estuaries. This Van der Burgh model has performed surprisingly well around the world. However, the physical basis of the empirical Van der Burgh coefficient (K) is still weak. This study provides a theoretical basis for the Van der Burgh method and presents alternative equations.

MacCready [2004] presented a theoretical expression for the dispersion coefficient following a reductionist approach. Comparing the density-related parts of the equations of the dispersion coefficient developed by Savenije and MacCready, a predictive equation is obtained for the coefficient K using physical parameters. In addition, a new box-model has been developed considering the longitudinal density-driven gravitational circulation and the lateral tide-driven horizontal circulation. The coefficient K (closely related to the Van der Burgh's coefficient) is used as an index of the density-driven mixing mechanism while the tide-driven part is included by assuming that it is proportional to the longitudinal dispersion. This model is validated in sixteen alluvial estuaries worldwide by using calibrated K values (and the boundary conditions). These calibrated values correspond well with the predicted values from the theoretical derivation, revealing that K has smaller values when the tide is stronger.

From a system perspective, alluvial estuaries are free to adjust dissipation processes to the energy sources that drive them. The potential energy of the river flow drives mixing by gravitational circulation. The maximum power concept assumes that the mixing takes place at the maximum power limit. To describe the complex mixing processes in estuaries holistically, different assumptions had to be made. The maximum power concept did not work satisfactorily when estuaries were assumed as isolated systems. However, by including the accelerating moment provided by the freshwater discharge, the open estuary system could be solved in analogy with Kleidon [2016] applying the maximum power concept. A new expression for the dispersion coefficient due to gravitational circulation has been derived and solved in combination with the advection-dispersion equation. This maximum power model works well in eighteen estuaries with a large convergence length, providing an alternative equation for the dispersion. These estuaries also have larger

calibrated K values by the Van der Burgh method, revealing a relation between the empirical coefficient K and the geometry.

All these models: the Van der Burgh model, the box-model, and the maximum power model, can describe the longitudinal salinity profiles. The comparison between these models implies that the empirical Van der Burgh coefficient is associated with the geometry and stratification conditions. Finally, new predictive equations have been obtained by regression with physical-based parameters which make the Van der Burgh salinity intrusion method predictive with a solid theoretical basis.

Samenvatting

De indringing van zout water is een belangrijk fenomeen in estuaria. De verspreiding van het zout wordt mathematisch bepaald door de Dispersiecoëfficiënt. Van der Burgh [1972] ontwikkelde een empirische relatie om deze dispersiecoëfficiënt te relateren aan de rivierafvoer. Door deze te combineren met de zoutbalans, leidde Savenije [1986] een één-dimensionale vergelijking af die de zoutindringing in estuaria beschrijft. Dit VanderBurgh-model bleek in de praktijk buiten verwachting goed te werken in verschillende delen van de wereld. Echter, de fysische basis voor de VanderBurgh-vergelijking was nog steeds zwak. Deze studie verschaft een theoretische basis voor deze vergelijking en presenteert alternatieve methoden om de evenredigheidsfactor (de VanderBurgh K) te bepalen.

Via een reductionistische methode leidde MacCready [2004] een theoretische uitdrukking af voor de dispersiecoëfficiënt. Door deze met die van het Savenije-model te vergelijken, wordt er in deze studie een voorspellende formule voor de VanderBurgh K verkregen, op basis van fysische parameters. Daarnaast wordt er middels een box-model een betrekking gevonden om laterale getij-gedreven circulatie aan longitudinale circulatie te koppelen. Dit model is in 16 alluviale estuaria, in verschillende delen van de wereld, gevalideerd met gecalibreerde K-waarden. Deze gecalibreerde K waarden kwamen goed overeen met de theoretische waarden, waaruit geconcludeerd kan worden dat een kleine K-waarde overeenkomt met een sterker getij.

Redenerend vanuit een systeem-perspectief, kan men stellen dat alluviale estuaria de menging van zoet en zout water aanpassen als functie van de energiebronnen die erop werken. De potentiële energie van het zoete rivierwater drijft de zwaartekracht-gedreven menging aan. Het zogenaamde Maximum Power (MP) concept veronderstelt dat deze menging plaatsvindt dicht bij de maximum power limiet (de Carnot limiet). Om deze methode toe te passen moesten een aantal aannames worden gemaakt. Het MP-concept werkte niet goed als estuaria als gesloten systemen werden beschouwd. Echter, als wij een estuarium als een open systeem beschouwen, waarbij het rotatie-moment uitgeoefend door het zoete water beschouwd wordt als het aandrijvende mechanisme, dan blijkt het MP-concept, in analogie met Kleidon [2016], goede resultaten te geven. Op basis daarvan is een nieuwe betrekking voor de dispersiecoëfficiënt voor zwaartekrachtscirculatie verkregen en–in combinatie met de zoutbalans–analytisch opgelost. Deze MP-methode blijkt goed te werken in 18 estuaria met een lange convergentielengte (met matige

convergentie). Deze estuaria hebben ook grotere K-waarden, wat erop duidt dat de VanderBurgh K aan de geometrie gerelateerd is.

Zowel het VanderBurgh model, het box-model, als het MP-model, bleken de longitudinale verdeling van het zoutgehalte goed te kunnen beschrijven. Uit deze vergelijking kan geconcludeerd worden dat de VanderBurgh K gerelateerd is aan de geometrie en de mate van gelaagdheid. Ten slotte is er, middels regressie, een voorspellende vergelijking voor de VanderBurgh K verkregen, als functie van fysische parameters. Hiermee is het VanderBurgh model een voorspellende methode geworden met een stevige theoretische basis.

1

Introduction

Do not sit by idly,
for young men will grow old in regret.

Fei YUE (1103 ~ 1142)

莫等闲 白了少年头
空悲切

岳飞［宋］

1

1.1. Importance of estuaries and the main issue

Estuaries, where rivers with fresh water meet the salty open sea, play an essential role in the human-earth system. The estuary serves as a superb habitat for a vast array of plants and animals. Of the thirty-two largest cities all over the world, twenty-two are located on estuaries. Humans rely on estuaries for water, food, leisure, transport, and coastal protection.

Estuaries are subject to marine and riverine influences. A crucial element of estuarine dynamic is the interaction between saline and fresh water. The river flow flushes fresh water into the estuary, pushing out the salt, while saline water penetrates landward due to mixing. The temporal and spatial distributions of salinity in an estuary are determined by the competition between freshwater flow and tidal currents. Sea water intruding upstream can lead to contamination of drinking water sources, diversified habitat loss, reduced production and quality of crops, and other consequences. This makes salt water intrusion in estuarine system functioning an important field of research.

1.2. Dispersion and salinity

In estuaries, the key to describe the spread of salinity is the dispersion coefficient. The transfer of salinity between streamlines at microscopic scale results from internal mixing (such as entrainment and turbulent diffusion) and boundary layer turbulence [Dyer, 1973]. Averaging small-scale turbulent diffusion over estuarine depth including both internally generated mixing and boundary generated mixing leads to a bulk transport, named depth average dispersion. It is used to describe the instantaneous mixing. If, in addition, we average depth-averaged dispersion over a full tidal cycle, then we obtain the tidal average dispersion, describing salinity spreading over a tidal period.

1.3. Reductionism research on dispersion

The study of the mathematical description of the salinity mixing, dispersion, dates back to the 1950s. Taylor [1954] pointed out the fundamental principles of dispersion due to shear flow in pipes. In that study, the longitudinal dispersion (D) was given by $D = 10.1ru_*$, where r [L] is the radius of the pipe and u_* [LT^{-1}] is the shear velocity. Subsequently, (dye) observational techniques were applied to flumes and open channel flows, and some researchers determined different ratios between the dispersion coefficient and the product of the flow depth and the shear velocity (reviewed by Fischer [1976]).

Then, analytical techniques matured rapidly, by which researchers decomposed the velocity and salinity profiles. Following the pioneering work by, for instance, Hansen and Rattray [1966], Fischer [1972, 1973], and Dyer [1974], a wide vari-

ety of researchers using the reductionist approach derived equations and different dispersive terms to determine different mixing mechanisms in specific estuaries [e.g., Chatwin, 1976; Smith, 1980; Hunkins, 1981; Prandle, 1981; McCarthy, 1993; Svendsen and Putrevu, 1994; MacCready, 2004, 2007, 2011; Lerczak et al., 2006]. Meanwhile, with the advance of computer software, a range of numerical and (semi-) analytical models, yielding colorful cross-sectional and/or vertical distributions of salinity, were used to investigate what the most effective mechanism is in a particular estuary [e.g., Ralston and Stacey, 2005; Burchard and Schuttelaars, 2012; Pein et al., 2014; Wang et al., 2017].

It is easy to understand why they tried to obtain more accurate and detailed salinity and current fields: it helps our understanding of dispersion processes if we have accurate estimates of salt fluxes. Fischer [1976] remarked that "it is not yet possible to look at a given estuary, compute the values of some appropriate dimensionless parameters, and say with certainty which mass-transport mechanisms are the most important or what factors control the intrusion of salinity", but researchers never stopped developing more advanced methods to observe and simulate the salinity and current fields in estuaries. It indeed provided some insights into the dominant mixing mechanism, but mostly limited to particular circumstances.

1.4. The holistic empirical method

In contrast to the reductionist approach, the holistic view regards the complex estuarine system as a whole. For instance, Van der Burgh [1972] developed a purely empirical method on the basis of the effective tidal average dispersion under equilibrium conditions. He made use of a considerable number of salinity measurements carried out in the Rotterdam Waterway over a period of eighty years. This method used one equation to describe all mixing mechanisms:

$$\frac{\partial D}{\partial x} = -K\frac{|Q|}{A}\,, \tag{1.1}$$

where D [L^2T^{-1}] is the dispersion, x [L] is the distance, K [-] is the Van der Burgh coefficient, Q [L^3T^{-1}] is the freshwater discharge, and A [L^2] is the cross-sectional area. The positive direction of flow is in the upstream direction.

Combining Van der Burgh's equation with the salt balance equation, Savenije [1986] published a one-dimensional model for salinity distribution in estuaries. [Savenije, 1989] then derived the analytical solution where the empirical Van der Burgh coefficient K was assumed constant along the estuary. Predictive equations for the empirical coefficient and the dispersion at the boundary were subsequently developed [Savenije, 1993b]. This salt intrusion model appeared to have excellent performance in a wide range of estuaries [e.g., Savenije, 2005; Nguyen and Savenije, 2006; Zhang et al., 2011; Kuijper and Van Rijn, 2011; Gisen et al., 2015b;

Xu et al., 2017]. The re-analysis by Gisen et al. [2015a] provided improved predictive equations using an expanded database, and the results were subsequently tested in estuaries like the Yangtze [Cai et al., 2015] and the Shatt al-Arab [Abdullah et al., 2016]. Overall, with scarce—or even without—field observations, salt water intrusion methods applying Van der Burgh's coefficient appeared to work surprisingly well in estuaries around the world.

However, the complicated predictive expressions for the empirical Van der Burgh coefficient provided by Savenije and Gisen, even though with significant mathematical correlation, did not reveal a physical meaning of this parameter. Whereas, for a full understanding of mixing and salinity distributions in estuaries, it is imperative that a solid theoretical basis is obtained for such an empirical coefficient.

1.5. Objectives and outline

This research is about trying to understand the complex interactions between tide, geometry, salinity, and fresh water that govern mixing in alluvial estuaries. The objective is to find a theoretical basis for the empirical Van der Burgh coefficient, or to find an alternative that functions equally well, while providing a physical basis for dispersion processes and salinity distributions in estuaries. The outline of the thesis is shown in Figure 1.1.

In this chapter, the importance of understanding salinity profiles in estuaries is firstly introduced. The empirical Van der Burgh equation is introduced, and the need for providing a physical basis for the empirical coefficient (K) is discussed.

Chapter 2 provides theories about the estuary, tide, salt transportations, and mixing mechanisms in estuaries. The previous empirical salinity intrusion model is introduced.

One possible physical basis behind the empirical coefficient is presented in Chapter 3, which links one equation derived from traditional reductionist methods ([MacCready, 2004]) to the empirical approach. In addition, a salt intrusion box-model including large-scale residual circulation in wide estuaries is developed.

Besides the reductionist approach, the saline and fresh water mixing using the maximum power concept in a holistic view is introduced. Estuaries are assumed as isolated systems firstly (Chapter 4), then discussed as open systems in Chapter 5. The Van der Burgh method is then applied making use of the maximum power method.

Chapter 6 provides an analysis of tidal strength on saltwater intrusion by data collected in the Rotterdam waterway (RW) and the Scheldt estuary (SE).

The physical basis for the empirical coefficient is discussed, making the Van der Burgh method predictable. Finally, conclusions, limitations, and recommendations are summarized in Chapter 7.

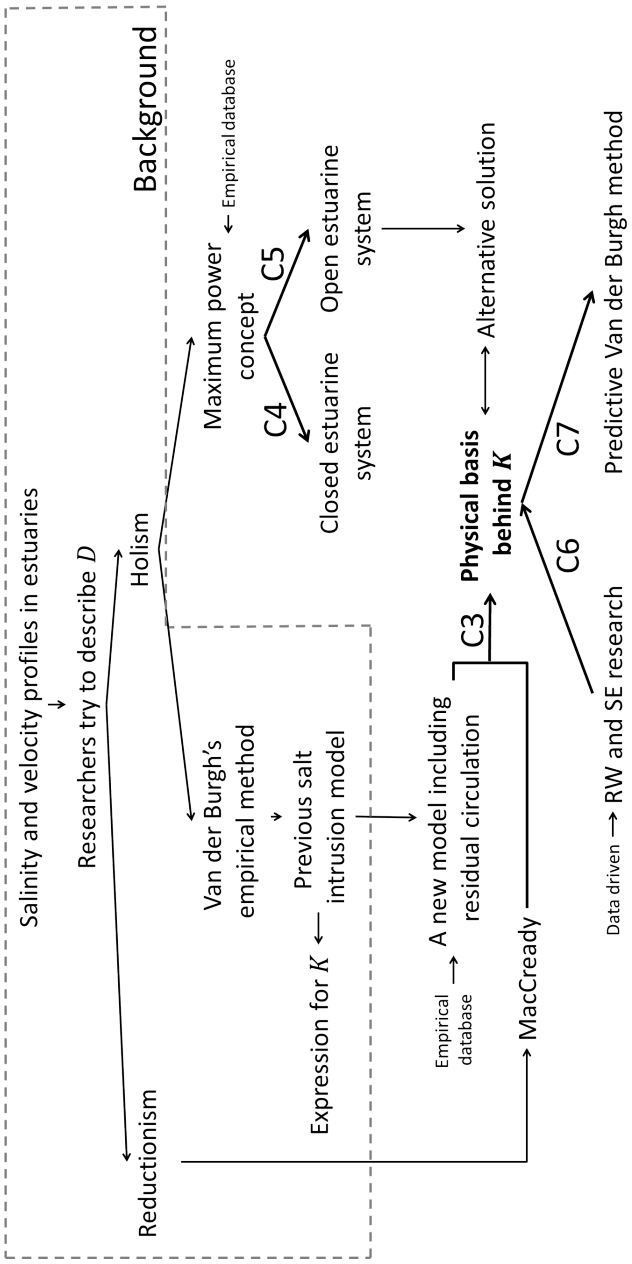

Figure 1.1: Outline of the thesis. Numbers direct the chapters.

2

Theories on estuary, salinity, and mixing

Nature has its own laws,
not depending on the will of people.

Kuang XUN (313 ~ 238 B.C.)

天行有常
不为尧存
不为桀亡

荀况［战国］

2.1. Coastal plain convergent estuaries

In an estuary, water movement depends on the topography, and the topography in turn depends on the hydraulics from seaside and riverside. Different characteristic shapes are distinguished: fjord-type, coastal plain, bar-built, tectonic, and the rest. The geomorphology of these shapes is too variable to study in general besides the coastal plain type. In coastal plain estuaries, due to the long-term dynamic equilibrium between sedimentation and erosion by tidal currents, the cross-sectional area converges towards the land. Even though spits may modify the shape near the mouth, this kind of alluvial estuary is ideal to generalize and it is the main research object in this study.

Figure 2.1 shows the sketch of a representative coastal plain estuary from the top, with the width (B) converging landward, showing a trumpet near the mouth. This kind of shape is composed of a wide mouth and a narrow stem with an inflection point in between. The downstream part has a much shorter convergence length, resulting from ocean waves dissipating their energy. The longitudinal distance of the wider part is generally not longer than about 10 km except for very wide estuaries (for instance, the Elbe and the Corantijn). Beyond the inflection point, the shape is determined by the combination of the kinetic energy of the tide and the potential energy of the river flow. If the tidal energy is dominant over the potential energy of the river, then the convergence to river is short; if the potential energy of the river is large due to regular and substantial flood flows, then the convergence is long. The interdependence between hydraulics and topography is important because it permits us to derive hydraulic information from the estuary shape and to derive geometric information from the hydraulics. The exact position of the mouth is often difficult to determine, but it can generally be found by connecting the adjacent shorelines [Savenije, 2005].

Not all coastal plain estuaries have a geometric inflection point. A near prismatic estuary (with a large convergence length) develops when tidal waves do not penetrate the estuary.

2.2. Description of the estuary shape

It is beneficial to represent the estuary shape in a mathematic way. As the shape converges landward, the geometry, especially the width is considered to follow an exponential function [e.g., Savenije, 1986; Friedrichs et al., 1998; Davies and Woodroffe, 2010]. The topography can be represented as

$$A(x) = \begin{cases} A_m \mathrm{e}^{-x/a_0} & 0 < x \leq x_1 \\ A_1 \mathrm{e}^{-(x-x_1)/a_1} & x_1 < x \end{cases}, \tag{2.1}$$

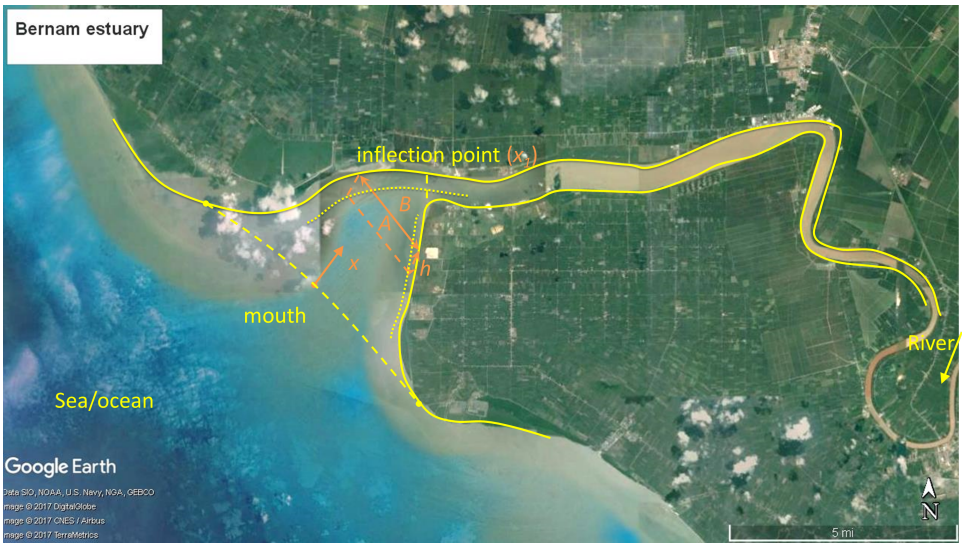

Figure 2.1: Geometry of an alluvial estuary in general: example of the Bernam in Malaysia. Yellow lines describe the geometry (The solid lines show the sketch of the shape, while the dot lines are part of the (invisible) shape at the bottom). Orange lines describe the parameters, where A is the cross-sectional area, B is the estuarine width, and h is the depth.

$$B(x) = \begin{cases} B_m e^{-x/b_0} & 0 < x \leq x_1 \\ B_1 e^{-(x-x_1)/b_1} & x_1 < x \end{cases} , \tag{2.2}$$

and

$$h(x) = \frac{A}{B} , \tag{2.3}$$

where A (A_m, A_1) [L^2] and B (B_m, B_1) [L] are the cross-sectional area and the width at location x (estuary mouth $x = 0$, inflection point $x = x_1$), respectively. a [L] and b [L] are the cross-sectional and width convergence length (a_0 and b_0 downstream of the inflection point; a_1 and b_1 upstream). Smaller values of a and b indicate that the geometry is more convergent. h [L] is the depth. In estuaries without the inflection point, x_1 equals zero.

As an example, Figure 2.2 shows the compilation of the geometry in two estuaries: the Maputo with an inflection point and the Thames without an inflection point. It can be seen that the natural geometry fits well on semi-logarithmic paper, supporting an exponential variation of cross section and width.

Equations (2.1)–(2.3) are widely used based on the exponentially varying geometry. However, in nature, the cross section converges upstream toward the cross

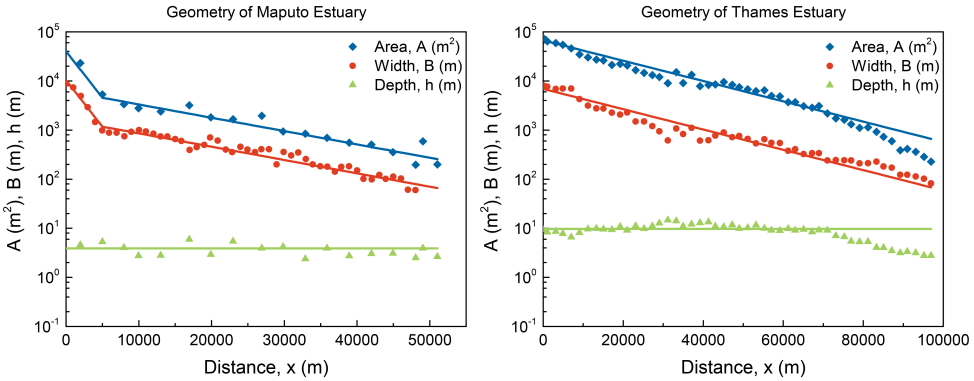

Figure 2.2: Semi-logarithmic presentation of estuary geometry, comparing simulated (lines) to the observations (symbols), including cross-sectional area (blue diamonds), width (red dots), and depth (green triangles).

section of the river (A_f) connecting to the bankfull stream width (B_f)[1]. In macrotidal estuaries, the part of the estuary where the salt intrusion occurs has a much larger cross section than the upstream river, such that $A_f \ll A$. However, in riverine estuaries, A_f should not be ignored. Then, the expression of the cross-sectional area can be modified as

$$A(x) = \begin{cases} (A_m - A_f)\mathrm{e}^{-x/a_0} + A_f & 0 < x \leq x_1 \\ (A_1 - A_f)\mathrm{e}^{-(x-x_1)/a_1} + A_f & x_1 < x \end{cases} . \tag{2.4}$$

Similarly, the equation for the width can be presented:

$$B(x) = \begin{cases} (B_m - B_f)\mathrm{e}^{-x/b_0} + B_f & 0 < x \leq x_1 \\ (B_1 - B_f)\mathrm{e}^{-(x-x_1)/b_1} + B_f & x_1 < x \end{cases} . \tag{2.5}$$

Based on equations (2.3)–(2.5), Figure 2.3 shows the geometry of the Maputo and the Limpopo. It can be seen that in the Maputo, A_f (50 m^2) is not important, while in the Limpopo, the size of the river cross section (750 m^2) is not negligible, showing a slight curve in the exponential functions.

One can see that equations (2.4)–(2.5) describe the geometry more precise than equations (2.1)–(2.2), however, the convergence length does not reveal the real convergence of the estuaries. Take the Limpopo as an example, based on the measurements, the cross section further than 30 km has a large convergence

[1] B_f is measurable, A_f can be estimated based on [Savenije, 2015]:

$$A_f = \begin{cases} 0.32{B_f}^{1.67} & B_f < 100 \\ {B_f}^2/25 & B_f \geq 100 \end{cases} .$$

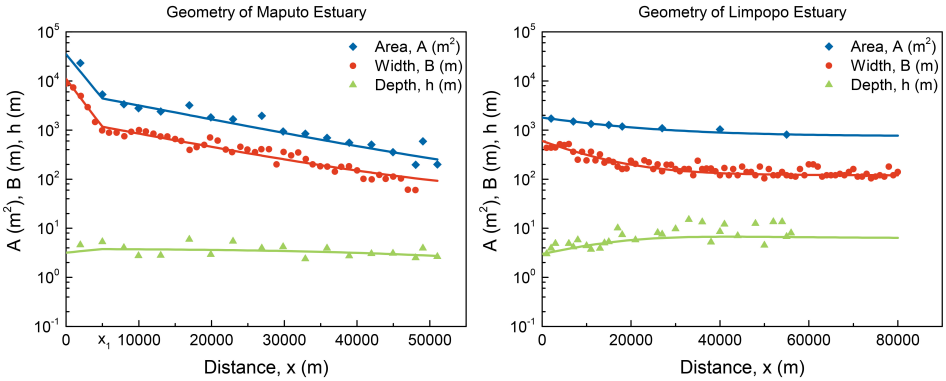

Figure 2.3: Semi-logarithmic presentation of estuary geometry, comparing simulated (lines) to the observations (symbols), including cross-sectional area (blue diamonds), width (red dots), and depth (green triangles). The cross section of the upstream river is considered when the river is wide compared to the salt intrusion part.

length, while this parameter is small if A_f is taken into account. Therefore this paremeter no longer represents the near prismatic geometry upstream.

In the equations describing the geometry, A_m and A_1 are the boundaries of two segments, the wide mouth and the narrow stem. For salt water intrusion analysis, a boundary condition (subscript "0") at a well-chosen location is required. Since salinity generally intrudes further than the geometric inflection point, the boundary condition is best taken at this point (at $x = x_1$) if the estuary has one. If the estuary has no inflection point, then the boundary is taken at the estuary mouth.

2.3. Propagation of the tide

In coastal plain convergent estuaries, the bottom is near horizontal, and the bottom slope only begins where the estuary gradually changes into the river [Pethick, 1984; Savenije, 2005]. Figure 2.4 shows the sketch of a longitudinal cross section of an estuary. Some instantaneous tidal waves are drawn. At all times, the water levels in the estuary remain between the envelopes of high water (HW) and low water (LW). The two envelopes converge to the water level of the river, which is sloped, upstream. Averaging instantaneous water levels over one tidal cycle at fixed locations, the mean water level (blue horizontal line in between HW and LW) is obtained. Accordingly, the cross-sectional area, width, and depth discussed in Section 2.2 are tidal-averaged. In nature, a full tidal wave seldom fits within the length of an estuary except in very long estuaries, because the length of the wave is in the order of hundreds of kilometers. In addition, two important vertical parameters, the tidal range (H) and the mean depth (h) are introduced. The amplitude

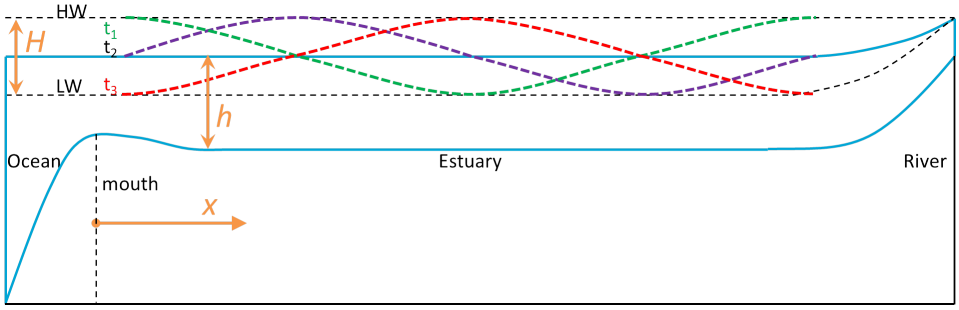

Figure 2.4: Instantaneous water levels (dash curved lines) contained between envelopes (horizontal dash lines) of high water (HW) and low water (LW). Area in between blue lines presents the water body. Orange lines describe the parameters, where H is the tidal range.

(η) of the tidal wave equals half the tidal range. In macro-tidal estuaries mentioned in Section 2.2, the tidal range is over 4 m. An estuary with a tidal range between 2 and 4 m is named meso-tidal estuary and with the range less than 2 m is micro-tidal. A significant assumption in this study is that the amplitude to depth ratio (η/h) is much smaller than unity. If the amount of energy per unit width lost by friction is stronger than the amount of energy gained by convergence of the banks, the tide damps; on the contrary, if the convergence is stronger than friction, the tide amplifies. In an alluvial estuary, the tidal range is more or less constant along the estuary, although it may be slightly damped or amplified. Being a schematic picture, these processes are somewhat exaggerated.

Different types of tidal waves in an estuary can be identified with respect to the wave celerity: standing wave, progressive wave, and mixed wave. Figure 2.5 shows the variation of water level (solid lines) and velocity (dash lines) for different types of waves at a fixed location within one tidal cycle. The moment of high water slack (HWS) occurs some time after high water, whereby the incoming current stops and changes direction. Similarly, the low water slack (LWS) happens some time after low water.

For a standing wave, the wave reaches its highest (lowest) level at HWS (LWS), like a pendulum. This type of waves occurs in short estuaries, semi-enclosed bodies, or estuaries with a closing structure blocking the progression of the wave. A progressive wave, however, occurs in prismatic frictionless channels with infinite length. The high water happens at the same time as the maximum flow velocity.

In alluvial estuaries, the tide propagates as a wave of a mixed type that has elements of both a standing and a progressive wave. The phase lag (ε) between HW and HWS or between LW and LWS is determined by the shape of the estuary and is very important in tidal hydraulics [e.g., Savenije, 2005; Cai and Savenije, 2013]. This phase lag is typically in the order of 0.3, resulting in a time lag of

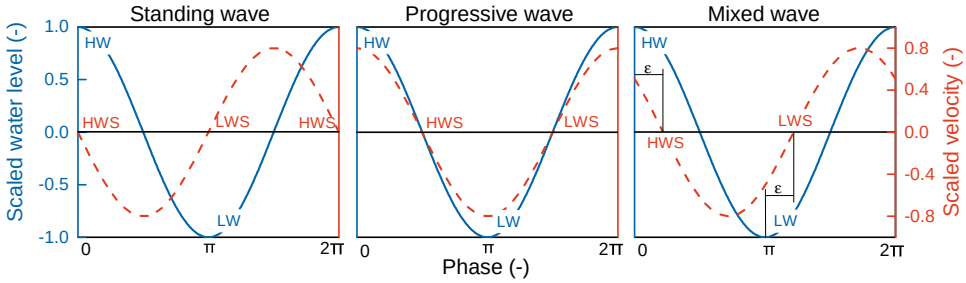

Figure 2.5: Types of waves. A phase of 2π is in consonance with one tidal cycle.

around 30 to 45 minutes for a semi-diurnal tide which has two nearly identical tidal cycles in a day. A tide which has only one complete tidal cycle in a day is a diurnal tide, which has a phase lag about twice as large.

Finally, a sketch about how one water particle moves longitudinally and vertically is shown in Figure 2.6. The particle flows in with the flood flow and out with the ebb flow to its original position (orange cross) after every tidal cycle, when the effect of river discharge is ignored. The longitudinal scale of the trajectory is the distance one particle can travel along the estuary, which is named the tidal excursion (E), which is in the order of about ten kilometers for a semi-diurnal tide. The vertical scale of the trajectory is the tidal range.

In field observations, the moments of slacks can be determined much easier than that of high water and low water which also represent the maximum and minimum local salinity. So the salinity observations are adequately measured at HWS and LWS. Figure 2.7 shows a sketch of the longitudinal cross-sectional average salinity distribution along an estuary that has an inflection point. There are three lines: at HWS, LWS, and tidal average (TA). Averaging the condition between HWS and LWS yields the TA condition. We can see that the TA intrusion has a change in curvature near the inflection point where there is a sudden change in the convergence. The tidal excursion is more or less constant landward, slightly affected by tidal damping or amplification, if any.

At fixed sites, the instantaneous salinity varies with the rise and fall of the tide. The average salinity during one tide cycle is the same as the TA condition, which lies in the middle of the HWS an LWS lines, horizontally, in Figure 2.7.

2.4. Salt transport and steady state in estuaries

Dynamics in estuaries are subject to sea/ocean and river flow. On one hand, rivers discharge fresh water seaward, pushing out the saline water. On the other hand, saline water enters and leaves estuaries on the rhythm of the tide. One can imagine

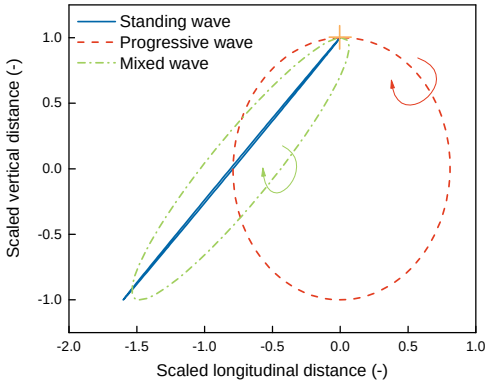

Figure 2.6: The movements of one water particle in different types of waves. The orange cross is the beginning. Arrows show the direction of movement.

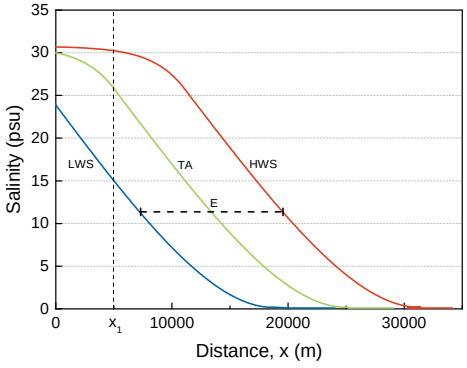

Figure 2.7: Typical longitudinal salinity distributions at high water slack (HWS), low water slack (LWS), and tidal average (TA) condition. Vertical dash line shows the location of the geometric inflection point.

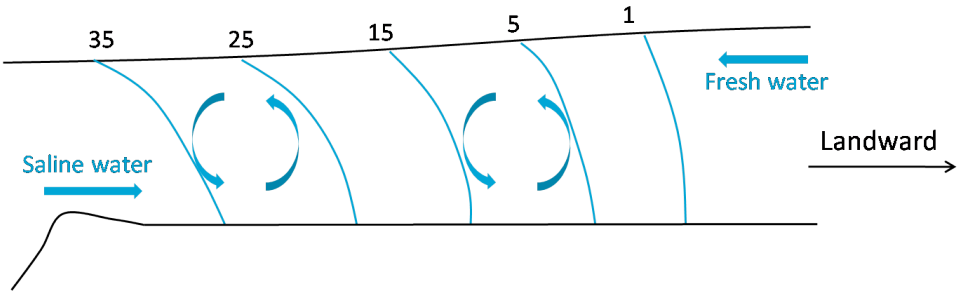

Figure 2.8: Sketch of longitudinal salt transportation in estuaries. Numbers show the isohalines (blue lines).

that the salt penetrates landward due to mixing, otherwise all the saline water would be pushed out in an estuary and the brackish environment is imbalanced. Figure 2.8 represents an example of how the fresh water and the salt water interact in a partially-mixed condition.

The mixing of fresh and saline water in estuaries is governed by the advection-dispersion equation, which results from the combination of the salt balance and the water balance. The one-dimensional advection-dispersion equation averaged over the cross section reads [e.g., Savenije, 2005]

$$A\frac{\partial S}{\partial t} - |Q|\frac{\partial S}{\partial x} - \frac{\partial}{\partial x}\left(AD\frac{\partial S}{\partial x}\right) = 0\ , \tag{2.6}$$

where S [psu] is the salinity, t [T] is time, and Q [L^3T^{-1}] is the water flow in the estuary. The first term reflects the change in the salinity over time as a result of the balance between advection by the water flow (second term) and mixing of water with different salinity by dispersive exchange flows (third term). If there is no other source of salinity, then the sum of these terms is zero. If we average this equation over a tidal period, then the first term reflects the long-term change in the salinity as a result of the balance between the advection of fresh water from the river and the tidal average exchange flows. In a steady state, in which the first term is zero, the equation can be simply integrated with respect to x, yielding

$$|Q|(S - S_f) + ADS' = 0 \tag{2.7}$$

with the condition that at the upstream boundary, the salinity gradient S' $(= \mathrm{d}S/\mathrm{d}x)$ approaches zero and $S = S_f$, which is the salinity of the fresh river water. In the steady-state situation the discharge Q then equals the freshwater discharge coming from upstream, which has a negative value moving seaward; similarly, the salinity gradient is negative with the salinity decreasing in the upstream direction.

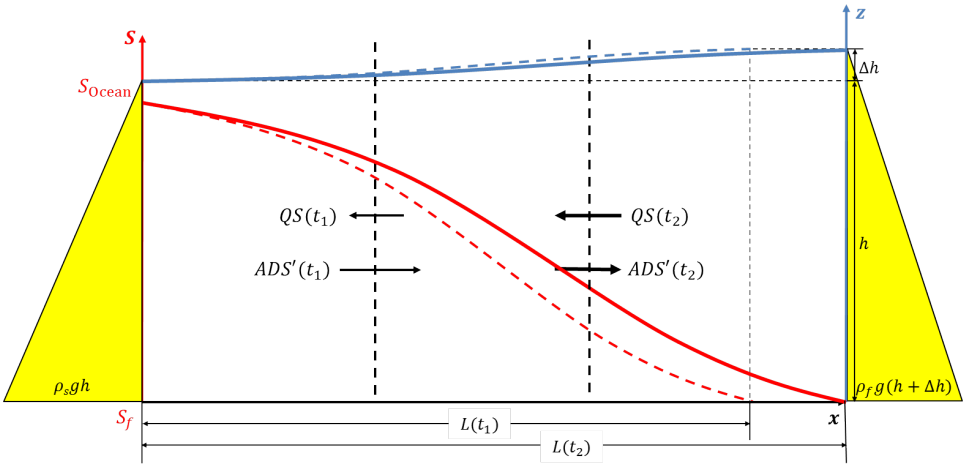

Figure 2.9: Systematic salt transport in estuaries, with the seaside on the left and the riverside on the right. The water level (in blue) has a slope as a result of the salinity distributions (in red) in different time (t_1 in dash lines and t_2 in solid lines). The black arrows show the corresponding salinity fluxes at cross sections (black vertical lines). ρ_s and ρ_f are the density at the seaside and riverside, g is the gravitational acceleration, and L is the salt water intrusion length. $(S - S_f)$ is simplified by S.

In the steady state, the flushing out of salt by the river discharge is balanced by the exchange of saline and fresh water resulting from a combination of mixing processes, which causes an upriver flux of salt along the estuary.

The sketch in Figure 2.9 presents the instantaneous system description of salt transportation in estuaries (the average value between HWS and LWS), with a typical longitudinal salinity distribution (in red). It also shows the associated water level z (in blue), which has an upstream gradient due to the decreasing salinity.

Within a salinity intrusion length (L) the salinity difference between the seaside (S_{Ocean}) and the toe (S_f) is invariant, then the increase of water level (Δh) is constant at moments t_1 (dash lines) and t_2 (solid lines). At t_1 when the value of $\Delta h/L(t_1)$ is large (salinity gradient S' is large), the salt flux by dispersive exchange flows from downstream ($ADS'(t_1)$) at any location within the salt intrusion length is larger than the advection by the water flow ($|Q|S(t_1)$), then the salinity intrudes. Hence, the salinity intrusion length increases, diminishing the salinity gradient, which would again affect the salt fluxes. The spread of salinity adjusts the system from unsteady states towards steady states (t_2) when the salt fluxes seaward and landward are equal. The efficient dispersion coefficient describes the spread of salinity. In estuaries, there are many different mixing processes at work instantaneously. Here in a system approach in which the assumption is that the different mechanisms are not independent but are jointly at work (in the form of D) to achieve the steady state.

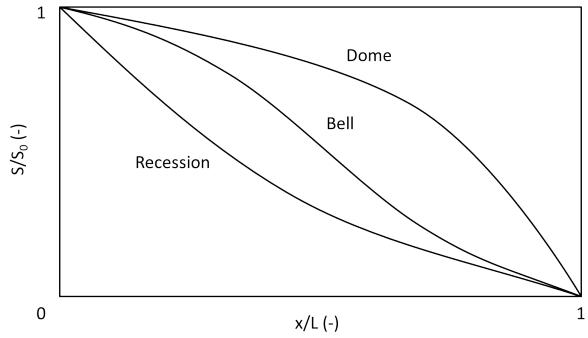

Figure 2.10: Types of salt distribution curves.

Different types of salinity distributions are distinguished: recession, bell, and dome (Figure 2.10). These types are determined by the topography of an estuary [Savenije, 2005]. The example in Figure 2.9 belongs to the bell type, which is achieved in an estuary with a clear inflection point. A dome shape appears in large and wide estuaries, and a recession shape in estuaries with a long convergent length. In estuaries where the evaporation exceeds rainfall and fresh water inflow (hypersaline estuaries), a totally different type (humpback) occurs, which goes beyond this study. How the salt intrudes is similar, no matter what the salinity distribution type is.

2.5. Maximum power concept in estuaries

Kleidon [2016] defines Earth system processes as dissipative systems that conserve mass and energy, but export entropy. These systems tend to function at maximum power, whereby the power of the system can be defined as the product of a process flux and the gradient driving the flux. The ability to maintain this power (i.e., work through time) in steady state results from the exchange fluxes at the system boundary. When work is performed at the maximum possible rate within the system ("maximum power"), this state reflects the conditions at the system boundary. The key parameter describing the process can then be found by maximizing the power.

Alluvial estuaries are systems that are free to adjust dissipation processes to the energy sources that drive them, primarily the kinetic energy of the tide and the potential energy of the river flow and to a minor extent the energy in wind and waves. We use the concept of maximum power (MP), as described by Kleidon, to see the mixing of saline and fresh water in estuaries which is a process of energy dissipation. Looking from the ocean to the river, there is a gradual transition from saline to fresh water and an associated rise in the water level in accordance with the increase in potential energy. This potential energy gradient triggers gravitational

circulation processes. Because the strength of the mixing of fresh and saline water in turn deplete this gradient, there is an optimum at which the mixing process due to density difference performs at maximum power.

The sketch of this system description of salt intrusion is similar to Figure 2.9. From an energy perspective, the freshwater flux pushing out saltwater decrases the salinity intrusion length L (at t_1), then the salt flux by dispersion ($ADS'(t_1)$) increases. The salinity disperses further upstream till the power is maximazed (an optimum at t_2). In this estuarine system, density-driven circulation is the dominant mixing mechanism.

In addition, the time needed to achieve the optimum situation is not sure (larger or less than a tidal period). In a low flow situation (which is the critical circumstance for salt intrusion) the variation of the river discharge is slow (following an exponential decline). If the time scale of flow recession is large compared to the time scale of salinity intrusion then it is reasonable to assume that maximum power optimum is achieved based on the steady-state assumption.

2.6. The cause of mixing

Different processes causing saline and fresh water mixing can be distinguished. Researchers split up mixing mechanisms in different processes at different scales [e.g., Hansen and Rattray, 1966; Park and James, 1990; Banas et al., 2004]. Fischer et al. [1979] mentioned three main drivers: wind, tide, and river. The effect of wind in coastal plain estuaries is ignorable. The river providing density difference along the estuary triggers baroclinic transport processes. For the dispersion over a tidal period in coastal plain estuaries, the tide facilitates barotropic processes in two ways: shear effect by friction at bottom turbulence and the interaction with bathymetry. The latter type includes tidal pumping which causes residual flow in flood and ebb channels, and trapping of low velocity water along the sides of an estuary, which is the effect of side embayments and small branching channels.

The tidal average dispersion is then expressed as

$$D = D_g + D_t \ , \tag{2.8}$$

where D_g and D_t with the dimension of [L^2T^{-1}] are the density- and tide-driven dispersion. The tide is an active hydraulic driver that creates shear stresses in the flow as momentum, resulting from friction along the boundaries, transferred to the heart of the channel by turbulence. To quantify the dispersion in estuaries due to the shear effect, Fischer et al. [1979] described the theory and methods in detail. However, this effect is limited over a tidal cycle, and it is considered only when the shear effect appears to be the dominant mechanism for dispersion. In alluvial estuaries without many asymmetric topography, trapping is not considered as a

strong mixing mechanism. By using the tidal excursion as the mixing length, tidal trapping can be incorporated into a predictive equation [Fischer et al., 1979]. In this study, residual circulation in preferential ebb and flood channels (D_{ef}) is considered as the main tide-driven mechanism.

Gravitational circulation

Besides describing the salt transportation, Figure 2.9 also shows the reason for density-driven mechanism in estuaries. Because of the longitudinal density difference, the hydrostatic pressures on both sides (in yellow) are not equal, so the water level at the toe of the salt intrusion curve is Δh higher, resulting in a seaward pressure difference near the surface and an inland pressure difference near the bottom. Although the hydrostatic forces (the integrals of the hydrostatic pressure distributions) are equal and opposed in steady state, they have different working lines that are a distance $\Delta h/3$ apart. This triggers an angular moment, which drives the gravitational circulation [Savenije, 2005]. When we have a strong density gradient, gravitational circulation is often a dominant transport mechanism and it is the main process in the maximum power concept.

The balance of the hydrostatic forces per unit width yields

$$\frac{1}{2}\rho_s g h^2 = \frac{1}{2}\rho_f g\,(h+\Delta h)^2 \ , \tag{2.9}$$

leading to the result of Δh:

$$\Delta h = \frac{(\rho_s - \rho_f)h}{2\rho_f} = \frac{\Delta\rho h}{2\rho_f} \ , \tag{2.10}$$

where ρ_s and ρ_f are the density (ρ [ML^3]) at the seaside and riverside, and g [LT^{-2}] is the gravitational acceleration.

Vertical density differences essentially affect the gravitational circulation. When the salinity gradient over the depth is large, the system is more stratified, with a sharp interface (a saline wedge) as the most extreme stratification. On the other hand, complete mixing occurs when there is very small stratification. Three basic types of alluvial estuaries are distinguished according to the stratification condition: the salt wedge estuary, the partially mixed (or slightly stratified) estuary, and the well mixed (or vertically homogeneous) estuary. The salt wedge estuary is highly stratified due to a large flow of the river. In this case, flooding is a more significant issue than saltwater intrusion. In this study, we focus on partially to well mixied estuaries. Due to variation in river discharge and tide, the stratification condition changes with time. Stratification is well depicted by the estuarine Richardson number (N_R):

$$N_R = \frac{\Delta\rho}{\rho}\frac{gh}{v^2}\frac{|Q|T}{AE} \ , \tag{2.11}$$

where $\Delta\rho/\rho$ $(= c_S S)$ [-] is the relative density difference between river water and saline water, c_S [psu^{-1}] is the saline expansivity equal to 7.7×10^{-4}, υ $(= \pi E/T)$ [LT^{-1}] is the tidal velocity amplitude, and T [T] is the tidal period.

This estuarine Richardson number describes the balance between the potential energy of the fresh water flowing into the estuary ($\rho g h|Q|T/2$) and the kinetic energy of the tidal flood flow ($\rho v^2 AE/2$). Linking the gravitational circulation (D_g) with the stratification number (N_R) is consistent with energy dissipation in estuaries. If N_R is large, the potential energy of river discharge dominates and stratification occurs, D_g is enhanced; if it is small, the estuary is well-mixed due to sufficient kinetic energy to reduce the density gradient, D_g is reduced. In this study, we connect D_g and N_R with a power, which is further discussed in Chapter 3.

The parameter N_R is widely used in theoretical and practical studies [e.g., Fischer, 1972; Fischer et al., 1979; Kuijper and Van Rijn, 2011]. Other estuary numbers such as the Canter Cremers' estuary number [e.g., Savenije, 2005], the Prandle's estuary number [e.g., Prandle, 1985], and the Simpson number [e.g., Simpson et al., 1990; MacCready and Geyer, 2010; Stacey et al., 2001; Stacey and Ralston, 2005] are also used.

Residual circulation in wide estuaries

Residual circulation is complicated. It can be a very powerful mechanism where the tide causes mixing by the cross-over of preferential ebb and flood channels which develop in a wide estuary. For example, Figure 2.11 shows different channels in the Scheldt estuary, exhibiting a remarkable pattern: a number of consecutive loops around the major shoal complexes. The ebb channel is the main channel and the flood channel is the side channel. Similar patterns can be observed in a number of convergent estuaries, such as the Pungue, the Columbia, the Thames, the Mersey, and the Yangtze River. In the Scheldt and the Columbia this mechanism happens downstream from the point where the width to depth ratio is about 100.

Previous researchers focused on longitudinal dispersion in prismatic estuaries [e.g., Hansen and Rattray, 1966], while the fact that cross sections of natural alluvial estuaries obey an exponential function is relevant. Even though the one-dimensional tide-driven mixing should be included in the dispersion coefficient, traditional researches have ignored this kind of large-scale lateral mixing by residual circulation. However, the presence of preferential ebb and flood channels is a major mechanism in wide estuaries, affecting salt transportation, sediment movement, and long-term morphodynamic development [e.g., Bowden and Gilligan, 1971; Wang et al., 2001; Van Veen, 2001; Savenije, 2005; Nguyen et al., 2008; Guo et al., 2015].

How can we parameterize the large-scale residual circulation? Nguyen et al. [2008] provided an equation for the dispersion due to residual circulation based on

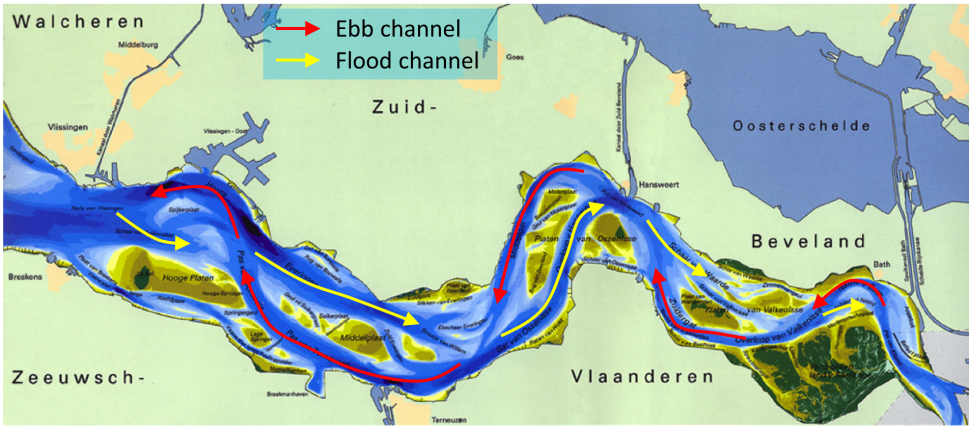

Figure 2.11: Ebb and flood channels in the Scheldt estuary. Shortcut and ebb- or flood-channel are not specified. Based on Van Veen [2001].

a box-model:

$$D_{ef} = 0.5 e_p \frac{E}{T} L_{ef} \ , \tag{2.12}$$

where 0.5 is a factor assumed as the ratio of cross-sectional area of the flood channel and total area, e_p [-] is the pumping efficiency (relative difference of the tidal velocity amplitude between flood and ebb currents in the flood channel), and L_{ef} [L] is the length of an ebb-flood channel loop which is forced by the width. This simple equation implies that the effective longitudinal dispersion generated by the flood-ebb channel interaction is directly proportional to the efficiency of the tidal pumping, the tidal excursion, and the estuary width.

2.7. Previous empirical salinity intrusion models

Assuming that in a given estuary the geometry $A(x)$ is known, as is the observed salinity and discharge of the fresh river water, the salt balance equation (2.7) has two unknowns $D(x)$ and $S(x)$. Van der Burgh's empirical equation (1.1) provides an additional equation for $D(x)$ to describe the mixing of salt and fresh water in estuaries. Integrating the combination of these two equations yields [Savenije, 1986]

$$\frac{D}{D_0} = \left(\frac{S - S_f}{S_0 - S_f} \right)^K \ , \tag{2.13}$$

where the subscript "0" defines the boundary condition for all distance-dependent parameters. This boundary is conveniently chosen at the inflection point, or at the mouth if there is no inflection point. This equation links the dispersion directly to the salinity which is special because most other researchers link the dispersion to

the salinity gradient [e.g., Fischer, 1976; Prandle, 1981; Thatcher and Najarian, 1983].

Substituting equation (2.1) for the cross section into the integration of (1.1) and assuming that K is constant gives [Savenije, 1989]

$$\frac{D}{D_0} = 1 - \beta\left(\mathrm{e}^{x/a} - 1\right) , \tag{2.14}$$

where β [-] is the dispersion reduction rate:

$$\beta = \frac{K|Q|a}{A_0 D_0} . \tag{2.15}$$

Combining equations (2.13) and (2.14), the salinity distribution $S(x)$ is solved along an estuary:

$$\frac{S - S_f}{S_0 - S_f} = \left[1 - \beta\left(\mathrm{e}^{x/a} - 1\right)\right]^{1/K} . \tag{2.16}$$

The Van der Burgh method works only if the boundary conditions (S_0 and D_0) and the empirical coefficient (K) are known or calibrated. To make the empirical salinity intrusion model predictive, Savenije [1993b] presented predictive equations for K and D_0 (S_0 is easy to estimate):

$$K = 0.16 \times 10^{-6}\left(\frac{h}{b}\right)^{1.10}\left(\frac{H}{h}\right)^{1.66}\left(\frac{h}{B}\right)^{0.13}\left(\frac{T\sqrt{gh}}{H}\right)^{2.24} , \tag{2.17}$$

$$\frac{D^{\mathrm{HWS}}}{\upsilon E} = 1400\frac{h}{a}{N_R}^{0.5} , \tag{2.18}$$

where D^{HWS} is dispersion at high water slack. Bulk parameters which are not time-dependent were considered and K is suggested in between zero and unity. Although equation (2.18) is based on the high water slack situation, one can compute the salinity distribution for both tide average and low water slack by shifting the curve over $E/2$ and E in the seaward direction.

Later, Savenije [2005] modified the predictive equation (2.17) involving more parameters:

$$K = 0.3 \times 10^{-3}\left(\frac{E}{H}\right)^{0.65}\left(\frac{g}{C^2}\right)^{0.39}(1 - \delta_H b)^{-2.0}\left(\frac{b}{a}\right)^{0.58}\left(\frac{Ea}{A'_m}\right)^{0.14} , \tag{2.19}$$

where C [$\mathrm{L}^{1/2}\mathrm{T}^{-1}$] is the coefficient of Chézy's, δ_H [L^{-1}] is the tidal damping rate, and A'_m [L^2] is the cross-sectional area at mouth which is obtained by extending the second segment of the exponential function of the area to the mouth.

Gisen [2015] then provided another equation for the Van der Burgh coefficient:

$$K = 8.03 \times 10^{-6}\left(\frac{B_f}{B}\right)^{0.30}\left(\frac{g}{C^2}\right)^{0.09}\left(\frac{E}{H}\right)^{0.97}\left(\frac{\overline{h}}{b_1}\right)^{0.11}\left(\frac{H}{\overline{h}}\right)^{1.10}\left(\frac{\lambda}{E}\right)^{1.68} , \quad (2.20)$$

where $\overline{h}$ [L] is the averaged depth after the inflection point and λ [L] is the length of the tidal wave. The boundary condition of these distance-dependent parameters is then adjusted from the estuary mouth to the inflection point. Gisen [2015] also tested eighteen predictive equations for predicting dispersion at the boundary by multiple regression analysis, obtaining the following two equations that performed best:

$$D_0 = 0.1167{N_R}^{0.57} \upsilon E , \quad (2.21)$$

$$D_0 = 0.2558{f_D}^{-0.21}{N_R}^{0.57} \upsilon E , \quad (2.22)$$

where f_D [-] is the Darcy-Weisbach friction factor.

Subsequently, although the processes of mixing and saline water intrusion are clearly complex and three-dimensional, this empirical salinity intrusion model, based on Van der Burgh's relationship, provides an analytical approach to estimate the longitudinal salinity distribution in estuaries which appeared to have excellent practical performance. The purely empirical K combines into one parameter the effects of all mixing mechanisms. However, the predictive equations (2.17), (2.19), and (2.20) are still very complicated, and the physical foundation of the empirical coefficient is still weak. To provide a theoretical basis for the empirical Van der Burgh coefficient is the main challenge in this study, which will be dealt with in the following chapters.

3

Physics behind the empirical method by reductionism

Water benefits everything and does not compete with anything.

Laozi (around 571 ~ 471 B.C.)

水善利万物而不争

李耳［春秋］

This chapter is based on:

Zhang, Z. and Savenije, H. H. G.: The physics behind Van der Burgh's empirical equation, providing a new predictive equation for salinity intrusion in estuaries, Hydrol. Earth Syst. Sci., **21**, 3287-3305, 2017.

3.1. Background

Using the steady state equation (2.7) at a boundary condition, we can derive the dispersion as a function of the salinity gradient [Savenije, 2015]:

$$\frac{D}{D_0} = \left(-\frac{AD_0}{|Q|S_0} \frac{\mathrm{d}S}{\mathrm{d}x} \right)^{\frac{K}{1-K}}, \tag{3.1}$$

which connects the dispersion coefficient to local variables (A, $\mathrm{d}S/\mathrm{d}x$), boundary conditions (D_0, S_0), and K. It reveals the dispersion can be shown to be proportional to the salinity gradient to the power of $K/(1-K)$.

Traditional literature presents different values for this power. Transferring these back with this relationship to Van der Burgh's coefficient, we found a value of $1/2$ [Kuijper and Van Rijn, 2011], of 1 [Hansen and Rattray, 1966], a series of 0, $1/2$, and $2/3$ [Prandle, 1981; MacCready, 2004] or an empirical range of 0.20–0.75 [Gisen, 2015]. It is important to have such different values, which means that the Van der Burgh coefficient may be not a constant.

One objective of this chapter is to provide a theoretical background for this coefficient. This chapter also aims to provide an approach to describe large-scale tide-driven residual circulation caused by preferential ebb and flood channels that develops in the wider part of estuaries, following from Nguyen et al. [2008].

3.2. Linking Van der Burgh to MacCready

Following from the reductionist approach by Hansen and Rattray [1966], MacCready [2004, 2007] derived an equation for the exchange term theoretically:

$$\begin{aligned} \overline{\tilde{u}\tilde{S}} - K_H \frac{\mathrm{d}S}{\mathrm{d}x} = &\left(m_1 \frac{h^2 {u_f}^2}{K_S} + K_H \right) \left(-\frac{\mathrm{d}S}{\mathrm{d}x} \right) + m_2 \frac{g c_S h^5 u_f}{K_S K_E} \left(-\frac{\mathrm{d}S}{\mathrm{d}x} \right)^2 \\ &+ m_3 \frac{g^2 {c_S}^2 h^8}{K_S {K_E}^2} \left(-\frac{\mathrm{d}S}{\mathrm{d}x} \right)^3, \end{aligned} \tag{3.2}$$

where $\tilde{u}$ [LT^{-1}] is the depth-varying velocity, $\tilde{S}$ [psu] is the depth-varying salinity, and the over-bar denotes tidal average and cross-sectional average. $m_1 = 2/105$, $m_2 = 19/(420 \times 48)$, and $m_3 = 19/(630 \times 48^2)$ are constant values following MacCready's vertical integration. u_f ($= |Q|/A$) [LT^{-1}] is the velocity of fresh water, K_H [$\mathrm{L}^2\mathrm{T}^{-1}$] is the along-channel diffusion coefficient, K_S [$\mathrm{L}^2\mathrm{T}^{-1}$] is the effective vertical eddy diffusivity, and K_E [$\mathrm{L}^2\mathrm{T}^{-1}$] is the effective hydraulic eddy viscosity. For the eddy viscosity, there are different empirical expressions [Fischer et al., 1979]; in

this study, following equations are used:

$$K_E = 0.1\frac{2}{\pi}u_* h \ , \tag{3.3}$$

$$u_* = \frac{\sqrt{g}}{C}v \ , \tag{3.4}$$

$$C = K_M h^{1/6} \ , \tag{3.5}$$

where K_M [$L^{1/3}T^{-1}$] is Strickler's coefficient, generally known by its inverse value n ($K_M = 1/n$), Manning's coefficient, representing the bed friction.

Comparing the salt balance equation of MacCready to the steady state equation (2.7) implies that equation (3.2) is identical to $-D\mathrm{d}S/\mathrm{d}x$. MacCready assumed the estuary to be narrow and rectangular, in the sense that cross-sectional shape does not basically modify the width-averaged dynamics. In the derivation, he also assumed the effective vertical eddy viscosity to be constant with depth, following Hansen and Rattray [1966], and that the salinity gradient of the depth-varying part is much smaller than the depth-averaged part, following Pritchard [1952]. Additionally, other effects like salt storage, internal hydraulics and the Coriolis acceleration were considered negligible.

After division of all terms by the salinity gradient, equation (3.2) becomes an equation for the dispersion coefficient:

$$D = \left(m_1 \frac{h^2 {u_f}^2}{K_S} + K_H\right) + m_2 \frac{g c_S h^5 u_f}{K_S K_E}\left(-\frac{\mathrm{d}S}{\mathrm{d}x}\right) + m_3 \frac{g^2 {c_S}^2 h^8}{K_S {K_E}^2}\left(-\frac{\mathrm{d}S}{\mathrm{d}x}\right)^2 \ , \tag{3.6}$$

whereby the first term is not dependent on the salinity gradient, the second is directly proportional to it, and the third term depends on the square of the salinity gradient.

Based on equation (3.1) we can also derive an expression for the dispersion:

$$D = D_0\left(\frac{A_0 D_0}{l|Q|}\right)^{\frac{K}{1-K}}\left(-\frac{A}{A_0}\frac{l}{S_0}\frac{\mathrm{d}S}{\mathrm{d}x}\right)^{\frac{K}{1-K}} \ , \tag{3.7}$$

where l ($= L - x_1$) [L] is the distance from the inflection point to where salinity becomes the same as the fresh water salinity.

Hence $D \propto \gamma^{K/(1-K)}$ with $\gamma = -\frac{A}{A_0}\frac{l}{S_0}\frac{\mathrm{d}S}{\mathrm{d}x}$. Given the function $F(\gamma) = \gamma^{K/(1-K)}$, a

Taylor series expansion near $\gamma = 1$ can be derived as

$$F(\gamma) = \frac{(2K-1)(3K-2)}{2(1-K)^2} + \frac{K(2-3K)}{(1-K)^2}\left(\frac{A}{A_0}\frac{l}{S_0}\right)\left(-\frac{\mathrm{d}S}{\mathrm{d}x}\right) + \frac{K(2K-1)}{2(1-K)^2}\left(\frac{A}{A_0}\frac{l}{S_0}\right)^2\left(-\frac{\mathrm{d}S}{\mathrm{d}x}\right)^2 + R_2(x) \ , \tag{3.8}$$

where $R_2(x)$ is the residual term, considered to be small. If $K = 0$, $F(\gamma) = 1$, dispersion is independent on the salinity; if $K = 1/2$, dispersion is proportional to the salinity gradient; and if $K = 2/3$, dispersion is proportional to the square of the salinity gradient, which means that the dispersion is more sensitive to the salinity gradient.

To analyze the importance of the different terms in equation (3.8), Figure 3.1 presents the factors

$$g_1 = \frac{(2K-1)(3K-2)}{2(1-K)^2} \ , \tag{3.9}$$

$$g_2 = \frac{K(2-3K)}{(1-K)^2} \ , \tag{3.10}$$

$$g_3 = \frac{K(2K-1)}{2(1-K)^2} \ , \tag{3.11}$$

when K is between $1/2$ and $2/3$. g_1 seems a closure term which compensates for g_2 and g_3 so as to make $\sum g_p = 1$ ($p = 1, 2, 3$). It is clear that the absolute value of the first term is much smaller than the density-related terms. Also, the larger the value of K, the more important the third term is.

Considering only the density-dependent terms in equations (3.6) and (3.8), the proportionality results in

$$\frac{2-3K}{2K-1} = 36\frac{K_E|Q|}{gc_S h^3 A_0}\frac{l}{S_0} = \frac{7.2E|Q_f|}{\sqrt{g}c_S h^2 A_0 CT}\frac{l}{S_0} = \omega \ , \tag{3.12}$$

leading to an analytical expression for K:

$$K = \frac{2+\omega}{3+2\omega} \ . \tag{3.13}$$

One should realize that the coefficient K is not exactly the Van der Burgh coefficient, since it only considers the density-related mechanisms, but in the part of the estuary where density-driven mixing is dominant, it is likely a good approximation. According to equation (3.12), K is not time independent; rather, it is determined by the tidal excursion and the fresh water discharge. In the case of a relatively constant discharge, a larger tidal excursion implies larger values of ω, hence K ap-

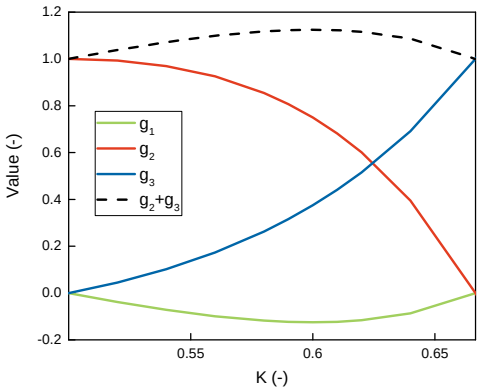

Figure 3.1: Comparison between the factors in the Taylor series expansion of $F(\gamma)$ as a function of the Van der Burgh coefficient K.

proaches the lower limit $(1/2)$. On the other hand, a smaller tidal excursion implies more stratification, a smaller value of ω, and K approaching the higher limit $(2/3)$. Additionally, averaging over a tidal cycle, the parameters in equation (3.12) are almost constant, hence, it is reasonable to assume K is invariable along the estuary as long as gravitational circulation is dominant. We have used this expression to calculate K values in sixteen real estuaries using the empirical database of Savenije [2012]. These K values are in a range of 0.51–0.64 (see Appendix A.4).

Overall, there are three results for the estimation of K: 1) by comparison with traditional studies ($K = 1/2$ or $2/3$), 2) by comparison with MacCready considering the salinity relevant terms ($1/2 < K < 2/3$), and 3) based on empirical calculation.

3.3. Model including residual circulation

3.3.1. A box-model approach for wide estuaries

For calculating the effect of residual circulation, a different approach is followed than Nguyen et al. [2008], trying to combine lateral and longitudinal circulation in the regular one-dimensional advection-dispersion equation.

Figure 3.2 presents a sketch of a box-model used to include lateral exchange in longitudinal dispersion. Water particles in the middle can mix longitudinally and laterally within their respective mixing lengths. For the longitudinal mixing length we consider the tidal excursion and for the lateral exchange half of the estuary

width. The mass balance can then be described as

$$\frac{V\Delta S_2}{\Delta t} = |Q|(S_2 - S_1) + i(S_1 - 2S_2 + S_3) + j(S_L - 2S_2 + S_R) \ , \tag{3.14}$$

where $V\ (= AE)$ [L^3] is the water volume, S_p [psu] is the salinity at different locations p, and i and j [L^3T^{-1}] are longitudinal and lateral exchange discharges.

The balance equation then becomes

$$V\frac{\partial S}{\partial t} - |Q|\frac{\partial S}{\partial x}\Delta x - i\frac{\partial^2 S}{\partial x^2}(\Delta x)^2 - j\frac{\partial^2 S}{\partial y^2}(\Delta y)^2 = 0 \ , \tag{3.15}$$

where Δx and Δy [L] are the mixing lengths, which are taken as $\Delta x = E$ and $\Delta y = B/2$.

The assumption used is that the lateral exchange is proportional to the longitudinal exchange [Fischer, 1972]:

$$j\frac{\partial^2 S}{\partial y^2} \propto i\frac{\partial^2 S}{\partial x^2} \ . \tag{3.16}$$

As a result, longitudinal and lateral processes can be combined into one single one-dimensional equation:

$$\frac{\partial S}{\partial t} - \frac{|Q|}{A}\frac{\partial S}{\partial x} - \frac{iE}{A}\left(1 + C_2\left(\frac{B}{E}\right)^2\right)\frac{\partial^2 S}{\partial x^2} = 0 \ , \tag{3.17}$$

where C_2 determines how important lateral exchange is in relation to longitudinal exchange. Comparing equation (3.17) with the traditional salt balance equation (2.6), if the variation of the cross section and dispersion is slight, the effective longitudinal dispersion is

$$D = \frac{iE}{A}\left(1 + C_2\left(\frac{B}{E}\right)^2\right) \ . \tag{3.18}$$

Subsequently, the longitudinal exchange discharge i is assumed to be proportional to the amplitude of the tidal flow ($\widehat{Q_t} = Av$), and to the stratification number to the power of K:

$$i = C_1 {N_R}^K \widehat{Q_t} \ , \tag{3.19}$$

where C_1 is a factor. Here the tide-driven residual circulation is presented by the C_2 term and K considers only density-driven processes, which is consistent with equation (3.13). Tidal shear effect and trapping are assumed to be relatively small. If not, it can be included in the C_2 part.

We then obtain a simple dimensionless expression for the dispersion coefficient,

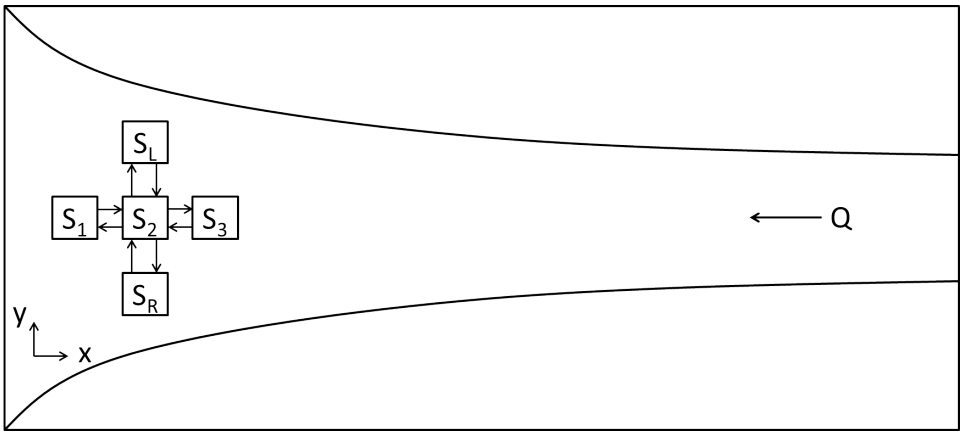

Figure 3.2: Conceptual sketch for lateral and longitudinal mixing. Longitudinal and lateral mixing lengths are Δx and Δy, respectively.

similar to the one by Gisen et al. [2015a] but incorporating lateral processes:

$$\frac{D}{vE} = C_1 {N_R}^K \left(1 + C_2 \left(\frac{B}{E}\right)^2\right) . \tag{3.20}$$

3.3.2. Analytical solution

In almost all estuaries especially in the upstream part, the ratio of width to excursion length is quite small. This is the part where salinity problems are important to water users and the environment. So for analytical solutions of the salt balance equation we shall focus on the first part of equation (3.20):

$$D = C_1 {N_R}^K vE . \tag{3.21}$$

The traditional approach by Savenije [2012] uses this equation for the boundary condition, after which $D(x)$ values are obtained by integration of Van der Burgh's equation along the estuary axis. But, in principle, with this equation the dispersion can be calculated at any point along the estuary, provided local hydraulic and geometric variables are known. Using the expression for N_R, equation (3.21) can be elaborated into

$$D(x) = C_1 (c_S g \pi)^K \left(\frac{S|Q|}{v^3 B}\right)^K vE , \tag{3.22}$$

where all local variables are merely a function of x.

The following equations are used for the tidal velocity amplitude, width, and

tidal excursion:

$$v(x) = v_0 e^{\delta_v (x - x_1)} , \tag{3.23}$$

$$B(x) = B_0 e^{-(x - x_1)/b} , \tag{3.24}$$

$$E(x) = E_0 e^{\delta_H (x - x_1)} , \tag{3.25}$$

where δ_v ($\approx \delta_H$) [L^{-1}] is the damping/amplifying rate of tidal velocity amplitude.

At the boundary, the predicted equation is given by:

$$D_0 = C_1 (c_S g \pi)^K \left(\frac{S_0 |Q|}{{v_0}^3 B_0} \right)^K v_0 E_0 . \tag{3.26}$$

Substitution of equations (3.23)–(3.26) into (3.22) gives

$$D(x) = D_0 \left(\frac{S}{S_0} \right)^K e^{\Omega (x - x_1)} , \tag{3.27}$$

with $\Omega = 2\delta_H - 3K\delta_H + K/b$.

Differentiating D with respect to x and using equation (3.27) results in

$$\frac{dD}{dx} = K \frac{D}{S} \frac{dS}{dx} + \Omega D . \tag{3.28}$$

Combining the result with the salt balance equation (2.7), equation (3.28) results in

$$\frac{dD}{dx} = \Omega D - K \frac{|Q|}{A} . \tag{3.29}$$

If $\Omega = 0$, equation (3.29) becomes Van der Burgh's equation. A small value of Ω occurs in estuaries with a long convergence length and limited damping. This is why the exchange flow is a function of the stratification number to the power K in equation (3.19). Even though K here considers only the density-driven mechanism and therefore is not exactly the same as the Van der Burgh coefficient (which includes all mixing mechanisms), it is clearly closely related to the Van der Burgh coefficient.

The cross-sectional area A is given by

$$A(x) = A_0 e^{-(x - x_1)/a} . \tag{3.30}$$

Substitution of equation (3.30) into (3.29) gives

$$\frac{dD}{dx} = \Omega D - K \frac{|Q|}{A_0} e^{(x - x_1)/a} . \tag{3.31}$$

In analogy with Kuijper and Van Rijn [2011], the solution of this linear differential

equation is

$$\frac{D}{D_0} = \mathrm{e}^{\Omega(x-x_1)} - \frac{K|Q|}{A_0 D_0}\zeta\left[\mathrm{e}^{(x-x_1)/a} - \mathrm{e}^{\Omega(x-x_1)}\right] , \tag{3.32}$$

with

$$\zeta = \frac{a}{1-\Omega a} . \tag{3.33}$$

The maximum salinity intrusion length is obtained from equation (3.32) after substitution of $D = 0$ at $x = L$:

$$L = \zeta \ln\left(1 + \frac{A_0 D_0}{K|Q|\zeta}\right) + x_1 . \tag{3.34}$$

This is the same equation as in Savenije [2005] if $\zeta = a$.

Using equation (3.27), the longitudinal salt distribution becomes

$$\frac{S}{S_0} = \left\{1 - \frac{K|Q|}{A_0 D_0}\zeta\left[\mathrm{e}^{(x-x_1)/\zeta} - 1\right]\right\}^{1/K} . \tag{3.35}$$

This solution is the same as equation (2.16) if $\Omega = 0$ and it is similar to the solution by Kuijper and Van Rijn [2011], with the difference that Kuijper and Van Rijn used a constant value of $K = 1/2$ and that their value of Ω depended on the bottom slope.

So with these new analytical equations, the local dispersion and salinity can be obtained, using the boundary conditions. This method is limited since it only works if $B/E < 1$. If we want to account for residual circulation using equation (3.20), then we have to use numerical integration of equation (2.7) using (3.20) for D.

3.4. Empirical validation

3.4.1. Summary information

Sixteen alluvial estuaries, covering a diversity of sizes, shapes, and locations, are used for empirical validation of the new box-model. The general geometry of these estuaries using equations (2.1)–(2.3) are compiled in Appendix A.1. It shows that all these estuaries can be schematized in one or two segments separated by a well-defined inflection point. The general geometry of these estuaries is summarized in Appendix A.2. The same values of a and b indicate that the depth is constant.

Summary information on different measurement dates is presented in Appendix A.3 and A.4, where E_m [L] is the tidal excursion at estuary mouth and $\alpha = D/|Q|$ [L^{-1}] is the mixing coefficient. Tidal excursion and tidal period are more or less the same in all estuaries, except for the Lalang and the Chao Phraya with a diurnal tide. Most estuaries damp upstream, with negative values of δ_H. In addition, most estuaries have a small tidal amplitude to depth ratio, which means relatively simple

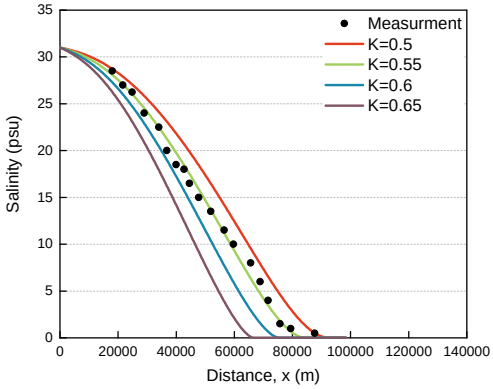

Figure 3.3: Salinity profiles using different values of K: using data from the Thames at tidal average.

solutions of hydraulic equations are possible [Savenije, 2005].

K values have been obtained by calibration of simulated salinities to observations in these estuaries. How the simulated salinity distribution changes for different values of K is presented in Figure 3.3. The smaller the value, the further the salinity intrudes. The value of K affects the salinity mostly in the upstream reach. The dispersion at the boundary has a range of $50 - 600$ m^2/s in a variety of estuaries, which is consistent with Prandle [1981]. The mixing coefficient demonstrates to what extent the dispersion overcomes the flushing by river flow. The larger the river discharge, the smaller the α, meaning it is difficult for the salinity to penetrate into the estuary. The dispersion reduction ratio β determines the longitudinal variation of dispersion. Fischer et al. [1979] suggested that the transition from a well-mixed to a strongly stratified estuary occurs if the values of stratification number N_R are in the range of 0.08–0.8. With a ratio of π between Fischer's and our expressions for the stratification number, the range becomes 0.25–2.51. It is obvious that all estuaries are partially to well mixed, with N_R below 2.51.

Using the automatic Solver, the best result was obtained with $C_1 = 0.10$, $C_2 = 12$, and $K = 0.58$. For individual estuaries, K values were obtained ranging between 0.45 and 0.78.

3.4.2. Sensitivity to C_2

Through the use of C_2 we can use a single dispersion equation accounting for two-dimensional effects in a one-dimensional model. The assumption that lateral exchange is proportional to longitudinal dispersion suggests C_2 to be independent of x. To check the sensitivity to C_2, different values (mainly 1, 10, and 50) have

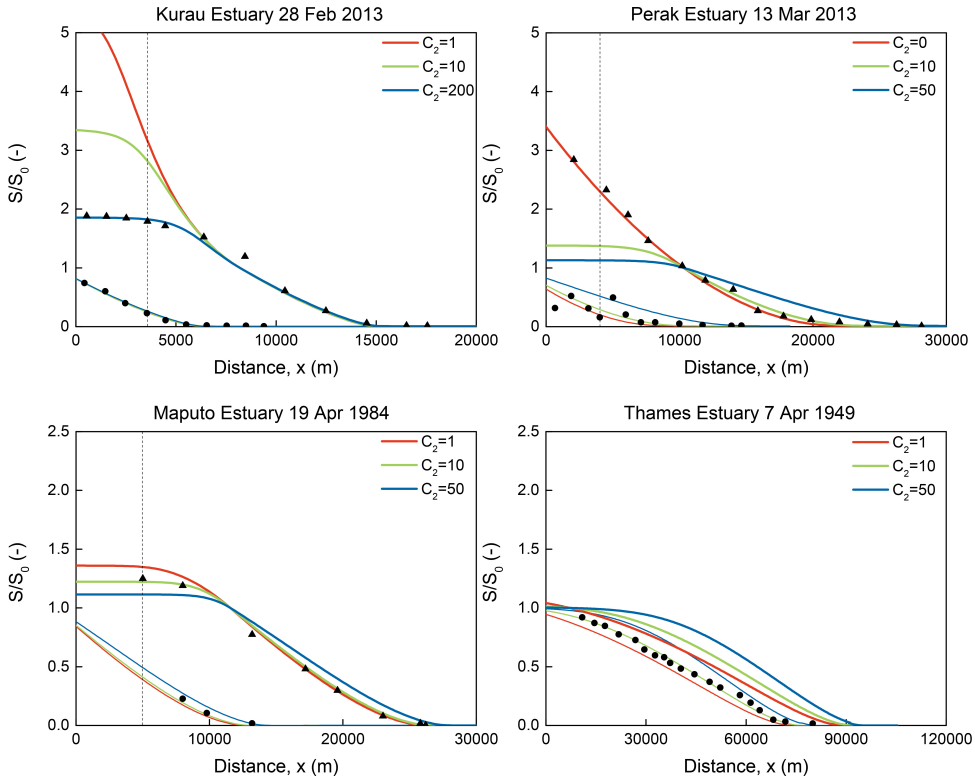

Figure 3.4: Comparison between simulated and observed salinity at high water slack (thin lines) and low water slack (thick lines), scaled by the boundary salinity S_0 for different C_2 values. Observations at high water slack are represented by triangles and low water slack by circles. The Thames only has low water slack observations.

been used to calculate salinity curves. Figure 3.4 and Appendix A.5 demonstrate how salinity changes with varying C_2 values. Salinities were simulated by numerical solution of equation (2.7) with (3.20) based on the boundary condition normally at $x = x_1$. There is almost no effect on narrow estuaries like the Lalang, the Limpopo, the Tha Chin, and the Chao Phraya. However, typically, C_2 matters near a wide mouth part. It is demonstrated that the larger the value of C_2, the smaller the salinity gradient and the flatter the salinity curve near the estuary mouth. Additionally, because of the interdependence of D, S, and $\mathrm{d}S/\mathrm{d}x$ through equation (2.7) in the upstream part, a larger value of C_2 can lead to larger salinities upstream (e.g., the Thames, the Elbe, the Edisto, the Maputo, and the Corantijn). Overall, the inclusion of the residual circulation improves the accuracy of salinity simulation in wide estuaries and more particularly near the mouth of the estuaries where the ratio of width to tidal excursion is relatively large.

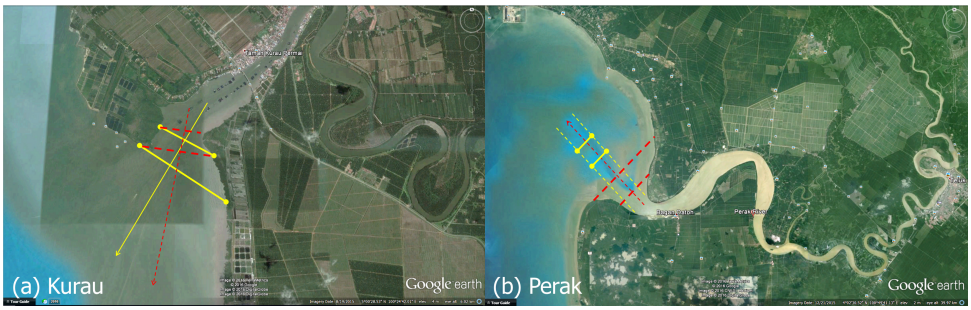

Figure 3.5: Estuary mouth shapes of (a) the Kurau and (b) the Perak. Thick lines show the estimation of width and thin lines show reference streamlines. In yellow presents the situation may be the case instead of the misinterpretation in red.

Basically, $C_2 = 10$ (green lines) can perform perfectly in 12 out of 16 estuaries, for instance, in the Maputo and the Thames in Figure 3.4. Hence, a general value of $C_2 = 10$ is recommended.

Tailor-made C_2 values are needed in some estuaries that have peculiar shapes near the mouth. A larger value of C_2 ($= 200$) applies to the Kurau. This may be because the width is underestimated in the estuary mouth (Figure 3.5), due to misinterpretation of the direction of the streamline (the width is determined according to a line perpendicular to the streamline). As a matter of fact, the width should be larger (yellow solid lines) and dispersion should be larger with smaller salinity gradients, which would then result in a lower value of C_2. The same applies to the Endau ($C_2 = 35$). By contrast, a smaller value of C_2 ($= 0$) in Perak fits better, because of overestimation of the width (Figure 3.5). Here the topographical map suggests a wide estuary mouth, whereas the tidal flow is concentrated in a much narrower main channel due to a the north bank protruding into the estuary and a spur from the south projecting into the mouth. The Selangor has a similar situation ($C_2 = 3$). It shows that the configuration of the mouth is important for the correct simulation of the salinity near the estuary mouth. But, fortunately, a relatively poor performance near the mouth of these estuaries does not affect the salinity distribution upstream as long as C_2 is not too large. In conclusion, $C_2 = 10$ appears to be a suitable default value as long as the trajectory of the tidal currents can be considered properly.

The poor fit in the downstream parts of the Lalang and the Chao Phraya, in which measured salinities are lower than simulated, can be explained by a complex downstream boundary. The Lalang estuary has a pronounced riverine character and is a tributary to the complex estuary system of the Banyuasin, sharing its outfall with the larger Musi river. So the salinity near its mouth is largely affected by the Musi. Also, pockets of fresh water can decrease the salinity near the confluence.

The Chao Phraya opens to the Gulf of Thailand where the salinity is influenced by historical discharges rather than ocean salinity, remaining relatively fresh. Other measurement uncertainties may cause outliers as well.

3.5. Reductionist approach to the coefficient

The physical meaning of the coefficient K has been analyzed, linking it to the traditional theoretical research. Equation (3.12) shows a direct relation between this parameter and MacCready's parameters, which are measurable quantities. Hence, the coefficient is affected by tide, geometry, and freshwater discharge. Shaha and Cho [2011] also found K values to depend on river discharge while considering the value to increase upstream in a range of $(0,\ 1)$ due to different mechanisms along the estuary.

A 1:1 plot is presented in Figure 3.6, relating the empirical K values by calibration applying the box-model to the predicted values using equation (3.13). The predicted K values are close to the calibrated ones, even though the former have a smaller range (0.51–0.64) than the latter (0.45–0.78). It can be seen that there is a steep linear relation between predicted and calibrated K values, which reveals that the predictive method overestimates the low calibrated K values and underestimates the high values. Or, the range of $(1/2,\ 2/3)$ appears too narrow. Mixing mechanisms not related to density, corresponding to $K = 0$, are strictly avoided in the predictive method. While even though the non-density driven mechanism is represented in the C_2 term, it may affect the empirical calibration. An increase of tide which deminishes the stratification would also decrease the K value. As a result, the predicted values are higher than the calibrated ones in the lower region. On the other hand, the Taylor series to approximate $F(\gamma)$ could have more terms, resulting K to equal, for instance, $3/4$, $4/5$, approaching unity. According to Hansen and Rattray [1966], K equals 1 under their central regime assumption, where the salinity gradient is maximized. Hence, a larger range than $[1/2,\ 2/3]$ may be feasible. However, considering that the K values have been obtained from different approaches, they are still reasonably similar. As a result, this correspondence provides a physical basis to K, which is connected to the Van der Burgh coefficient. Finally, all K values are very close to 0.58, which may be a good starting value in estuaries where information on geometry and channel roughness is lacking.

Overall, there are quite some uncertainties in calibrating an empirical model to data in real estuaries, as a result of a whole range of uncertain factors related with observational errors, data problems, the assumption of steady state, flows in the geometry, and other factors. The outlier from the Thames ($\#8$ in Figure 3.6) is most likely due to the geometry. Maybe the Thames is too wide for the dispersion to be dominant by density differences which is underlying MacCready's method. The outlier estuary $\#1$ (Kurau) may be because of an underestimated freshwater

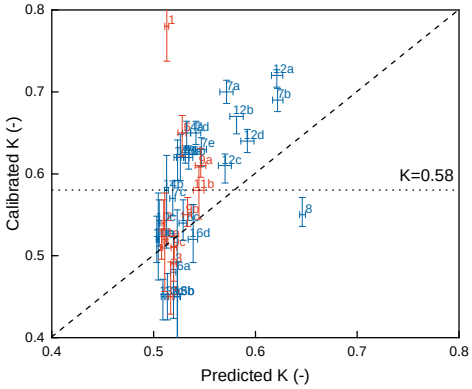

Figure 3.6: Comparison between predicted and calibrated K values. Labels are used to distinguish estuaries. The blue marks use K_M from Cai et al. [2012] and the red ones from Gisen [2015]; 25 % sensitivity of fresh water discharge is indicated by the whiskers.

discharge.

3.6. Concluding remarks

The coefficient K determines the way the density-relevant process of dispersion relates to the stratification number by a power function. Two approaches, theoretical derivation from the traditional literature using a reductionist approach and empirical validation based on observations in a large set of estuaries, provided similar estimates of K. Under MacCready's assumptions, there are three ways to estimate K: $0.51 < K < 0.64$ from empirical application of equations (3.12) and (3.13); $1/2 < K < 2/3$ as the physical boundaries of equation (3.13); and the comparison with traditional approximations ($K = 1/2$ and $2/3$). After validation of the new box-model to the database of field observations, the values of K are in a range of $0.45 - 0.78$ for a wide range of conditions, with an average of 0.58, close to the predicted values. Although these one-dimensional expressions of velocity and salinity may be simplifications of reality, the good correspondence provides a promising theoretical basis for K, revealing that the Van der Burgh coefficient has a lower value when the estuary is less stratified due to a stronger tide.

A previous analytical salinity intrusion model was developed by Gisen [2015], from which the Van der Burgh coefficient values resulted in a range of 0.20–0.75 by calibration and 0.22–0.71 by prediction. These solutions cover a wider range than our estimates because of Gisen's assumption that Van der Burgh's coefficient does not depend on river discharge and the absence of the two-dimensional tide-

driven mixing near the mouth. Moreover, three improvements have been made in this chapter. Firstly, we used the local hydraulic parameters to simulate the salinities, while Gisen used a constant depth and no damping. In addition, by using an uncertainty bound of 25% on freshwater discharge we could reduce the inaccuracy of the tail of the salinity curve and obtain a better fit (where K matters most). And finally, all geometric analyses were improved by revisiting the fit to observations.

An important consequence of this study is that K depends on time. Where Gisen assumed the Van der Burgh coefficient to be constant for each estuary, we find substantial variability for estuaries where a larger range of discharges is available: e.g. in the Maputo, $0.57 < K < 0.70$ and in the Limpopo, $0.61 < K < 0.72$.

Overall, the single one-dimensional salinity intrusion model including residual circulation appears to work well in natural estuaries with a diversity of geometric and tidal characteristics, by both analytical and numerical computation. The new equation is a simple and useful tool for analyzing local dispersion and salinity directly on the basis of local hydraulic variables. In a calibration mode, K is the only parameter to be calibrated using $C_1 = 0.10$ and $C_2 = 10$. In a predictive mode, a value of $K = 0.58$ can be used as a first estimate. If information on river discharge, roughness, and geometry is available, K can be determined iteratively by taking $K = 0.58$ as the predictor and subsequently substituting S_0 and l from the first iteration by equations (3.12) and (3.13) and repeating the procedure until the process converges.

The addition of the factor $(1 + C_2(B/E)^2)$ in the dispersion equation proved valuable near the wide mouth of estuaries where the interacting ebb and flood channels dominate dispersive actions. The value $C_2 = 10$ was found to perform best in most estuaries.

In some particular cases, the simulated salinity with $C_2 = 10$ does not fit the observations near the estuary mouth. So one should be aware of peculiar configurations of streamlines and geometries near the estuary mouth when using this model. However, a poor fit near the estuary mouth has almost no effect on the total salinity intrusion. Finally, this predictive one-dimensional salinity intrusion model, having a stronger theoretical basis, may be a useful tool in ungauged estuaries.

4

Thermodynamics of saline and fresh water mixing in estuaries

To learn without thinking is blindness,
to think without learning is idleness.

Confucius (551 ~ 479 B.C.)

学而不思则罔
思而不学则殆
孔子［春秋］

This chapter is based on:

Zhang, Z. and Savenije, H. H. G.: Thermodynamics of saline and fresh water mixing in estuaries, Earth Syst. Dynam., **9**, 241-247, 2018.

4.1. Background

The freshwater flow that enters an estuary from the river contains potential energy with respect to the saline ocean water. This potential energy is able to perform work. Gravitational circulation is a process that dissipates the potential energy of the fresh water. The maximum power concept assumes that this dissipation takes place at maximum power [Kleidon, 2016].

The sketch in Figure 4.1 presents a typical longitudinal salinity distribution at the maximum power optimum. The seaward and landward salt fluxes are the same, at any location along the estuary. The power is described by the product of the upstream dispersive water flux and the gradient in geopotential height driving this flux or, alternatively, the product of the dispersive exchange flux and the water level gradient. In this chapter, the system is assumed closed hence these two aspects are considered affecting each other and can lead to a maximum product (toward thermodynamic equilibrium).

4.2. Maximum power in estuaries

The water level gradient follows from the balance between the hydrostatic pressures of fresh and saline water, resulting in

$$\frac{\mathrm{d}z}{\mathrm{d}x} = -\frac{h}{2\rho_f}\frac{\mathrm{d}\rho}{\mathrm{d}x}\,, \tag{4.1}$$

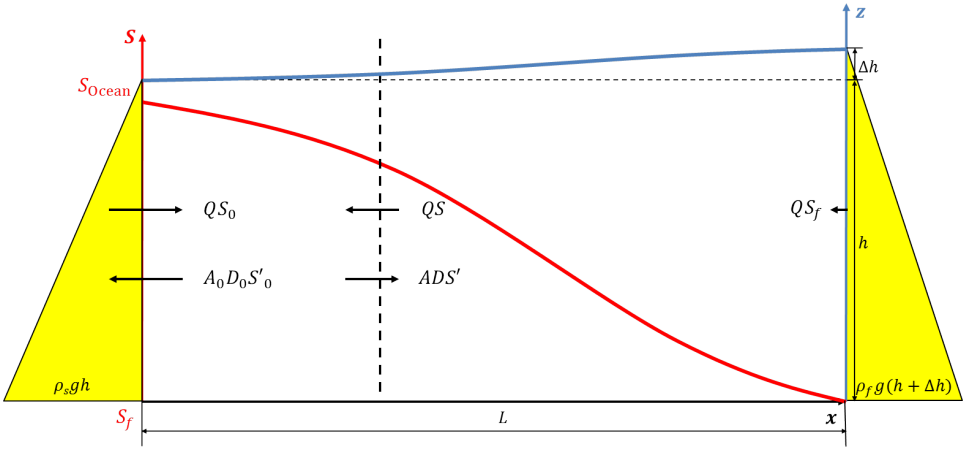

Figure 4.1: Salinity distribution at maximum power (at t_2 in Figure 2.9). The black arrows show the boundary fluxes.

where z $(= h + \Delta h)$ [L] is the tidal average water level (blue line in Figure 4.1). The depth gradient is essential for the density-driven mixing, but Δh is small compared to h (typically 1.2 % of h). Note that this equation applies to the case in which the river flow velocity is small, which is the case when estuaries are well mixed. Otherwise a backwater effect should be included, but this only applies to a situation of high river discharge when the salt intrudes by means of a salt wedge with a sharp interface.

One can express the density of saline water as a function of the salinity:

$$\rho = \rho_f (1 + c_S S) \ . \tag{4.2}$$

As a result, equation (4.1) can be written as

$$\frac{\mathrm{d}z}{\mathrm{d}x} = -c_S \frac{h}{2} \frac{\mathrm{d}S}{\mathrm{d}x} = -c_S \frac{h}{2} S' \ . \tag{4.3}$$

The upstream dispersive flux is implicit in the salt balance equation in steady state. Writing water fluxes both downstream and upstream results in

$$Q = \frac{ADS'}{S - S_f} \ . \tag{4.4}$$

The right-hand side is the water exchange flux, which is the flux that depletes the gradient. As equation (4.4) shows, in steady state this exchange flux is equal to the freshwater discharge. The combination of the flux and the gradient leads to the power of the mixing system per unit length (defined as a positive quantity):

$$\widehat{P} = |\rho g Q \frac{\mathrm{d}z}{\mathrm{d}x}| = -\frac{1}{2} c_S \rho g h |Q| S' \ . \tag{4.5}$$

Applying the theory of maximum power to the dispersive process, we need to maximize the power with regard to the dispersion coefficient, which is the parameter representing the mixing and which is the main unknown in salt intrusion prediction:

$$\frac{\mathrm{d}\widehat{P}}{\mathrm{d}D} = 0 \ . \tag{4.6}$$

Applying equation (4.6) with constant river discharge and constant depth, which is the property of an ideal alluvial estuary[1] according to Savenije [2005], leads to

$$\frac{\mathrm{d}S'}{\mathrm{d}D} = 0 \ . \tag{4.7}$$

[1]In an ideal estuary, the convergence of the estuary banks is just sufficient to balance the damping of the tidal range due to friction Langbein [1963]; there is no damping or amplification.

Using the salt balance equation, differentiation leads to

$$\frac{\mathrm{d}S'}{\mathrm{d}D} = \frac{\mathrm{d}S'}{\mathrm{d}x}\frac{\mathrm{d}x}{\mathrm{d}D} = -\frac{|Q|}{AD}\left\{\frac{S'}{D'} - \frac{A'(S-S_f)}{AD'} - \frac{S-S_f}{D}\right\}, \tag{4.8}$$

where the prime means the gradient of the parameters with respect to x. The application of equation (4.7) then yields:

$$\frac{DS'}{(S-S_f)D'} = \frac{A'D}{AD'} + 1\,. \tag{4.9}$$

4

4.3. Thermodynamic approach for the empirical coefficient

We introduce three length scales: $a = -(A-A_f)/A'$, $s = -(S-S_f)/S'$, and $d = -D/D'$, where s [L] is length scale of the longitudinal salinity variation and d [L] is length scale of the longitudinal variation of dispersion. A shape factor σ ($= 1-A_f/A$) [-] is included considering the effect of river cross section. In an exponentially shaped estuary, the convergence length a is a constant, but d and s vary with x. It can be shown that the proportion s/d equals the Van der Burgh coefficient K ($= -AD'/|Q|$) [Van der Burgh, 1972], which in this approach varies as a function of x. Using these length scales, equation (4.9) can be written as

$$\frac{s}{d} = \frac{a}{a+d\sigma} \tag{4.10a}$$

or:

$$s = \frac{ad}{a+d\sigma} \tag{4.10b}$$

or:

$$d = \frac{as}{a-s\sigma}\,, \tag{4.10c}$$

where in estuaries with a pronounced funnel shape σ approaches unity. Equation (4.10) is an additional equation to the salt balance, which in terms of the length scales reads $s = AD/|Q|$.

As a result, we have two differential equations with two unknowns: $S(x)$ and $D(x)$. Adding two boundary conditions at a given point S_0 and D_0 would solve the system. The first boundary condition is relatively simple to measure. Then the only unknown parameter left is the value for the dispersion at the boundary. If observations of salinity distributions are available, then the value of D_0 is obtained by calibration.

What the maximum power equation has contributed is that it provides an additional equation. In the past, a solution could only be found if an empirical equation

was added describing $D(x)$, containing an additional calibration parameter. In the approach by Savenije [2005] this was the empirical Van der Burgh equation containing the constant Van der Burgh coefficient K. However, with the new equation (4.10), which in fact represents a spatially varying Van der Burgh coefficient, this additional calibration parameter is no longer required. So this thermodynamic approach replaces the empirical equation with a new physically based equation and removes a calibration parameter, leaving only one unknown: the dispersion at a well-chosen boundary condition.

4.4. Applications

Besides sixteen estuaries used in Chapter 3, seven additional estuaries from a less reliable dataset have been added to the database for empirical validation. The general geometry of all these estuaries uses equations (2.3)–(2.5) and is compiled in Appendix A.6 and summarized in Appendix A.7. This compilation considers that the estuaries converge to rivers. Comparing to Appendix A.1 using equations (2.1)–(2.3), most of the estuaries have similar characteristics while in some of them, for example, the Thames and the Limpopo, the location of the inflection point has been changed by the revisiting of geometry. Salinity measurements of the first sixteen estuaries are displayed in Appendix A.3 and A.4, and information of new estuaries is presented in Appendix A.8.

Subsequently we have integrated equations (2.7) and (4.10) conjunctively by using a simple explicit numerical scheme in a spreadsheet and confronted the solution with observations. The solutions are fitted to the data by selecting values for S and D at the boundary condition. Figures 4.2 shows applications of the solution to selected observations in the Maputo and the Limpopo. In the Appendix A.9 more applications are shown for estuaries in different parts of the world. It is clear that the new equation appears to fit very well to the observations in these estuaries.

Salinity, dispersion, and estuarine Richardson number at the boundary condition are summarized in Appendix A.10.

4.5. Critical remarks

By making use of the maximum power concept, it was possible to derive an additional equation to describe the mixing of salt and fresh water in estuaries. Together with the salt balance equation, these two first-order and linear differential equations only require two boundary conditions (the salinity and the dispersion at a well-chosen boundary) to be solved. However, there is a problem.

An analytical solution of equation (4.9) with the steady-state equation (2.7) is possible (see below in Section 4.5.1). The solution shows that the longitudinal salinity gradient is a constant and the salinity curve is a straight line. Hansen and

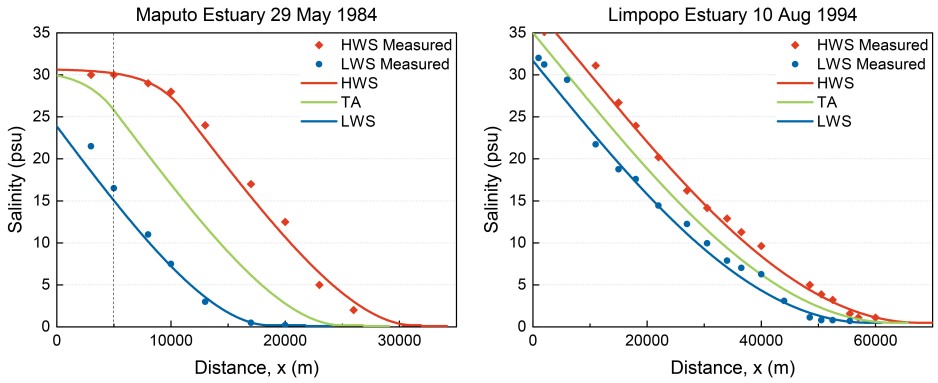

Figure 4.2: Application of the numerical solution to observations for high water slack (red) and low water slack (blue). The green line shows the tidal average condition. The symbols reflect the observations.

Rattray [1966], based on the data from Pritchard [1952], also claimed that the longitudinal salinity distribution in many coastal plain estuaries is almost linear with the maximum gradient in the central part. Nevertheless, even though the analytical solution can simulate the salinity in the central part, it is not yet satisfactory. The realistically looking profiles in the applications are an artifact of the numerical solution: a predictor-corrector method for the dispersion coefficient was used.

Alternatively we considered maximum power over a segment. This leads to a dome-shaped intrusion curve with $K = 1$ (see below in Section 4.5.2).

Subsequently, we considered the maximum power over the entire intrusion length. This leads to the trivial condition of steady state (see below in Section 4.5.3).

4.5.1. Analytical solution of the maximum power equation

Combining the steady-state equation (2.7) and (4.9), the salinity terms can be eliminated as

$$D' - \frac{1}{a}D = -\frac{|Q|}{A_0}\mathrm{e}^{(x-x_1)/a} \,. \tag{4.11}$$

The solution of the first-order linear differential equation (4.11) using a boundary condition that $D = D_0$ at $x = x_1$ is

$$D = \mathrm{e}^{(x-x_1)/a}\left[D_0 - \frac{|Q|}{A_0}(x - x_1)\right] \,. \tag{4.12}$$

Substituting equation (4.12) in the steady-state equation and integrating the

result using the boundary condition that $S = S_0$ at $x = x_1$,

$$S = S_0 - \frac{|Q|S_0}{A_0 D_0}(x - x_1) \ . \tag{4.13}$$

This analytical solution shows that the simulation of salinity is a straight line. Hence, the solution in equation (4.8) is not the correct approach to equation (4.6).

4.5.2. Maximum power at fixed location

Another solution is considered assuming the power achieves its maximum with time ($\mathrm{d}P/\mathrm{d}t = 0$). Then the resulting S and D distributions are no longer time-dependent and linked at any segment.

The solution of equation (4.7) then can be

$$\frac{\mathrm{d}S'}{\mathrm{d}D} = \frac{\partial S'}{\partial D} + \frac{\partial S'}{\partial S}\frac{\mathrm{d}S}{\mathrm{d}D} = 0 \ . \tag{4.14}$$

Substituting the steady-state equation yields

$$\frac{|Q|S}{AD^2} - \frac{|Q|}{AD}\frac{\mathrm{d}S}{\mathrm{d}D} = 0 \ . \tag{4.15}$$

Hence, the relation between the salinity and dispersion using the boundary condition that at $S = S_0$, $D = D_0$ is

$$\frac{S}{S_0} = \frac{D}{D_0} \ . \tag{4.16}$$

Combining the steady-state equation, the salinity along the estuary can be derived using the boundary condition that at $x = x_1$, $S = S_0$:

$$S = S_0\left[1 - \frac{a|Q|}{A_0 D_0}\left(\mathrm{e}^{(x-x_1)/a} - 1\right)\right] \ . \tag{4.17}$$

If we compare equations (4.16) and (4.17) to the traditional equations (2.13) and (2.16), the Van der Burgh coefficient K equals 1.

Correspondingly, the following equations are solved:

$$S' = -\frac{|Q|S_0}{A_0 D_0}\mathrm{e}^{(x-x_1)/a} \ , \tag{4.18}$$

$$S'' = -\frac{|Q|S_0}{aA_0 D_0}\mathrm{e}^{(x-x_1)/a} \ . \tag{4.19}$$

Both of these two equations have negative values for S' and S'' along the estuary, suggesting that the salinity distribution is a dome shape curve. This is certainly not

the common case in natural estuaries. It reveals that the maximum power concept is not used correctly assuming it is in thermodynamic equilibrium along the estuary.

4.5.3. Maximum power at a certain moment in time

Instead of considering that the thermodynamic equilibrium is achieved at fixed locations along the estuary, the solution may be that the power of the entile estuary is maximized at a certain moment. Then the maximization of the power along the estuary is considered as

$$\frac{\partial}{\partial t}\int_0^x P\,\mathrm{d}x = 0\ . \tag{4.20}$$

Under this circumstance,

$$\frac{\partial}{\partial t}\int_0^x S'\,\mathrm{d}x = \frac{\partial S}{\partial t} = 0\ , \tag{4.21}$$

which correspondence to the steady-state situation.

In conclusion, we have to admit that the thermodynamic approach of this chapter has a flaw. An estuary is an open system. Therefore the thermodynamics of saline and fresh water mixing in estuaries can not be solved easily assuming it as an isolated system. In the next chapter, the maximum power concept is explored in open estuarine systems.

5

Maximum power concept towards open estuarine systems

Three passions, simple but overwhelmingly strong,
have governed my life: the longing for love,
the search for knowledge,
and unbearable pity for the suffering of mankind.

Bertrand Russell

This chapter is based on:

Zhang, Z. and Savenije, H. H. G.: Maximum power concept towards saline and fresh water mixing in open estuarine systems, Earth Syst. Dynam., (under review).

5.1. Background

In Chapter 4, the maximum power concept was used trying to solve the saline and fresh water mixing as in thermodynamic equilibrium systems. The problem is that the freshwater discharge provides continuous potential energy into the estuary hence the system is not isolated.

Kleidon [2016] presented an example of the maximum power limit for non-thermal energy conversions. In the example, fluid is kept in motion by an accelerating force which provides kinetic energy to the system. The velocity of the fluid is slowed down by friction and the remainder is converted into another form of energy. If the velocity is too large, the friction is large and energy dissipation dominates, then the power of the force to generate work is limited. In contrast, if the velocity is too small, the power is not enough to generate work. Hence, there is an optimum value for the product of the force and velocity to produce maximum useful energy.

Estuaries are comparable to this non-thermal system. This chapter tries to solve the dynamics of an estuary using a similar concept considering it as an open system.

5.2. Maximum power concept for an open estuary system

In an estuary, the cross-sectional average hydrostatic forces have equal values along the estuary axis. Over a segment, the forces are opposed but working on different lines of action due to the density gradient in upstream and downstream directions. As a result, they exert an angular moment M_{acc} that drives the gravitational circulation, performing as accelerating energy. N_{fric} is the energy dissipation due to friction. The remainder moment M_{ex} drives the dispersive movement and performs work (Figure 5.1). Hence, the balance of work in steady state over a segment is

$$M_{\mathrm{acc}} - M_{\mathrm{ex}} - N_{\mathrm{fric}} = 0 \ . \tag{5.1}$$

Energy dissipation is expressed as

$$N_{\mathrm{fric}} = F_{\mathrm{fric}} l_m \ , \tag{5.2}$$

with F_{fric} [MLT^{-2}] being the friction that causes energy dissipation and l_m [L] the dispersive distance scale where energy dissipates due to mixing.

Friction is expressed as

$$F_{\mathrm{fric}} = \tau O \ , \tag{5.3}$$

where τ [$\mathrm{ML}^{-1}\mathrm{T}^{-2}$] is the shear stress and O [L^2] is the contact area. Since the process of mixing is essentially to move the saline water up in the vertical column

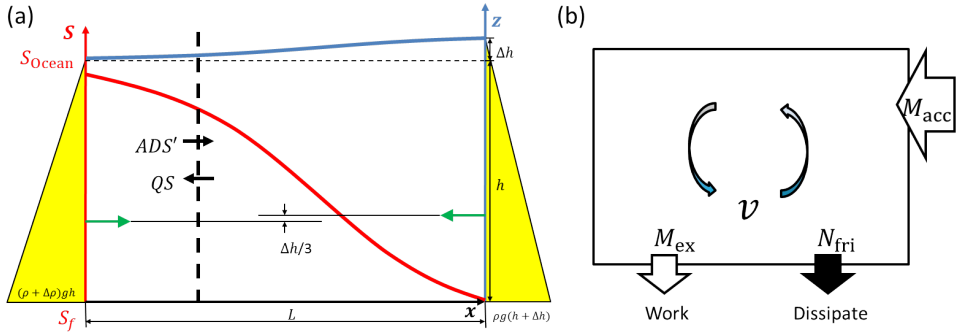

Figure 5.1: (a) Systematic salt transport in estuaries, with the seaside on the left and the riverside on the right. The water level (in blue) has a slope as a result of the salinity distributions (in red). The hydrostatic forces on both sides have different working lines, which triggers the gravitational circulation, providing an accelerating moment M_{acc} to the system. (b) A box-model displaying the moment balance in an open estuarine system.

(vertical salinity gradient essentially enhances gravitational circulation), the contact area may be dominated by the depth. Following that reasoning, O is assumed equal to $2Bh$, one Bh for the upward lift of saline water and one Bh for the downward push of relatively fresh water. The dispersive distance then equals the depth ($l_m = h$).

Because the velocity of the dispersive gravitational circulation is small, the mixing flow is assumed to be laminar. The shear stress is typically considered as a function of flow velocity (v): $\tau = \rho q v$, with q [LT^{-1}] being a laminar resistance, assumed to be proportional to the tidal velocity amplitude. The flow velocity represents the residual flow performing saline and fresh water exchange. Then, the expression for the velocity results in

$$v = \frac{M_{\text{acc}} - M_{\text{ex}}}{2\rho q B h^2} \ . \tag{5.4}$$

Figure 5.2 illustrates how the mixing moment (energy) and residual flow velocity vary. If the working moment is too large and causes fast mixing flow, the energy dissipation would increase and diminish the flow velocity. If it is too small, the mixing would also be sub-optional. In analogy with Kleidon [2016], the product of the working moment and velocity has a well-defined maximum.

Power is defined by the product of a force and its velocity. The power of torque (angular moment) is defined as the product of the moment and its angular velocity. Hence, the power is defined as

$$P = M_{\text{ex}}\omega = M_{\text{ex}}\frac{v}{h/2}2\pi = \frac{2\pi}{\rho q B h^3}\left(M_{\text{acc}} - M_{\text{ex}}\right)M_{\text{ex}} \ , \tag{5.5}$$

where ω [T^{-1}] is the angular velocity, or the rotational speed. The maximum power is obtained by: $\partial P/\partial M_{ex} = 0$, hence, the optimum values of the execution moment $M_{ex,opt}$ and the velocity v_{opt} are

$$M_{ex,opt} = \frac{1}{2} M_{acc} \tag{5.6}$$

and

$$v_{opt} = \frac{M_{acc}}{4\rho q B h^2} \ . \tag{5.7}$$

Here, the accelerating force that produces the moment is the hydrostatic force obtained by integrating the hydraulic pressure over the depth:

$$F_{acc} = \frac{1}{2}\rho_0 g h^2 B \ . \tag{5.8}$$

The accelerating moment has an arm $\Delta h/3$ [Savenije, 2005], subsequently the accelerating moment can be described as

$$M_{acc} = F_{acc}\frac{1}{3}\frac{\mathrm{d}h}{\mathrm{d}x}E = -\frac{1}{2}\rho_0 g h^2 B \frac{1}{3}\frac{h}{2}c_S S' = -\frac{1}{12}\rho_0 g h^3 B c_S S' E \ . \tag{5.9}$$

Accordingly, in steady state ($|Q|S + ADS' = 0$), the optimum velocity is

$$v_{opt} \propto \frac{c_S g h T}{48}\frac{|Q|S}{AD} \ . \tag{5.10}$$

Assuming that the steady state over a tidal cycle is driven mainly by the accelerating moment especially in the upstream part where tidal effects are small ($D \approx D_g$) and this gravitational circulation is proportional to the dispersive residual velocity ($D_g \propto vE$),

$$D_g \propto \left(\frac{c_S g}{48}\frac{S|Q|ET}{B}\right)^{1/2} \ . \tag{5.11}$$

5.3. Analytical solution for the dispersion equation

Equations derived from the maximum power concept are obtained along the estuary axis, hence they can be used at any point along the estuary. Then, equation (5.11) becomes

$$D_g(x) = C_3\left(\frac{S|Q|ET}{B}\right)^{1/2} \ , \tag{5.12}$$

where C_3 [$psu^{-1}LT^{-2}$] is a factor and all local variables are a function of x.

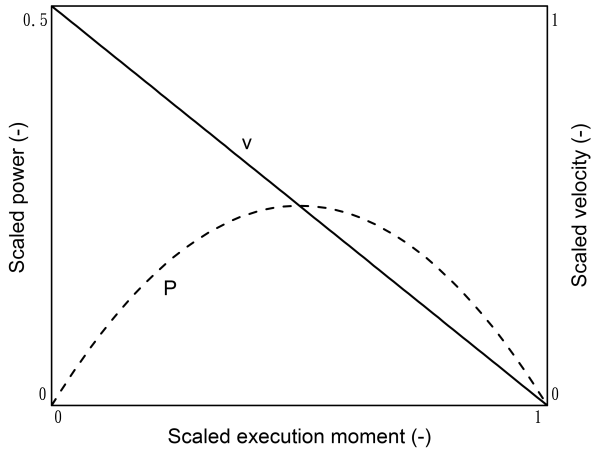

Figure 5.2: Sketch of the sensitivity of the exchange flow velocity v to the working moment M_{ex}.

In analogy with the solution in Section 3.3, this gives

$$D_g(x) = D_{g0}\left(\frac{S}{S_0}\right)^{1/2} e^{\Omega_2(x-x_1)} \tag{5.13}$$

with

$$\Omega_2 = \frac{\delta_H}{2} + \frac{1}{2b} \,. \tag{5.14}$$

Differentiating D_g with respect to x and using the steady state equation results in

$$D_g'(x) = \frac{D_g}{2S}\frac{\mathrm{d}S}{\mathrm{d}x} + \Omega_2 D_g = \Omega_2 D_g - \frac{1}{2}\frac{|Q|}{A} \,. \tag{5.15}$$

This is comparable to Van der Burgh's equation using dispersion due to gravitational circulation ($D_g' = -K|Q|/A$). In alluvial estuaries, $1/b$ is relatively large and Ω_2 is larger than zero. In this case, K is smaller than half. The stronger the convergence, the smaller the coefficient K. If tide damps heavily in a prismatic estuary (with large b value), Ω_2 becomes negative and K can be larger than half. Overall, the coefficient K is linked to the balance between the convergence of the geometry and tidal damping. If Ω_2 happens to equal zero, K equals half. The Van der Burgh coefficient which considers density-driven as well as tide-driven mixing proceses should be slightly smaller than the K discussed here.

Accordingly, the solution of the linear differential equation (5.15) is

$$\frac{D_g}{D_{g0}} = e^{\Omega_2(x-x_1)} - \frac{|Q|\zeta_2}{2A_0 D_{g0}}\left[e^{(x-x_1)/a} - e^{\Omega_2(x-x_1)}\right] \,, \tag{5.16}$$

with $\zeta_2 = a/(1-\Omega_2 a)$.

At the salinity intrusion limit ($x = L$), $D_g = 0$, resulting in

$$L = \zeta_2 \ln\left(1 + \frac{2A_0 D_{g0}}{|Q|\zeta_2}\right) + x_1 \ . \tag{5.17}$$

The solution for longitudinal salinity distribution yields

$$\frac{S}{S_0} = \left\{1 - \frac{|Q|\zeta_2}{2A_0 D_{g0}}\left[e^{(x-x_1)/\zeta_2} - 1\right]\right\}^2 \ . \tag{5.18}$$

These results are similar to the solutions in Section 3.3. Furthermore, the solution is the same as Kuijper and Van Rijn [2011] if a equals b in their cases. With these analytical equations, the dispersion and salinity can be obtained, using calibrated boundary conditions (D_0 and S_0).

5

5.4. Empirical validation and discussion

Appendix A.12 demonstrates how the new equation (5.12) based on the maximum power concept works in twenty-three estuaries including the less reliable database (in Appendix A.8 and A.11). The Van der Burgh (VDB) method (equations (2.14)–(2.16)) and curve fitting based on the observations are used for comparison. Density-driven gravitational circulation is one part of the dispersive actions in estuaries. Hence the total dispersive process (D_{VDB}) must be larger than the dispersion from the maximum power method (D_{MP}) (Appendix A.12). By fitting the real observations, total tidal average dispersion (D_{FT}) is calculated based on the steady state equation (2.7), and dispersion by gravitational circulation (D_{FG}) is evaluated by the new model (equation (5.12) using tailor-made C_3). Information is summarized in Appendix A.13.

It shows that the simulation curves by the new MP method are in recession shape, increasing seaward from the inflection point owing to the widening. The salinity observations can be simulated well landward from the inflection point in most estuaries. In the Bernam, the Pangani, the Rembau Linggi, and the Incomati estuaries, the part in the center, where D_{MP} closely approach D_{VDB}, fits well. In these estuaries, the calibration is slightly lower than the measurement near the intrusion limit. In general, the dispersion from the maximum power method declines upstream the inflection point approximately with the total dispersion from the empirical Van der Burgh method, which means that the gravitational circulation is the predominant mixing mechanism in the landward part of these estuaries.

However, in the Thames (#8), the Delaware (#20), the Scheldt (#21), and the Pungwe (#22), the new approach seems not to work, both from the salinity and dispersion profiles. Figure 5.3 shows the relation between the geometry and the

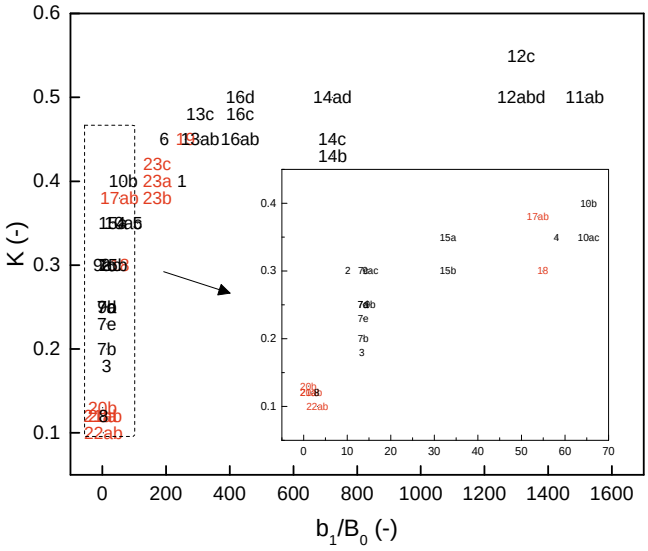

Figure 5.3: Comparison of the geometry to the Van der Burgh coefficient. The red color represents estuaries from a less reliable dataset.

K values. It can be seen that estuaries with poor performances by MP approach have lower b_1/B_0 and K values. However, not all estuaries with strong convergent geometry perform poor, revealing that the geometry is not the only effect. According to the expression of Ω_2, tidal damping can play a role. In wide estuaries with strong convergence, the role of gravitational circulation is insufficient to describe the mixing. Tidal mixing processes such as lateral circulation, tidal pumping, and tidal shear are dominant. The Scheldt with preferential ebb and flood channels is a case in point. Besides, the Corantijn (#9) is considered uncertain because it has a low b_1/B_0 value but contains few observations.

Appendix A.13 also shows that simulated salinity and dispersion by curve fitting (which follows the "truth") and the Van der Burgh method are basically similar except the near mouth part which is due to few salinity observtions. It supports that the Van der Burgh model is a useful tool to study the salinity intrusion in estuaries. Besides, reasons for outliers can be referred to the discussion in Chapter 3.

Overall, the maximum power approach in open systems is a useful tool to understand the mixing processes in most estuaries. In the upstream part where the effect of tide is small, gravitational circulation plays the main role. Meanwhile, observations upstream are more important for salinity intrusion research and more

relevant for water users. Where the salinity is high, it is less relevant since the water is already too saline to use.

This chapter provides an approach to define the dispersion coefficient which is proportional to the product of the velocity of the gravitational circulation and tidal excursion length. The latter parameter comes from the fact that water particles travel within this distance over a tidal cycle. The dispersive velocity actually represents the ability of dispersion due to gravitational circulation. Based on the maximum power method (equation (5.12)), the velocity can be described as

$$v \propto \left(\frac{c_S S g h}{48} \frac{|Q|T}{AE} \right)^{1/2} . \tag{5.19}$$

Here, the dispersive flow due to gravitational circulation strengthens with larger freshwater discharge and weakens with stronger tide.

Using the calibrated dispersion coefficient at the boundary, C_3 can be calculated. Except in estuaries with poor performance, C_3 values range from 3.47×10^{-3} to 9.95×10^{-3} with an average 6.76×10^{-3} (the relative standard derivation equals 0.2634). Finally, the R^2 of the regression between the predicted and calibrated values of the dispersion at the boundary equals 0.86. Considering all the uncertainties in the measurement, 6.76×10^{-3} is a promising approximation to predict D_{g0}.

5.5. Concluding remarks

An estuary is an open system which has a maximum power limit when the accelerating source is stable. This chapter has described a moment balance approach to non-thermal open systems, yielding a new equation (5.12) for the dispersion coefficient due to the density-driven gravitational circulation. It shows that the dispersive action is closely related to the salinity, the freshwater discharge, the tide, and the estuarine width. This equation has been used to solve the tidal average salinity and dispersion distributions together with the steady-state equation. The maximum power model has then been validated with fifty salinity observations in twenty-three estuaries worldwide and compared with the traditional Van der Burgh method. Generally, the new equation is a helpful tool to analyse the estuaries providing an alternative solution for the empirical Van der Burgh method where gravitational circulation is the main mixing mechanism. A predictive equation for dispersion at the boundary has been provided. More reliable observations in other estuaries are suggested to validate this maximum power method.

The maximum power method offers a connection between Van der Burgh's coefficient and the geometry, providing a physical basis for this empirical coefficient.

The fact that the relationship derived from the maximization works well in a wide range of estuaries is an indication that natural systems evolve towards max-

imum power, much like a machine that approaches the Carnot limit, which is the maximum efficiency that any machine can achieve that transforms free energy into work (whether it transforms potential energy from water into hydropower or chemical energy from fuel into motion by a combustion engine).

6

The influence of tidal strength on salinity intrusion

Stay hungry, stay foolish.

Stewart Brand

6.1. Background

Vertical stratification enhances gravitational circulation. Hence in slightly stratified estuaries tide decreases dispersion dominated by the gravitational circulation. On the other hand, tide triggers the tide-driven mixing mechanism. In natural estuaries, different mixing mechanisms occur together. The question then is: does tidal strength increase or decrease salt intrusion? This makes the influence of tidal strength on salinity distribution an interesting topic for study.

The salinity range between high water slack and low water slack is directly connected to the tidal excursion length hence the tidal strength. In this chapter, salinity observations in two different estuaries, the Scheldt estuary and the Rotterdam Waterway, are used to study the relation between the tide (represented by salinity range) and average salinity, under simple one-dimension consideration and over a tidal cycle, to see the effect of the tidal strength on salinity intrusion in estuaries.

6.2. Case study

6.2.1. Case description

Two different estuaries have been researched. The Scheldt estuary is a significant shipping route to the Port of Antwerp and has a great ecological value. It exhibits a well-developed funnel-shaped geometry, with exponentially decreasing cross-sectional area from the estuary mouth at Vlissingen to the head near Gent, while the width-averaged depth is almost constant up to Antwerp. The estuary is tide-dominated and the yearly-averaged discharge is about 120 m^3/s [Winterwerp et al., 2013].

The New Waterway is a man-made channel constructed to give the harbors in Rotterdam a better connection to the North Sea. Since there are no tidal flats between the New Waterway and the New Maas, they can be considered as the Rotterdam Waterway with almost rectangular cross section. Sea water enters the Rhine-Meuse estuary via the waterway, meanwhile, by operating the Haringvliet sluice gates, the waterway can discharge a rather constant value of about 1500 m^3/s for as long as possible [Rijkswaterstaat, 2011; Verlaan and Spanhoff, 2000].

6.2.2. Field study

The field measurements in the Scheldt estuary were made by Rijkswaterstaat of the Netherlands (NL) and Hydraulic Information Centre of Belgium (BE). Salinity and water level observations were carried out every 10 min at different locations along the estuary. The measurements in the Rotterdam Waterway were taken by Rijkswaterstaat, every hour for salinity and every 10 min for water level. Figure 6.1 gives the locations of the measuring sites. Salinity was measured at different depths, and detailed information is shown in Table 6.1. Fixed sensors are located

Table 6.1: Information about the salinity observation sites. The first five sites belong to the Scheldt estuary and the last three belong to the Rotterdam Waterway. Depth shows the vertical location of the sensors.

Site	Abbreviation	Depth (cm)	Description	Country
(1) Overloop van Hansweert	OVE	Top: -75	Floating	NL
		Bottom: -800	Fixed	
(2) Baalhoek	BAA	Top: -75	Floating	NL
		Bottom: -550	Fixed	
(3) Boei-84	B84	Top: 350	About the riverbed	BE
		Bottom: 100		
(4) Oosterweel	OOS	Top: 400		BE
		Bottom: 50		
(5) Driegoten	DRI	-300	Floating	BE
(6) Hoek van Holland	HOE	Top: -250	Fixed	NL
		Middle: -450		
		Bottom: -900		
(7) Lekhaven	LEK	Top: -250		NL
		Middle: -500		
		Bottom: -700		
(8) Brienenoordbrug	BRI	Top: -250		NL
		Bottom: -650		

below the water depth at mean sea level; floating sensors are settled below water level; and some sensors used in Belgium are fixed at a certain depth above the riverbed. There is only one sensor at site (5), and other sites without available data were not considered.

The freshwater discharge in the Scheldt estuary is taken as a combination of seven drain points (Eppegem, Aarshot, Hulshout, Grobbendonk, Melle, Dendermonde, and Bath) from different branches. The discharge in the Rotterdam Waterway is measured as the Rhine run-off, at Lobith near the Dutch-German border. During the dry seasons, most of the Rhine water flows through the waterway [Verlaan and Spanhoff, 2000; Stigter and Siemons, 1967].

Two study periods were chosen: 27-10-2011 to 26-11-2011 (begins with the 1st day of a lunar month) for the Scheldt estuary and 13-07-2003 to 23-08-2003 (begins with the 14th day of a lunar month) for the Rotterdam Waterway, due to the relatively constant freshwater discharge during these periods. Both the Scheldt estuary and the Rotterdam Waterway have semi-diurnal tide, hence, for simpler analysis, daily average values are used instead of tidal average.

Figure 6.1: Locations of measuring sites in (a) the Scheldt estuary and (b) the Rotterdam Waterway. Yellow labels with number refer to salinity (chloride) (and maybe also water level) observation sites; white labels refer to sites with only water level observations. The water level observation sites are the same as salinity observation sites or the nearest site downstream.

6.3. Results and discussion

6.3.1. The Scheldt estuary

The freshwater discharge in the Scheldt estuary is shown in Figure 6.2. The values were relatively stable from one month before (dot line), diminishing the effect of discharge on salinity intrusion in the estuary. It is during the dry season and the discharge varies between $5–55$ m^3/s.

Figure 6.3 shows statistics at five sites, containing several parts: (a) water level, (b) salinity and salinity range, (c/e) the relation between salinity and water level, and (d/f) the relation between salinity and salinity range. The first part shows the rise and fall of water level temporally, and the strength of the tide (spring or neap tide) is quite clear. Daily average water level was also shown, keeping relatively stable during the study period. In addition, the water level increases slightly upstream, showing the amplification of the Scheldt estuary (till Driegoten). From the (b) part, daily average salinity rises with time to some extent at all sites, which may be caused by low freshwater discharge for a long time and continuous sea water intrusion. The variation of salinity range basically fluctuates with the lunar cycle. Also, salinity ranges increase landward. Comparing the relations between data on top (c and d parts) and at bottom (e and f parts), the patterns are almost the same along the estuary.

The spring and neap tides are separated according to the lunar calendar. It is shown that the average water level is similar during spring and neap tides, only the former type causes a larger range. The average water level is slightly related to the salinity at all sites (c and e parts), which is because of a weak advection

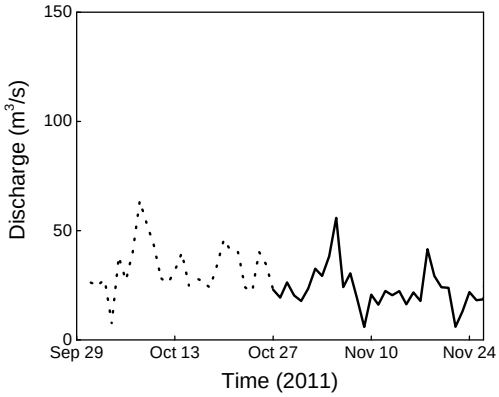

Figure 6.2: Freshwater discharge in the Scheldt estuary.

effect: more sea water entering the estuary leads to larger salinity concentration. For ideal waves, the average water level tends to be constant within a lunar cycle, and the variations here are due to outside influences. The wind set-up, for instance, displays sudden increase of water level on Nov 5, 2011 (Figure 4.3.1a). From (d) and (f) parts, there are slight positive relations between salinity range and average salinity, and the slopes are almost stationary at the first four sites. The relation at site (5) is because of the tail effect. The salinity range between LWS and HWS is reduced near the intrusion limit where the salinity values are low.

The vertical salinity gradient shows how well the saline and fresh water mix in estuaries. Figure 6.4 displays that the salinity gradients are small (less than 0.1 psu/m) except at site (3) which may be due to the fact that it is connected to a buoy, showing that the Scheldt estuary is well-mixed.

The Scheldt estuary is well-mixed and the stratification number is minor (N_R in the order 0.001 near the mouth). Gravitational circulation mechanism is much smaller than the tide-driven mechanism. The effect of tidal strength performs in different ways along the estuary which leads to a slightly positive relation between the salinity range and average salinity. Near the wide mouth, at the first two sites, the tide plays a role in the residual circulation in preferential ebb and flood channels, which increases the dispersive action. In the upstream, at sites (3) and (4), the residual circulation no longer exists. The effect of tide on other tide-driven mechanisms, such as tidal trapping and hydraulic shear stress, which are normally considered ignorable when they are not the dominant mechanism for dispersion, increses due to the tidal amplification.

6.3.2. The Rotterdam Waterway

The same analysis was done in the Rotterdam Waterway. According to Figure 6.5, the Rhine run-off at Lobith is relatively stable in July and August, 2003. The simulated discharge at Maassluis is presented for reference.

Figure 6.6 demonstrates similar results as in Figure 6.3, with three observation depths at two sites. The results are very similar to the Scheldt estuary, except the following three aspects. Firstly, the difference between the spring and neap tides are small during the study period. Besides, the relation between the average water level and salinity is stronger than the Scheldt estuary, which leads to a larger range of daily average salinity by the advection process. Last but not least, the trends between the salinity range and average salinity show negative relation at site (6).

From Figure 6.7, the vertical salinity gradient is relatively large at site (6). The black line, varying synchronized with the lunar cycle, demonstrates that the Rotterdam Waterway is strongly stratified and the stratification depends on the tidal strength: the statification is weaker during spring tide and stronger during neap tide. The line at site (7), however, shows different variation.

Near the mouth at site (6), the Rotterdam Waterway is stratified with N_R in the order 0.95. Gravitational circulation is strongly enhanced and is the predominant mixing mechanism. Tide-driven mixing mechanisms are not notable in the prismatic estuary. The tide decreases the degree of stratification hence declines the dispersive action. Pu et al. [2015] also reported that gravitational circulation is weaker during spring tide in the Yangtze River during wet and dry seasons. On the other hand, the effect of freshwater discharge seems more essential at site (7) where it is less stratified. The vertical salinity gradient varies to some extent following the discharge, which also explains why the salinity varies largely with small tidal variation there.

The negative relation at site (6) provides a view towards the Van der Burgh coefficient. According to equation (3.21), the effect of tidal strength on the dispersion coefficient is: $D \propto v^{2-3K}$. Previous research showed that the dispersion is proportional to salinity to the power K (equation (2.13)). Hence, the effect of tide is linked directly to the salinity distribution—eliminating the dispersion coefficient—$S \propto v^{(2-3K)/K}$. Only when K is larger than $2/3$, the stronger the tide, the smaller the salinity. The K discribing the density-driven mechanism is bound to Van der Burgh's coefficient. It suggests that the coefficient is large when the estuary is partially mixed where gravitational circulation is enhanced. Unfortunately, it is not easy to conclude whether K is constant or not along the estuary since the stratification and the mixing mechanisms vary.

6.3.3. Delft3D data of the Scheldt estuary

Delft3D simulation of the Scheldt estuary is studied as another approach to study the tidal effect. Two periods were chosen to show the cross-sectional average salinity: 14-01-2013 (spring tide) to 21-01-2013 (neap tide) and 16-06-2013 (neap tide) to 26-06-2013 (spring tide). Simulated freshwater discharges are 183, 144, 106, and 183 psu/m, and the tide excursion lengths are 13000, 7500, 8500, and 13000 m on the four days, respectively.

Salinities at high water slack, low water slack, and their average on spring and neap tides are shown in Figure 6.8. It can be seen that the saltwater intrudes further at HWS and shorter at LWS on spring tide than neap tide. For the average (in green), the salinity is slightly larger locally on spring tide than neap tide in January, 2013. In June, the difference between these two average values does almost not exist. This may be caused by an increase in the tidal strength and a decline in the freshwater discharge compared to that in January. It reveals that the saline and fresh water mixing in estuaries is complex under the interaction of different effects from downstream and upstream.

6.4. Concluding marks

In this Chapter we use actual observations and the Delft3D model, as a virtual laboratory, to study which velocity and length scale should be used in the empirical analysis to derive predictive equations. The intention was to test whether salt intrusion is positively or negatively correlated with tidal strength and under which conditions. This chapter is driven by data, using two different estuaries: the convergent Scheldt estuary and the prismatic Rotterdam Waterway. The influence of tidal strength on salinity intrusion depends on the mixing mechanisms in estuaries. When the estuary is partially mixed and the density-driven mixing mechanism is dominant, the stronger spring tide declines the gravitational circulation and the salinity intrudes less (for instance, at the mouth of the prismatic Rotterdam Waterway). When the estuary is well-mixed, the tidal strength is positively related to the dispersive actions if the tide-driven mechanisms play an important role (for instance, in the strongly convergent Scheldt estuary. Both the observation analysis and the numerical model reveal that the salt water intrudes slightly further in the well-mixed Scheldt estuary with stronger tide.

The negative relation between the tide and salinity supports that the Van der Burgh coefficient has a large value when the estuary is more stratified.

Comparing the simulation in Figure 6.8 with field observations in Appendix A.9, it seems that Delft3D can not represent salinity well in the Scheldt estuary. The salinity observation displays a dome shape in the estuary while in the model the curve is of the recession type. This may be an artefact of the schematization in Delft3D. Maybe the large-scale residual circulation is not well included in Delft3D.

However, the saline and fresh water mixing is a complex interaction between the sea and river, and the effect of freshwater discharge is also significant. More observations are always encouraged.

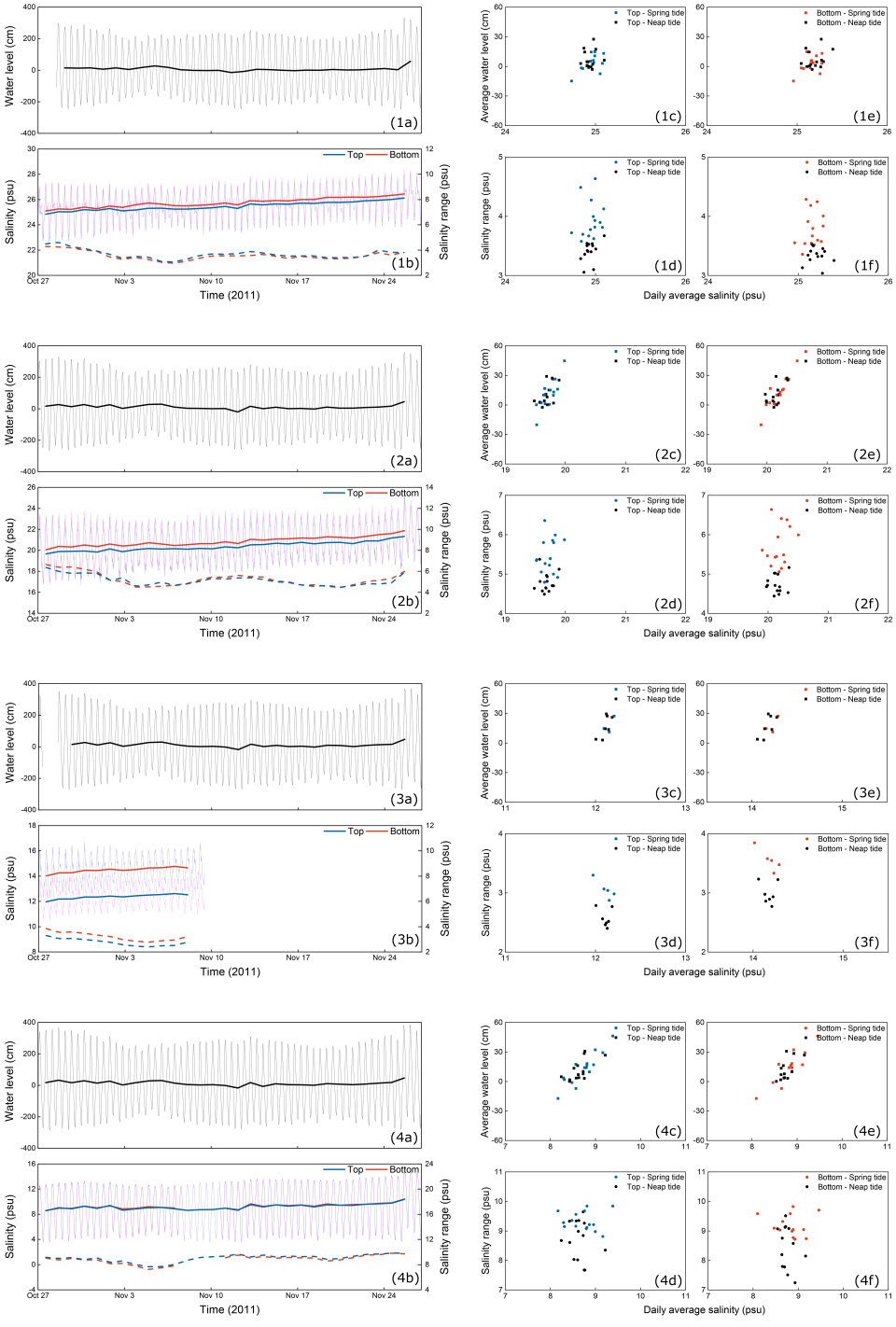
Water level (cm)
(1a)
Top
Bottom
Salinity (psu)
Salinity range (psu)
(1b)
Oct 27
Nov 3
Nov 10
Nov 17
Nov 24
Time (2011)
Top - Spring tide
Top - Neap tide
Average water level (cm)
(1c)
Bottom - Spring tide
Bottom - Neap tide
(1e)
Salinity range (psu)
(1d)
(1f)
Daily average salinity (psu)
(2a)
(2b)
(2c)
(2e)
(2d)
(2f)
(3a)
(3b)
(3c)
(3e)
(3d)
(3f)
(4a)
(4b)
(4c)
(4e)
(4d)
(4f)

6

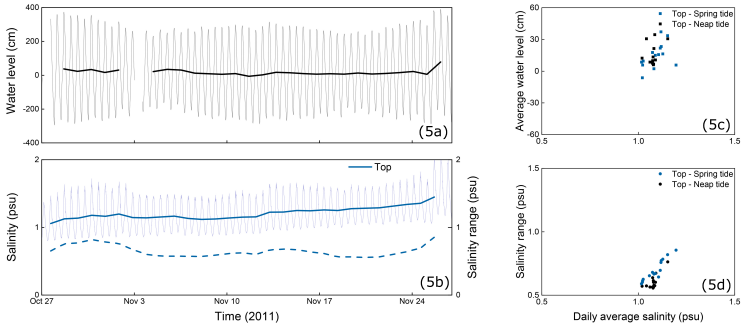

Figure 6.3: The statistics about the water level, salinity, and salinity range in the Scheldt estuary at sites: (1) OVE, (2) BAA, (3) B84, (4) OOS, and (5) DRI. Thin lines display the observations; thick lines show the daily average values; dash lines show the salinity range (right-Y); squares show the relation between the daily average salinity and water level (c and e parts); rounds show the relation between the average salinity and salinity range (d and f parts); colors follow the legends at different measurement depths and tides.

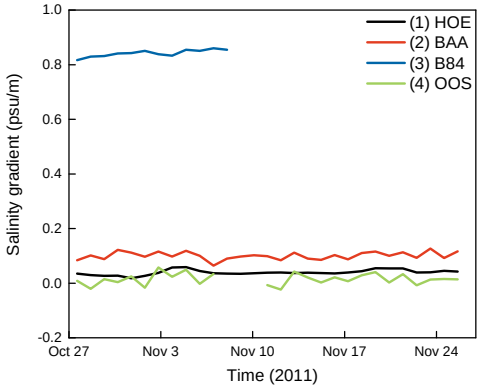

Figure 6.4: Vertical salinity gradient at different sites in the Scheldt estuary.

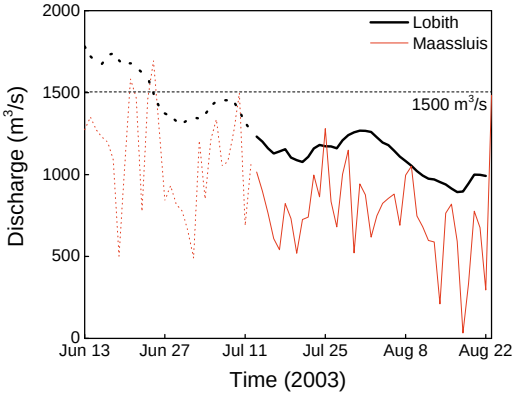

Figure 6.5: Freshwater discharge in the Rotterdam Waterway.

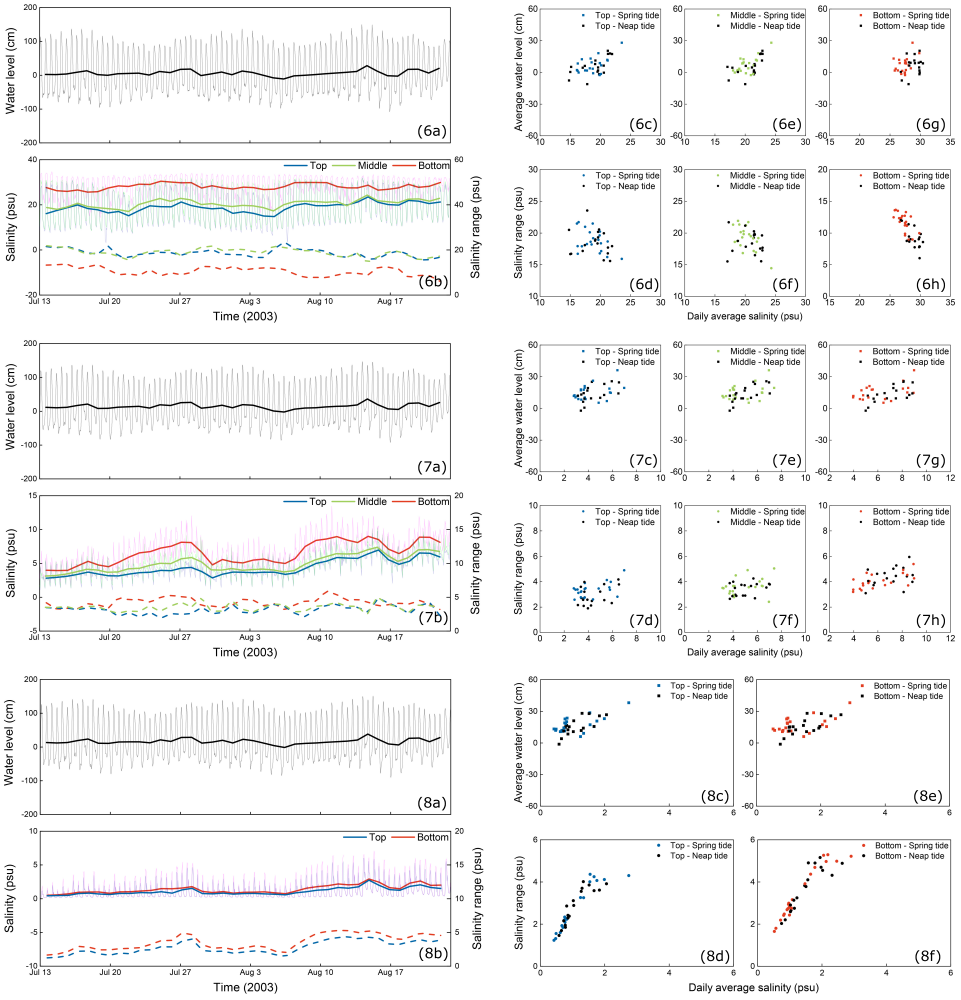

Figure 6.6: The same as Figure 6.3, except for in the Rotterdam Waterway at sites: (6) HOE, (7) LEK, and (8) BRI.

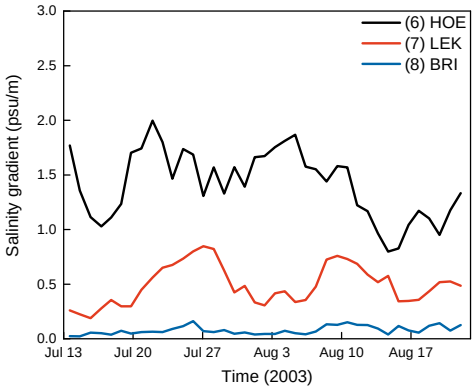

Figure 6.7: Vertical salinity gradient at different sites in the Rotterdam Waterway.

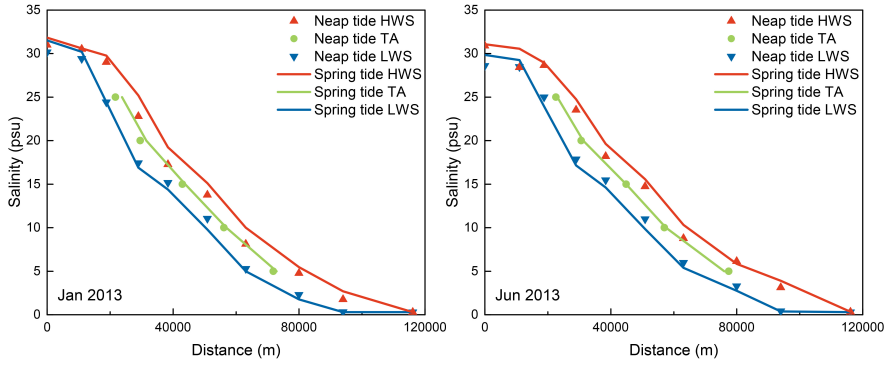

Figure 6.8: Simulated salinity in the Scheldt estuary by Delft3D in two study periods: (1) Jan 2013 and (2) Jun 2013. Symbols show values in neap tide while lines show values in spring tide at LWS (in blue), HWS (in red), and TA (in green).

7

Discussion and conclusions

I now see how owning our story
and loving ourselves
through that process is the bravest thing
that we will ever do.

Brené Brown

7.1. Predictive equations with a solid physical basis

7.1.1. The empirical Van der Burgh coefficient

In Chapter 3, the good performance of the predictive equation (3.12) suggests that the Van der Burgh coefficient decreases when the tide strengthens. In addition, the analytical solutions for dispersion due to gravitaional circulation in Chapters 3 and 5 demonstrate that Van der Burgh's coefficient is related to tidal damping and geometric convergence. Discussion in Chapter 6 also reveals that K can have a large value in the more stratified Rotterdam Waterway. Furthermore, the calibration of the Van der Burgh method based on the maximum power method reveals that Van der Burgh's coefficient is remarkably related to the geometry (Figure 5.3). Based on the discussion above, K is closely connected to the geometry and the competition between tide and freshwater discharge. The simple Canter-Cremers estuary number is a promising parameter to show the ratio between the amount of fresh and saline water entering the estuary during a tidal period [Savenije, 2005]. The combination of width and its convergence length is used to present the geometry. Hence, the Solver results in the following predictive equation:

$$K_{\text{predicted}} = 0.20\left(\frac{b_1}{B_0}\right)^{0.15}\left(\frac{|Q|T}{A_0E_0}\right)^{0.023} \quad ; K \in (0,\ 1)\ . \tag{7.1}$$

The correlation between the predictive value by equation (7.1) and calibrated value is shown in Figure 7.1, with $R^2 = 0.86$. The predictive equation works well in most estuaries. Outliers in the lower left corner (wide and convergent estuaries) imply that the value is overestimated when tide-driven dispersion plays a significant role. Considering all the uncertainties in the data, the physics-based equation (7.1) is a capable predictor for the empirical Van der Burgh coefficient.

When the freshwater discharge is not well-measured, the K value can be estimated based on the geometry only. Regression of the values in Figure 5.3 yields

$$K_{\text{predicted}} = 0.18\left(\frac{b_1}{B_0}\right)^{0.15} \quad ; K \in (0,\ 1)\ , \tag{7.2}$$

with $R^2 = 0.85$. It reveals that even though the K may be time-dependent according to the stratification condition, the effect of the geometry is predominant. Appendix A.13 shows that the K values vary in a small range in a certain estuary.

The average value of both calibrated and predicted K is 0.38. This can be a first estimation of the Van der Burgh coefficient.

It is notable that the empirical coefficient K is a result of complex interaction between the freshwater discharge, the tide, and the geometry. This kind of predictive equation helps in the practical application of the one-dimensional salt intrusion

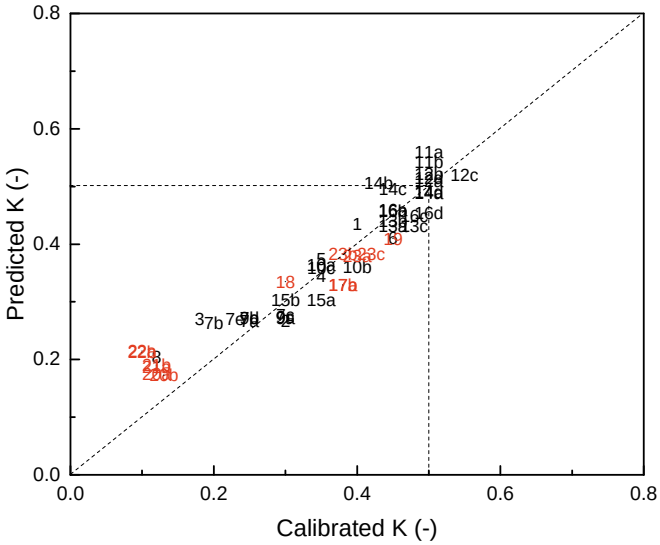

Figure 7.1: Comparison of calibrated and predicted K values. The red color represents estuaries from a less reliable dataset which have been used for validation.

model based on the Van der Burgh method.

7.1.2. The dispersion coefficient at the boundary

To make the Van der Burgh method fully predictive, an equation for the dispersion coefficient at the boundary is required. According to the nice performance by the maximum power concept, gravitational circulation is significant in most estuaries. Hence, the estuarine Richardson number describing the stratification which determines the strength of gravitational circulation is a significant parameter for dispersion. Regression for D_0 values by the pure Van der Burgh method gives:

$$D_{\text{predicted}} = 0.093 {N_R}^{0.50} v_0 E_0 \ , \tag{7.3}$$

with $R^2 = 0.75$. The result is comparable to previous predictive equations (2.18), (2.21), and (2.22), but with a lower value for the power of the estuarine Richardson number.

The relation between the predicted and calibrated values is shown in Figure 7.2. The outliers, which are all wide, reveal that the stratification number is not enough for describing the dispersion coefficient. Subsequently, the geometry is included to

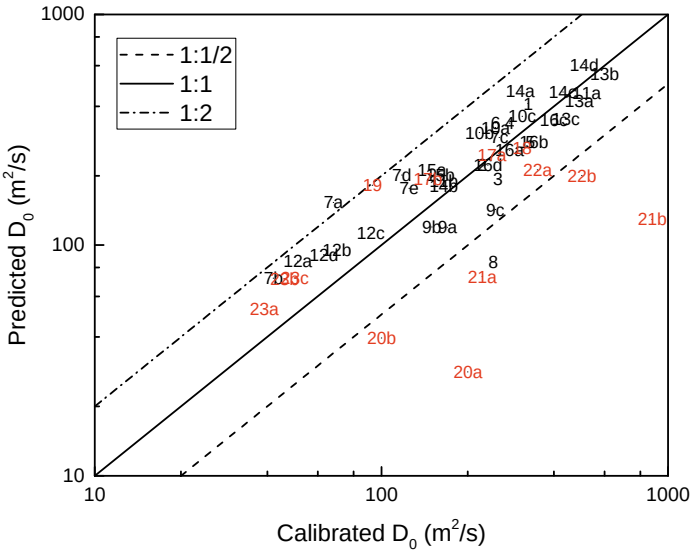

Figure 7.2: Comparison of calibrated and predicted D_0 values by equation (7.3).

represent the effect of tide. According to Section 2.6, the dispersion results in:

$$\frac{D_{\text{predicted}}}{\upsilon_0 E_0} = 0.095 {N_R}^{0.52} + 0.16 \left(\frac{B_0}{b_1} \right)^{2.25} , \tag{7.4}$$

with $R^2 = 0.79$. Figure 7.3 presenting how the predictive equation performs shows that almost all the data falls within a factor of 2, but equation (7.4) is obviously not suitable for the Delaware and the Scheldt estuaries, which have very large B_0/b_1 values (0.90 and 0.58, respectively). More precise equations could be developed, but for estuaries without extremely convergent geometry, the predictive equation is promising. The power of N_R increased after adding the tide term, supporting that K is overestimated if we consider only the density-driven mechanism. Consequently, the pure Van der Burgh method is predictable with a solid theoretical basis.

7.2. Conclusions

The tidal average salinity profile in an estuary follows the mass balance equation. Assuming that the estuary achieves the steady state over a tidal period, there are two unknown parameters ($S(x)$ and $D(x)$) in one equation, if the geometry, fresh-

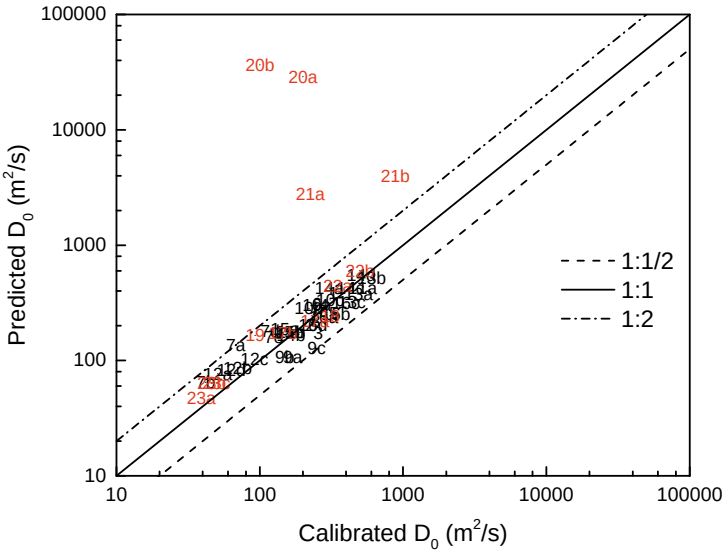

Figure 7.3: Comparison of calibrated and predicted D_0 values by equation (7.4).

water discharge, and tide condition are provided. Hence, an addition relation should be found to solve the salinity distribution along the estuary, which is the main core of saltwater intrusion research.

Van der Burgh [1972] found an expression for the dispersion coefficient (equation (1.1)). This purely empirical method was developed by Savenije [1986, 1989, 1993a] and Gisen [2015]. This method combines all mixing mechanisms into one empirical coefficient—the Van der Burgh coefficient K, which can be obtained by calibration on salinity observations. Chapter 5 has validated this Van der Burgh method based on the fact that the total dispersion is larger than the dispersion only due to gravitational circulation (D_g). The physical background of the empirical coeffient has then been developed based on the comparison with other theoretical methods. Finally, the Van der Burgh method becomes more powerful with predictive equations for the empirical coefficient (7.1) and the dispersion coefficient at the boundary (7.4).

A box-model has been built considering large-scale residual circulation in developed preferential ebb and flood channels, which resulted in a new equation (3.20). Combining it with the steady state equation, $S(x)$ and $D(x)$ have been solved. This model considers density- and tide-driven mixing mechanisms in seperate parts. Applying $C_1 = 0.10$, $C_2 = 10$, and predictive equation (3.13) helps the box-model to

perform well in most of the estuaries, making it an alternative solution. Besides, a physical basis for Van der Burgh's coefficient has been provided by linking a reductionist method with strong theoretical background.

From a system perspective, another method applying the maximum power concept in saline and fresh water mixing in estuaries has been derived. First, an unsatisfactory solution was derived because of the assumption that the system is isolated. This is impossible due to the continuous freshwater discharge. As a result, by including the accelerating moment provided by the freshwater discharge, the maximum power condition for an open estuary system has been solved. A new equation (5.12) describing the spread of salinity due to gravitational circulation has been found and the relevant salinity distribution model works well in estuaries with a large b_1/B_0 value. These estuaries also have larger K values in the pure Van der Burgh method. A predictive value for the dispersion coefficient at the boundary has also been provided, making this method a practical alternative for application in partially- to well-mixied estuaries.

In conclusion, the empircal Van der Burgh method which is accounts for all mixing mechanism is now predictive, based on the results from the new box-model and maximum power method. For an estuary with less available data, 0.38 can be a useful first estimate for the empirical Van der Burgh coefficient. This value appears to be a good estimate in estuaries with a large width convergence length. If, however, the proper geometric data and hydraulic characteristics are available, equations (7.1) and (7.2) are more powerful (and have a more solid physical basis) for predicting the Van der Burgh coefficient. However, these equations appear to be less accurate in wide estuaries with strong convergence.

7.3. Limitations and recommendations

7.3.1. Limitations

Limitations of this study mainly come from two aspects: the assumptions made and the uncertainties in the observations.

There are several assumptions used in this study. The geometry and the tide propagations are simplified. In addition, the large-scale lateral salinity exchange is assumed proportional to the longitudinal exchange and the proportionality is considered the same in different estuaries. This is how the two-dimensional box-model results in a one-dimensional equation and the two main mixing mechanisms are combined into one expression. Moreover, the maximum power condition is an assumption. Natural estuaries may not be in a steady state over a tidal cycle. Furthermore, other tide-driven mechanisms besides horizontal circulation have been ignored. Assumptions are also made in the analytical solutions dealing with the non-linear equations in Chapters 3.

Measurement uncertainties are unavoidable. Take the freshwater discharge as

an example, which is probably the most significant parameter in saline and fresh water mixing. It is not easy to measure the freshwater discharge in estuaries, and it may not be constant over a tidal cycle. Cross-sectional average salinity is also not easy to observe due to lateral variability, the complex topography, and the time required for detailed observations.

Due to the three-dimenssional charecter of wide estuaries, the capacity to describe the effect of tide in wide estuaries generally is also a limitation.

7.3.2. Recommendations

Here are some recommendations based on this study.

First of all, more field observations are necessary. It is important that these models can be tested in more estuaries. Also, most of the measurements were taken during spring tide. Even thought this is the case when the saltwater intrudes the furthest, cases during the neap tide are helpful to understand the mixing mechanisms.

Additionally, this study is focused on equations in steady-state condition. However, this is not always the case in estuaries. These models are recommended to be solved and tested in unsteady-state conditions.

Moreover, these tidal average salinity intrusion methods are recommended to trace other soluble substances in estuaries. It provides useful information for people concerned with water quality in alluvial estuaries.

The total dispersion is well described by the Van der Burgh method and the gravitational circulation can be described by the maximum power method. The difference between these two is regarded as the tide-driven dispersive processes. From Appendix A.12, the tidal effect is always large near the mouth and decreases landward. In Chapter 3, tidal effects are ideally included by using the C_2 part. However, C_2 can vary and tidal effects can be complicated since the geometry is so variable in estuaries around the world. General theories for the tidal effects separating from the density-driven part are suggested to be developed.

A

Appendix

A

A.1. Compilation of the geometry

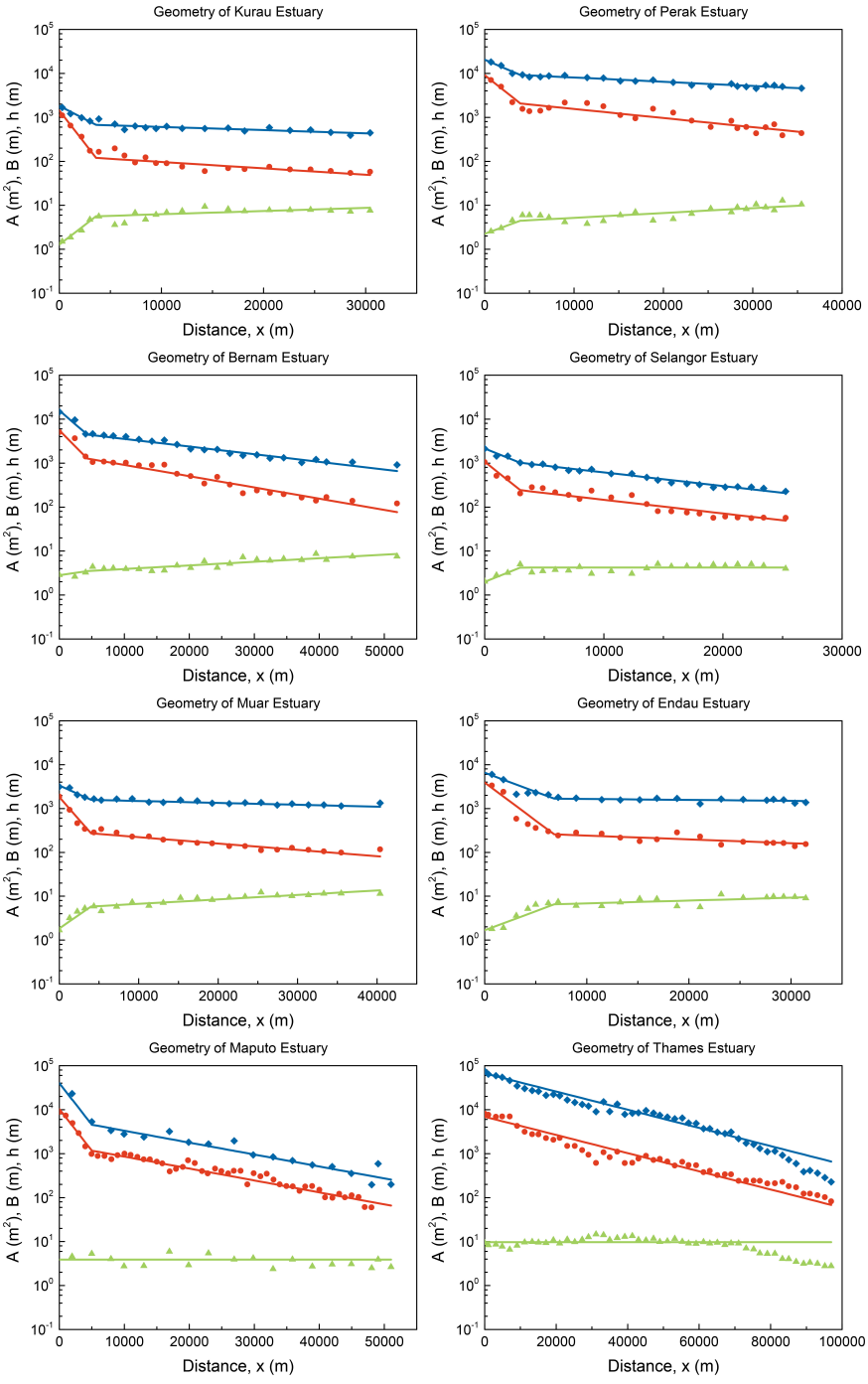

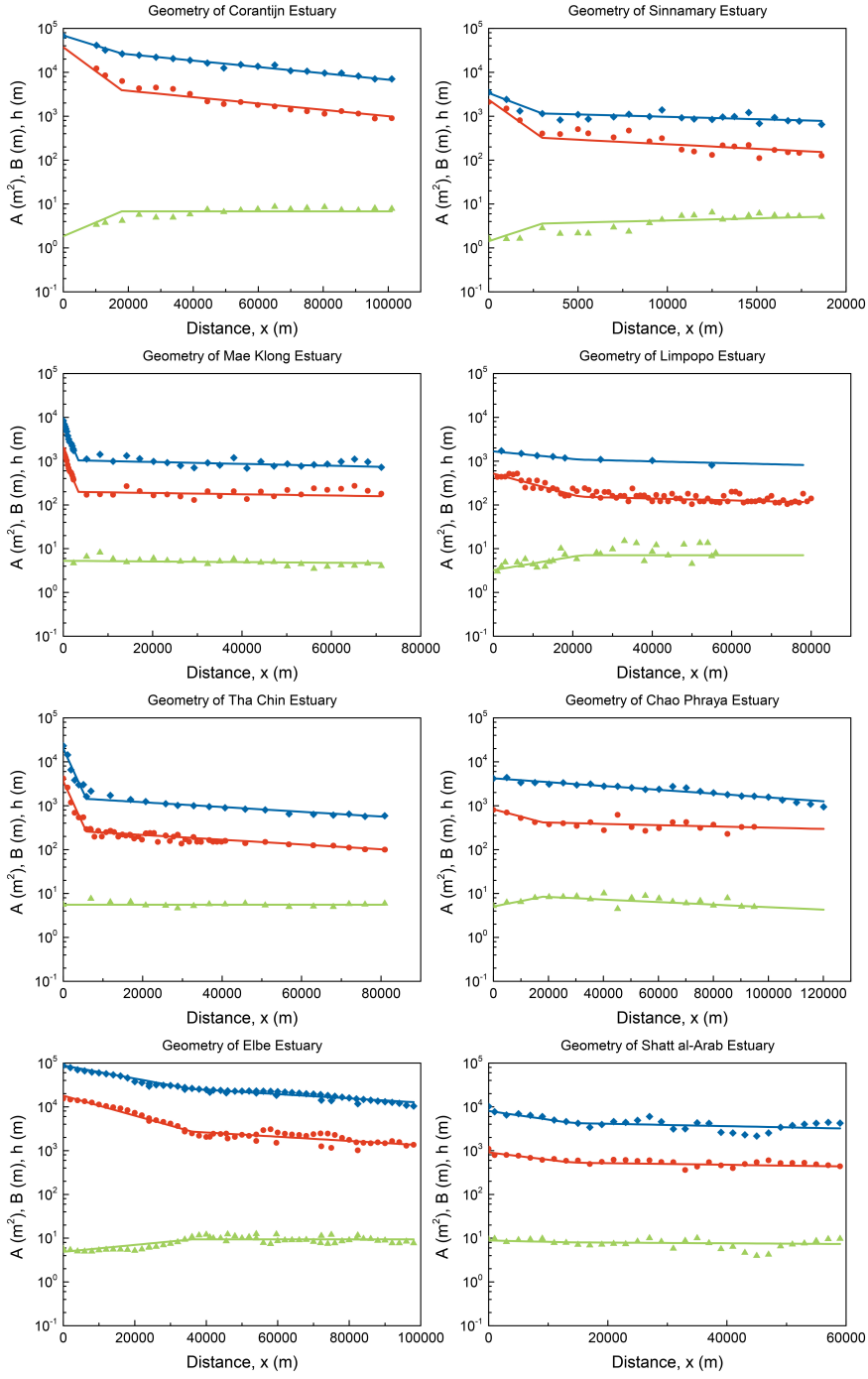

Figure A.1 The same as Figure 2.2.

A

A.2. Summary of the geometry

Table A.1: Summary of the geometry of the estuaries.

Label	Estuary	A_0 (m^2)	a_0 (km)	a_1 (km)	B_0 (m)	b_0 (km)	b_1 (km)	x_1 (m)	h_0 (m)	K_M ($m^{1/3}s^{-1}$)
1	Kurau	674	3.6	60	120	1.45	30	3600	5.6	30
2	Perak	9212	5	45	2068	2.7	21	4000	4.5	65
3	Bernam	4460	3.4	25	1270	2.9	17	4300	3.5	70
4	Selangor	1015	4	14	241	2	14	3000	4.2	40
5	Muar	1580	5.3	100	271	2.1	30	4000	5.8	45
6	Endau	1682	5	200	257	2.5	50	6800	6.5	45
7*	Maputo	4550	2.3	16	1170	2.3	16	5000	3.9	70
8*	Thames	67000	21	21	6900	21	21	0	9.7	51
9	Corantijn	26670	19	60	3923	8	60	18000	6.8	40
10*	Sinnamary	1155	2.8	40	321	1.5	21	3000	3.6	50
11	Mae Klong	1038	1.8	200	198	1.8	300	3400	5.2	40
12*	Limpopo	1075	50	200	152	18	200	22000	7.1	43
13*	Tha Chin	1430	2.2	80	260	2.2	80	5800	5.5	50
14*	Chao Phraya	3508	100	100	415	26	300	18000	8.5	51
15*	Elbe	25472	29	90	2715	19	90	36000	9.4	43
16*	Shatt al-Arab	4260	22	160	531	26	230	14000	8.0	38

[1]The estuaries with superscript used K_M from Cai et al. [2012], while others from Gisen [2015].
[2]Data about Shatt al-Arab Estuary comes from Abdullah et al. [2016].

A.3. Summary of measurements

In Table A.2 and A.3, the data chosen from each estuary with star-marked label is used in Appendix A.5. The subscript '0' represents parameters at the boundary condition.

Table A.2: Summary of salinity measurements.

Label	Date	E_m (m)	L (m)	T (s)	$\lvert Q\rvert$ (m^3/s)	δ_H (10^{-6} m^{-1})	H_0 (m)	η_0/h_0 (%)
1*	28/02/2013	9400	11000	44400	50	-6.3	2.8	25
2*	13/03/2013	11000	16000	44400	316	3	2.5	28
3*	21/06/2012	14000	42000	44400	42	1.7	3.5	50
4*	24/07/2012	12700	14000	44400	42	-3.7	4.0	47
5*	03/08/2012	11000	35000	44400	35	-2.68	2.0	17
6*	28/03/2013	10500	21000	44400	54	-1.3	1.9	14
7a	28/04/1982	13000	21000	44440	25	2	3.5	45
7b	15/07/1982	8000	30000	44440	8	2	2.1	27
7c*	19/04/1984	13000	20000	44440	120	2	3.3	43
7d	17/05/1984	13000	20000	44440	50	2	3.4	44
7e	29/05/1984	12000	23000	44440	40	2	3.0	39
8*	07/04/1949	14000	83000	44400	40	1.1	5.3	27
9a*	09/12/1978	12000	58000	44440	120	-1.7	1.8	13
9b	14/12/1978	13000	63000	44440	130	-1.7	2.2	16
9c	20/12/1978	13000	58000	44440	220	-1.7	1.6	11
10a	12/11/1993	8600	7600	44440	168	-5	2.6	36
10b	27/04/1994	11000	7800	44440	148	-5	2.9	40
10c *	03/11/1994	10000	9600	44440	112	-5	2.9	40
11a*	08/03/1977	10000	23000	44400	60	-4.2	1.5	14
11b	09/04/1977	8000	28000	44400	12	-4.2	2.1	20

continued on next page

continued from previous page

Label	Date	E_m (m)	L (m)	T (s)	$\lvert Q \rvert$ (m^3/s)	δ_H (10^{-6} m^{-1})	H_0 (m)	η_0/h_0 (%)
12a	31/12/1982	8000	67000	44440	2	1.7	1.1	8
12b	14/07/1994	7000	47000	44440	5	1.7	1.0	7
12c	24/07/1994	8000	58000	44440	5	1.7	0.93	7
12d*	10/08/1994	8000	62000	44440	3	1.7	1.0	7
13a*	27/02/1986	18500	37000	44400	40	-10.6	2.4	22
13b	01/03/1986	14000	42000	86400	40	-5.5	1.8	17
13c	13/08/1987	18500	32000	44400	39	-10.6	1.9	17
14a*	05/06/1962	24000	43000	86400	63	-2.2	2.1	12
14b	16/01/1967	14000	22000	86400	180	-2.2	2.4	14
14c	23/02/1982	19000	38000	86400	100	-2.2	1.5	9
14d	29/01/1983	26000	44000	86400	90	-2.2	1.5	9
15a	21/09/2004	20000	68000	44440	200	2	2.2	11
15b*	21/09/2004	18000	69000	44440	200	2	3.2	17
16a	26/03/2014	10000	40000	44000	114	-5	1.6	10
16b	16/05/2014	10000	48000	44000	96	-5	2.3	15
16c	24/09/2014	15500	65000	44000	58	-5	2.2	14
16d*	05/01/2015	10000	42000	44000	63	-5	2.4	15

A.4. Summary of parameters using the box-model method

Table A.3: Parameters using $C_2 = 10$, with data in bracket using a tailor-made C_2 value.

Label	$K_{\text{calibrated}}$ (-)	S_0 psu	D_0 (m^2/s)	α (m^{-1})	β (-)	N_{R0} (-)	$K_{\text{calculated}}$ (-)
1*	0.78	15	370 (382)	7.4	9.4	0.55	0.51
2*	0.54	8	255 (201)	0.81	3.3	0.041	0.51
3*	0.49	28	234	5.6	0.49	0.022	0.52
4*	0.51	14	314 (314)	7.5	0.94	0.084	0.51
5*	0.45	18	326	9.3	3.1	0.12	0.52
6*	0.65	17	282 (286)	5.2	15	0.23	0.53
7a	0.70	29	80	3.2	0.77	0.019	0.57
7b	0.69	32	47	5.9	0.41	0.028	0.62
7c*	0.57	22	281	2.3	0.86	0.068	0.52
7d	0.65	24	135	2.7	0.85	0.031	0.54
7e	0.63	26	133	3.3	0.67	0.030	0.55
8*	0.55	31	239	6.0	0.030	0.0044	0.65
9a*	0.61	14	178	1.5	0.92	0.018	0.55
9b	0.55	12	206	1.6	0.78	0.014	0.53
9c	0.51	10	292	1.3	0.86	0.019	0.52
10a	0.52	9	368	2.2	8.2	0.53	0.51
10b	0.52	7	335	2.3	8.0	0.17	0.51
10c*	0.54	12	359	3.2	5.8	0.30	0.51
11a*	0.52	24	484	8.1	12	0.51	0.51
11b	0.58	25	177	15	7.6	0.21	0.54
12a	0.72	24	45	23	5.9	0.038	0.62
12b	0.67	12	63	13	10	0.070	0.58
12c	0.61	15	86	17	6.6	0.059	0.57
12d*	0.64	17	62	21	5.8	0.040	0.59
13a*	0.44	21.5	532	13	1.9	0.043	0.51
13b	0.45	25	592	15	1.7	0.77	0.52
13c	0.46	16	431	11	2.3	0.031	0.51
14a*	0.65	11	336	5.3	3.5	0.068	0.53
14b	0.58	1	163	0.90	18	0.089	0.51
14c	0.62	8.5	402	4.0	4.4	0.17	0.53
14d	0.62	12	485	5.4	3.3	0.083	0.52
15a	0.62	10	142	0.71	3.1	0.0050	0.53
15b*	0.62	10.5	149	0.74	2.9	0.0073	0.53
16a	0.48	11	290	2.5	7.1	0.19	0.52
16b	0.45	15	323	3.4	5.0	0.22	0.52
16c	0.48	27	402	6.9	2.6	0.064	0.53
16d*	0.52	15	234	3.7	5.2	0.14	0.54

A

A.5. Sensitivity to C_2

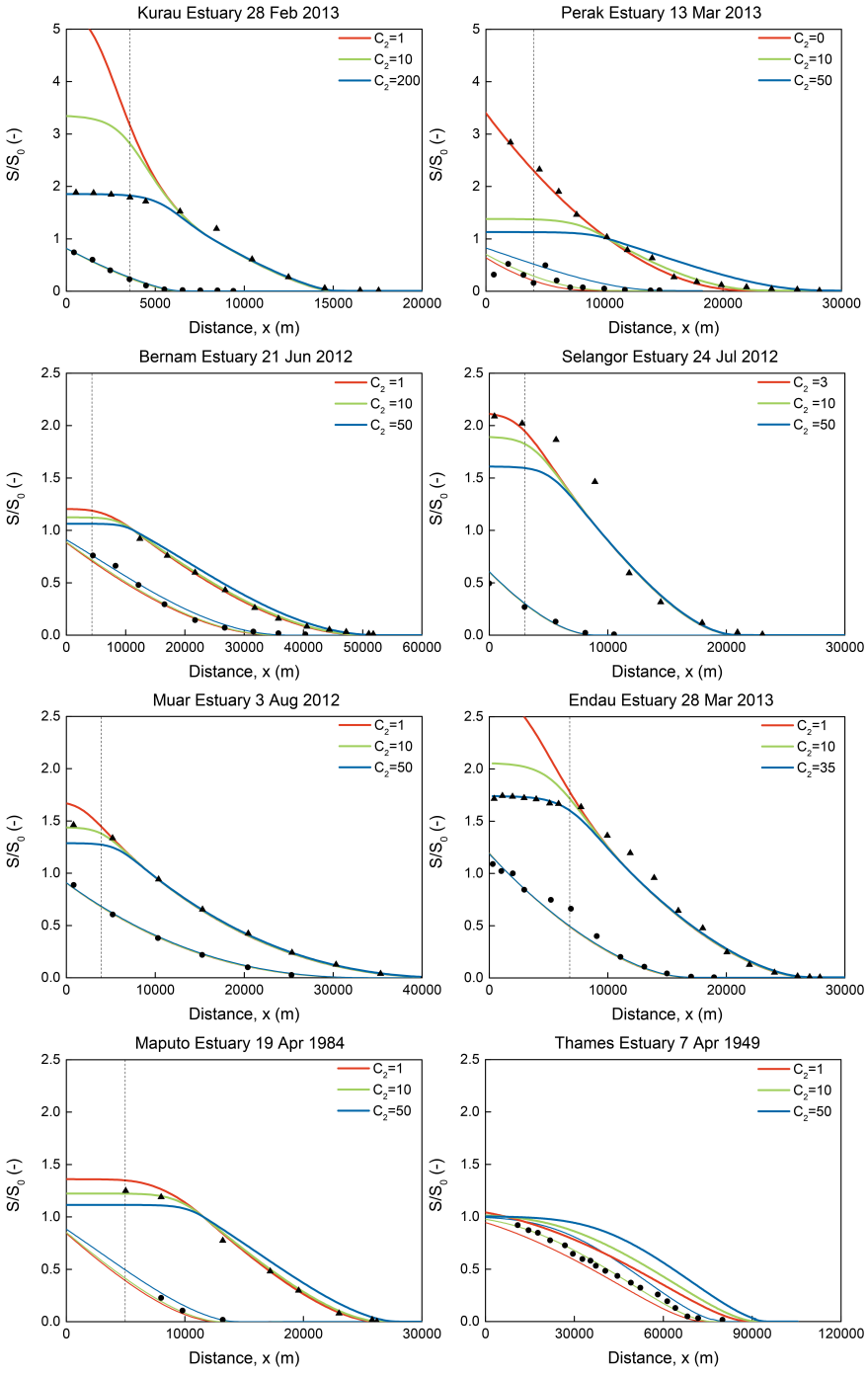

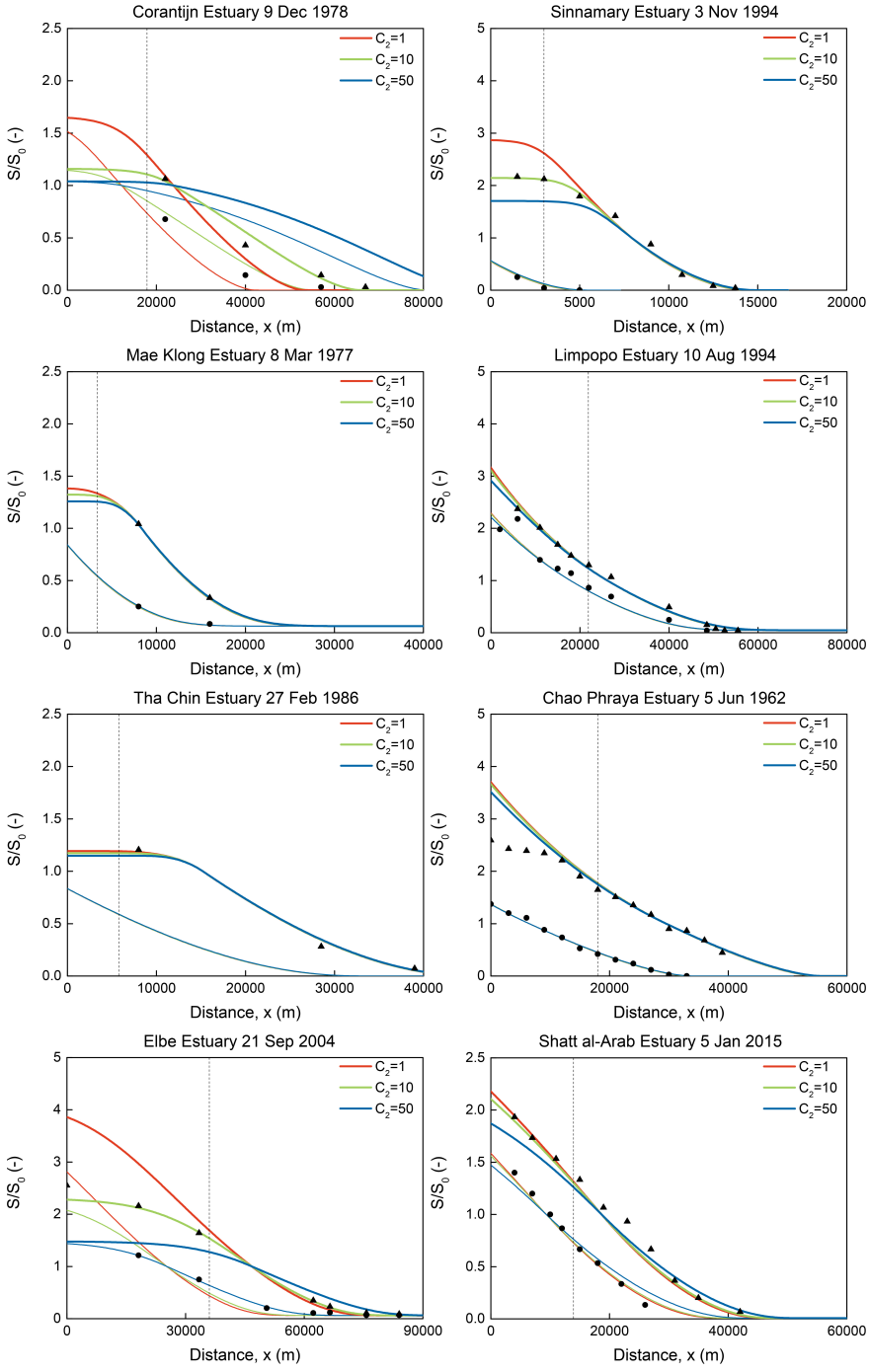

Figure A.2 The same as Figure 3.4.

A

A.6. Geometry considering the river cross section

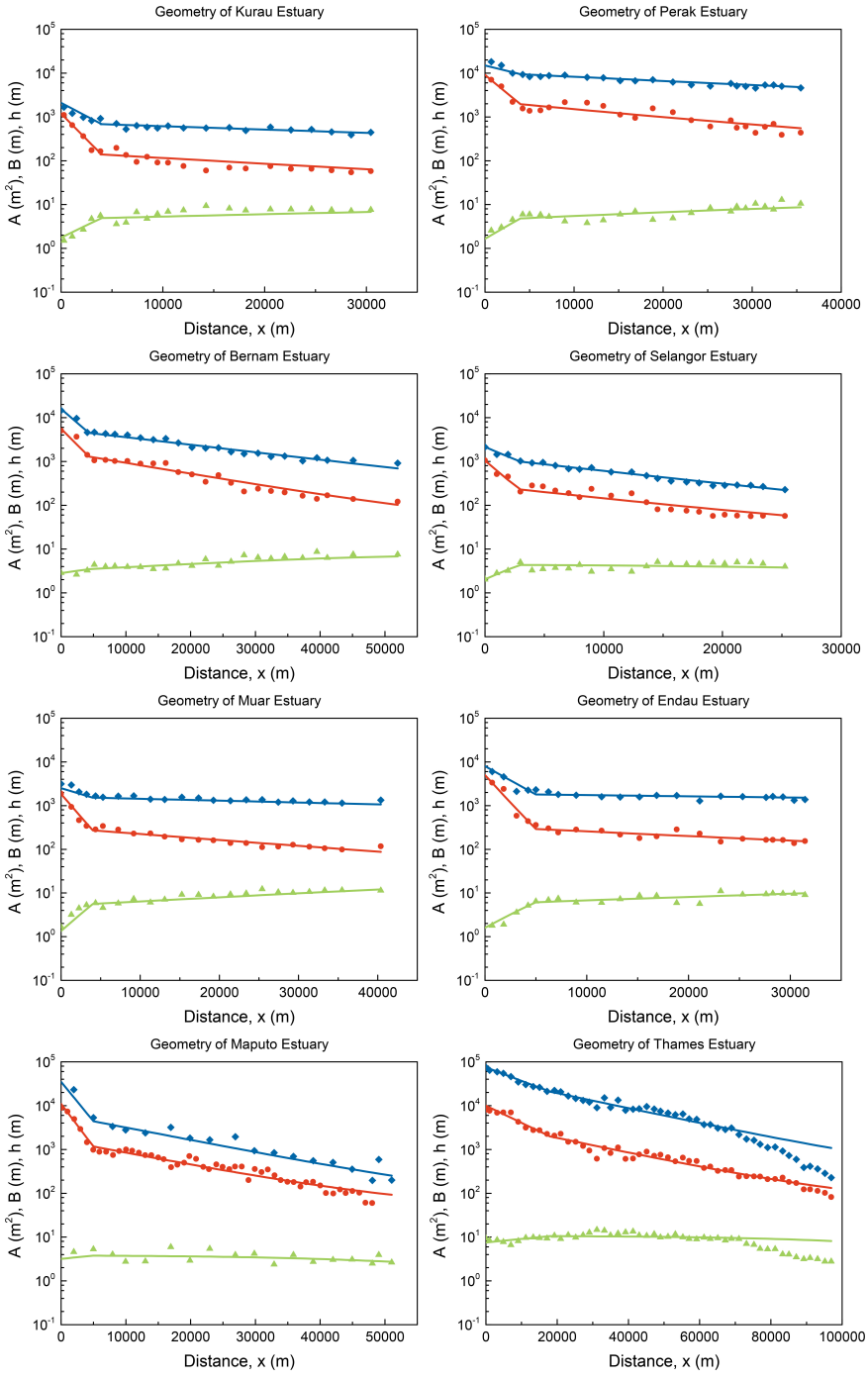

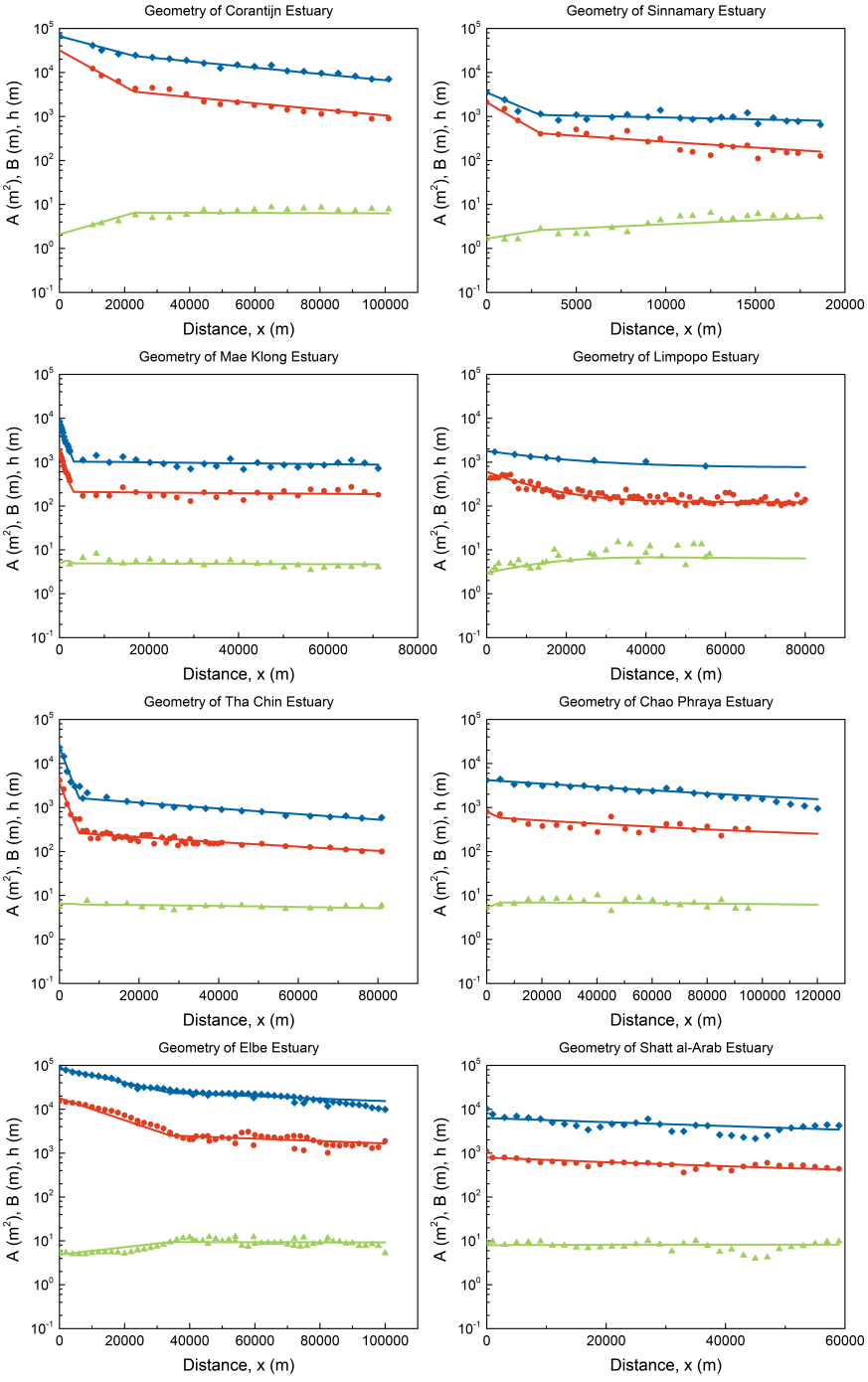
Geometry of Corantijn Estuary
Geometry of Sinnamary Estuary
Geometry of Mae Klong Estuary
Geometry of Limpopo Estuary
Geometry of Tha Chin Estuary
Geometry of Chao Phraya Estuary
Geometry of Elbe Estuary
Geometry of Shatt al-Arab Estuary
A (m²), B (m), h (m)
Distance, x (m)

A

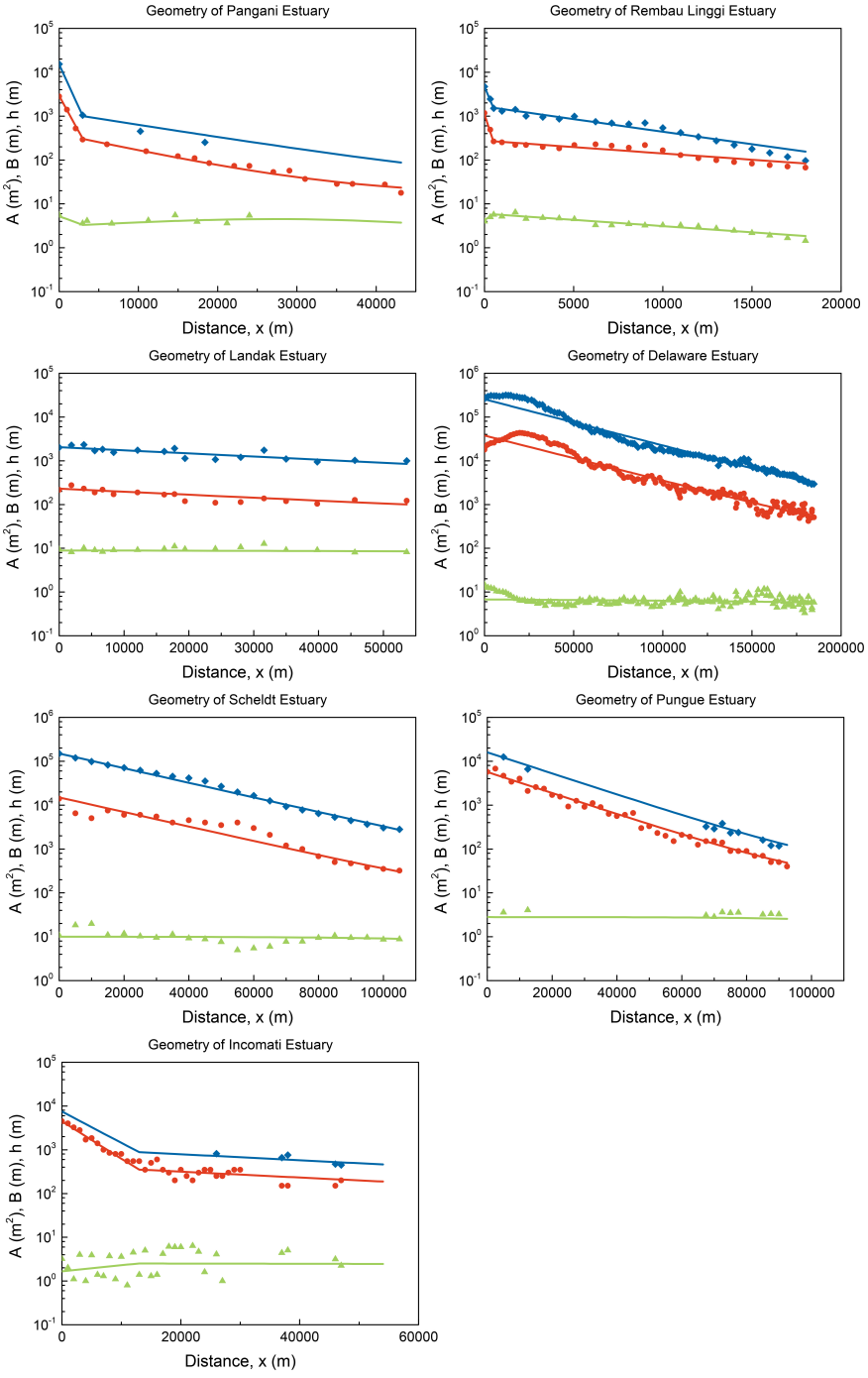

Figure A.3 The same as Figure 2.3.

A.7. Summary of the geometry considering the river cross section

Table A.4: Summary of the geometry of the estuaries considering the river cross section.

	Label Estuary	A_0 (m^2)	a_0 (km)	a_1 (km)	A_f (m^2)	B_0 (m)	b_0 (km)	b_1 (km)	B_f (m)	x_1 (km)	h_0 (m)
1	Kurau	683	3.5	55	20	139	1.8	30	10	4000	4.9
2	Perak	9452	8	40	900	1957	2.5	21	150	4000	4.8
3	Bernam	4482	3.4	25	30	1291	2.9	17	25	4300	3.5
4	Selangor	990	3.8	14	25	228	1.9	14	15	3000	4.3
5	Muar	1522	8	100	15	271	2.05	30	10	4000	5.6
6	Endau	1797	3.3	150	50	292	1.7	35	30	5000	6.1
7	Maputo	4402	2.4	15	50	1169	2.2	15	40	5000	3.8
8	Thames	20879	14	25	200	1987	11	25	50	18000	10.5
9	Corantijn	23650	22	60	150	3642	10.5	60	70	23000	6.5
10	Sinnamary	1082	2.5	50	40	413	1.8	15	20	3000	2.6
11	Mae Klong	1030	1.35	300	260	209	1.05	200	130	3200	4.9
12	Limpopo	1800	20	20	750	600	11	11	120	0	3
13	Tha Chin	1626	1.85	60	90	261	1.8	60	40	5000	6.2
14	Chao Phraya	4005	90	90	600	579	12	80	150	5000	6.9
15	Elbe	23674	26	150	200	2523	17	150	100	34000	9.4
16	Shatt al-Arab	6300	80	80	800	790	60	60	200	0	8
17	Pangani	1000	1.1	15	20	303	1.3	11	16	3000	3.3
18	Rembau Linggi	1551	0.45	7.5	5	267	0.35	14.5	5	500	5.8
19	Landak	2050	60	60	20	230	60	60	10	0	8.9
20	Delaware	255000	41	41	180	37655	42	42	60	0	6.8
21	Scheldt	150000	26	26	80	15000	26	26	40	0	10
22	Pungwe	16000	18	18	30	5700	18	18	15	0	2.8
23	Incomati	886	6	60	30	353	5	60	20	13000	2.5

A

A.8. Hydraulics of the extra database

Table A.5: Summary of hydraulic measurement in seven more estuaries.

Label	Date	E_m (m)	T (s)	$\|Q\|$ (m^3/s)	δ_H 10^{-6} m^{-1}
17a	27/10/2007	14000	44440	15	-10
17b	11/12/2007	12000	44440	11	-10
18	05/07/2012	8700	44440	26	-14
19	15/09/2009	15000	86400	10	-6.7
20a	23/08/1932	8000	44440	120	0.7
20b	04/10/1932	9000	44440	72	0.7
21a	01/07/1987	10000	44440	90	2.8
21b	02/11/2000	12000	44440	220	2.8
22a	27/02/2002	21000	44440	200	-8.5
22b	01/03/2002	27000	44440	150	-8.5
23a	05/09/1982	9000	44440	2	-19.9
23b	23/06/1993	11000	44440	4	-19.9
23c	07/07/1993	13000	44440	4	-19.9

A.9. Applications of the thermodynamic equation

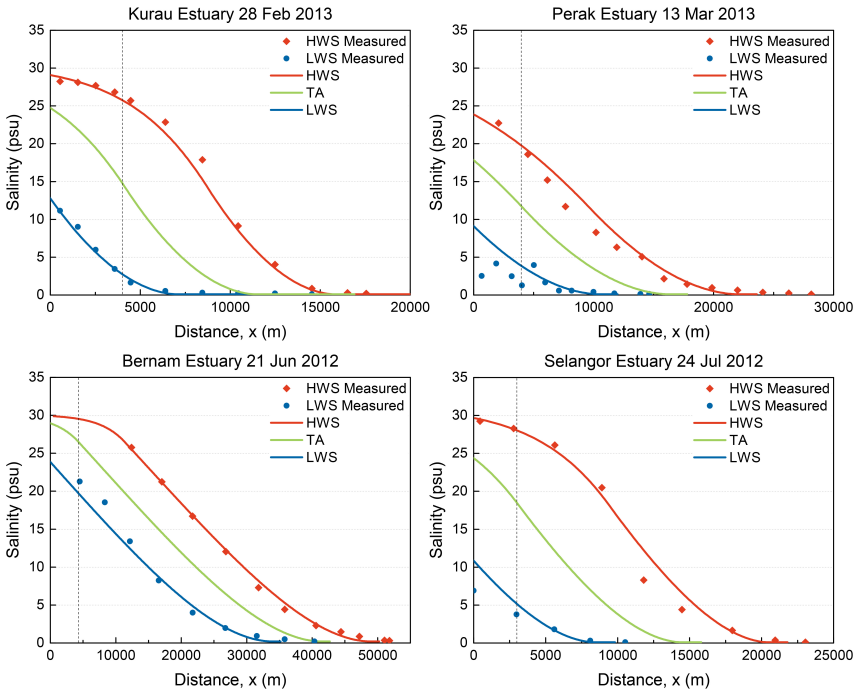

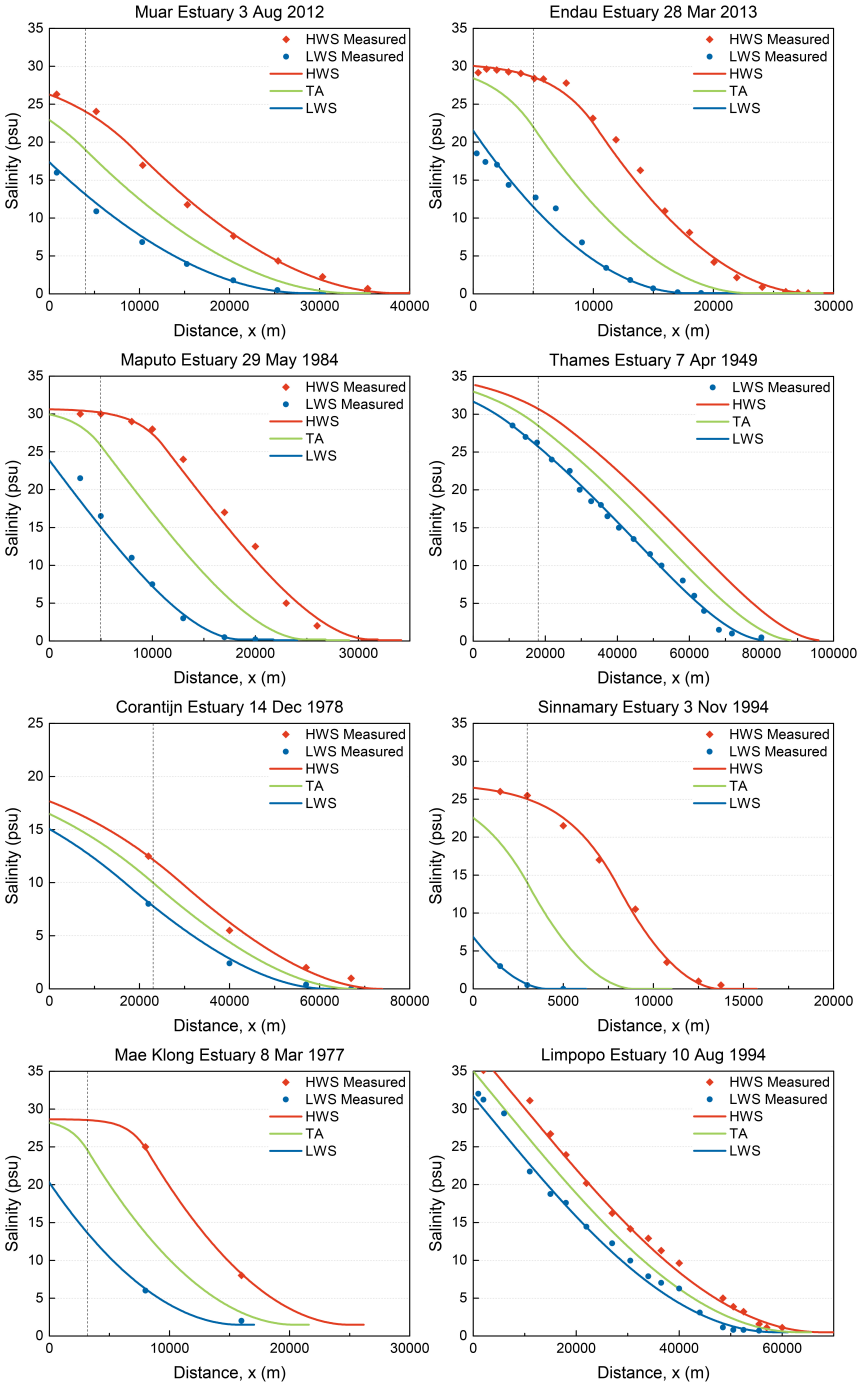
Muar Estuary 3 Aug 2012
Endau Estuary 28 Mar 2013
Maputo Estuary 29 May 1984
Thames Estuary 7 Apr 1949
Corantijn Estuary 14 Dec 1978
Sinnamary Estuary 3 Nov 1994
Mae Klong Estuary 8 Mar 1977
Limpopo Estuary 10 Aug 1994
HWS Measured
LWS Measured
HWS
TA
LWS
Salinity (psu)
Distance, x (m)

A

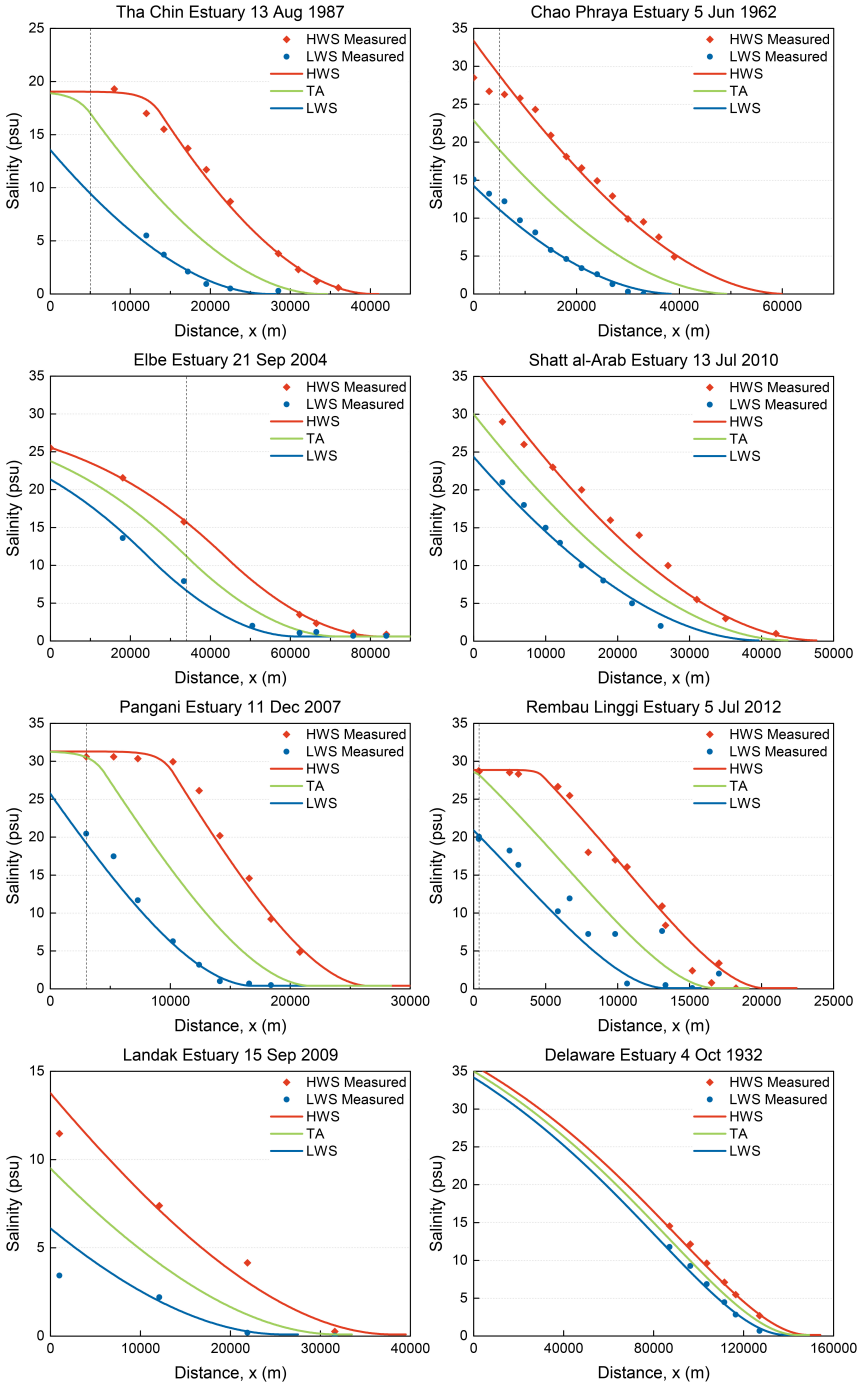
Tha Chin Estuary 13 Aug 1987
Chao Phraya Estuary 5 Jun 1962
Elbe Estuary 21 Sep 2004
Shatt al-Arab Estuary 13 Jul 2010
Pangani Estuary 11 Dec 2007
Rembau Linggi Estuary 5 Jul 2012
Landak Estuary 15 Sep 2009
Delaware Estuary 4 Oct 1932
HWS Measured
LWS Measured
HWS
TA
LWS
Salinity (psu)
Distance, x (m)

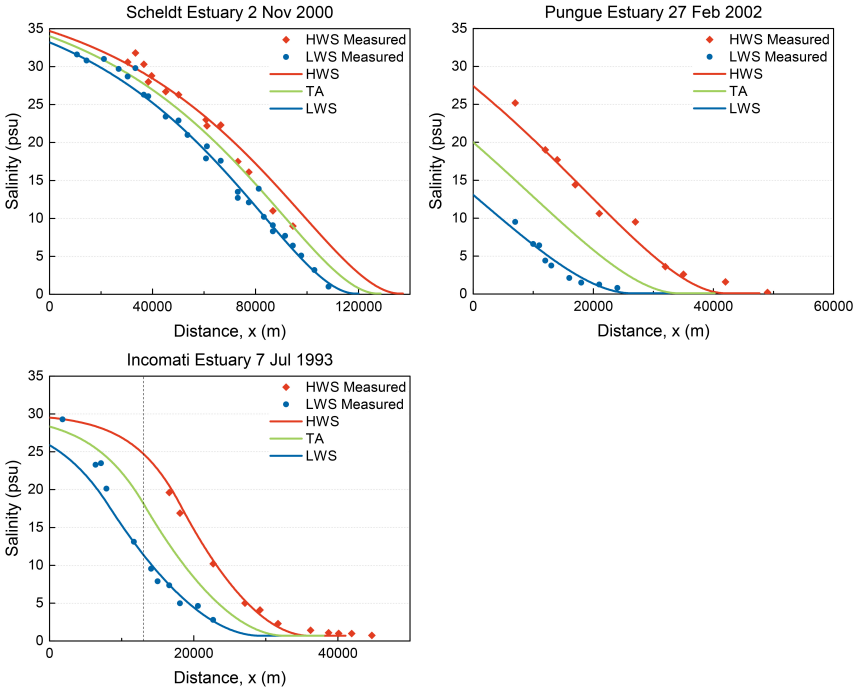

Figure A.4 The same as Figure 4.2.

A

A.10. Summary of the thermodynamic method

In Table A.6, the data chosen from each estuary with star-marked label is used in Appendix A.9.

Table A.6: Summary of boundary conditions using the thermodynamic equation.

Label	S_0 (psu)	D_0 (m^2/s)	N_{R0} (-)	Label	S_0 (psu)	D_0 (m^2/s)	N_{R0} (-)
1*	14.8	300	0.4705	13b	26	530	0.7875
2*	11.7	230	0.0932	13c*	17	395	0.0319
3*	26.5	260	0.0209	14a*	19	400	0.0774
4*	18.5	310	0.1168	14b	9	490	0.5274
5*	19	370	0.1293	14c	17.3	570	0.2253
6*	22	285	0.2428	14d	20	640	0.0915
7a	29	75	0.0186	15a	11	170	0.0060
7b	32	43	0.0282	15b*	11.2	175	0.0084
7c	22	285	0.0679	16a	24.5	380	0.2335
7d	24	130	0.0308	16b	29	380	0.2327
7e*	25.8	130	0.0337	16c	35	450	0.0456
8*	28.5	185	0.0167	16d*	30	250	0.1580
9a	11.7	155	0.0213	17a	28.7	205	0.0386
9b*	10.0	150	0.0124	17b*	28.5	130	0.0446
9c	8.4	230	0.0177	18*	28	250	0.2873
10a	7.8	225	0.3552	19*	9.5	90	0.0612
10b	6	190	0.1150	20a	13	100	0.0055
10c*	14	340	0.2703	20b*	35	55	0.0062
11a*	24.5	520	0.4963	21a	31	150	0.0127
11b	26	495	0.6172	21b*	34	400	0.0196
12a	35	55	0.0155	22a*	20	360	0.0052
12b	35	85	0.0579	22b	20	420	0.0018
12c	35	100	0.0388	23a	26	43	0.0299
12d*	35.0	70	0.0233	23b	20.2	47	0.0254
13a	23.0	470	0.0442	23c*	18.2	49	0.0139

A.11. Geometry of the extra database

The compilation and the summarized information of the geometry in the less reliable database are presented.

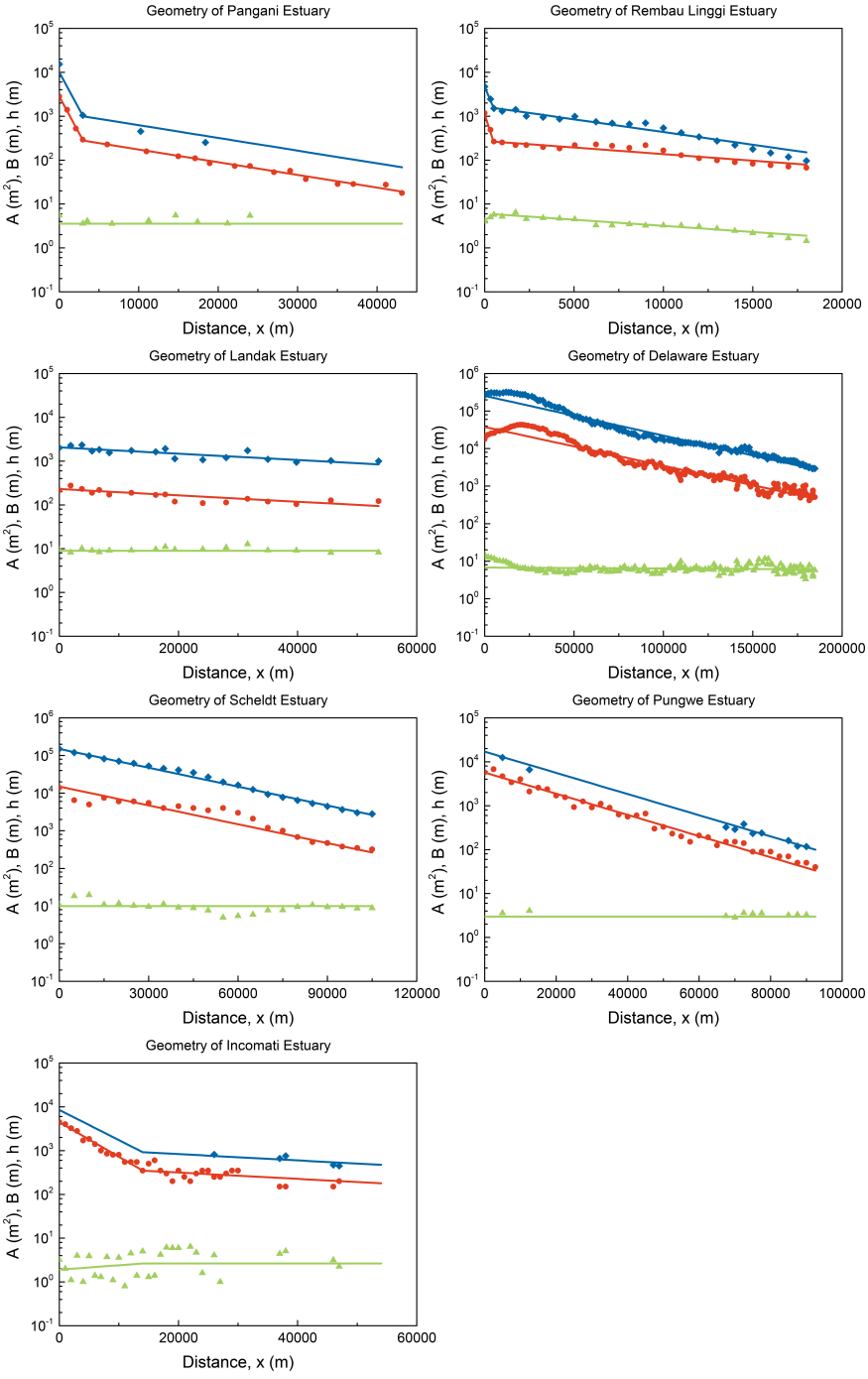

Figure A.5 The same as Figure 2.2.

A

Table A.7: Summary of the geometry of the less reliable database.

Label	A_0 (m^2)	a_0 (km)	a_1 (km)	B_0 (m)	b_0 (km)	b_1 (km)	x_1 (m)	h_0 (m)
17a	995	1300	15000	279	1300	15000	3000	3.57
17b	995	1300	15000	279	1300	15000	3000	3.57
18	1547	450	7500	264	350	14500	500	5.87
19	2060	60000	60000	230	60000	60000	0	8.96
20a	255000	41000	41000	37655	42000	42000	0	6.77
20b	255000	41000	41000	37655	42000	42000	0	6.77
21a	150000	26000	26000	15000	26000	26000	0	10.00
21b	150000	26000	26000	15000	26000	26000	0	10.00
22a	17000	18000	18000	5700	18000	18000	0	2.98
22b	17000	18000	18000	5700	18000	18000	0	2.98
23a	921	6300	60000	349	5500	60000	14000	2.64
23b	921	6300	60000	349	5500	60000	14000	2.64
23c	921	6300	60000	349	5500	60000	14000	2.64

A.12. Application of the maximum power method

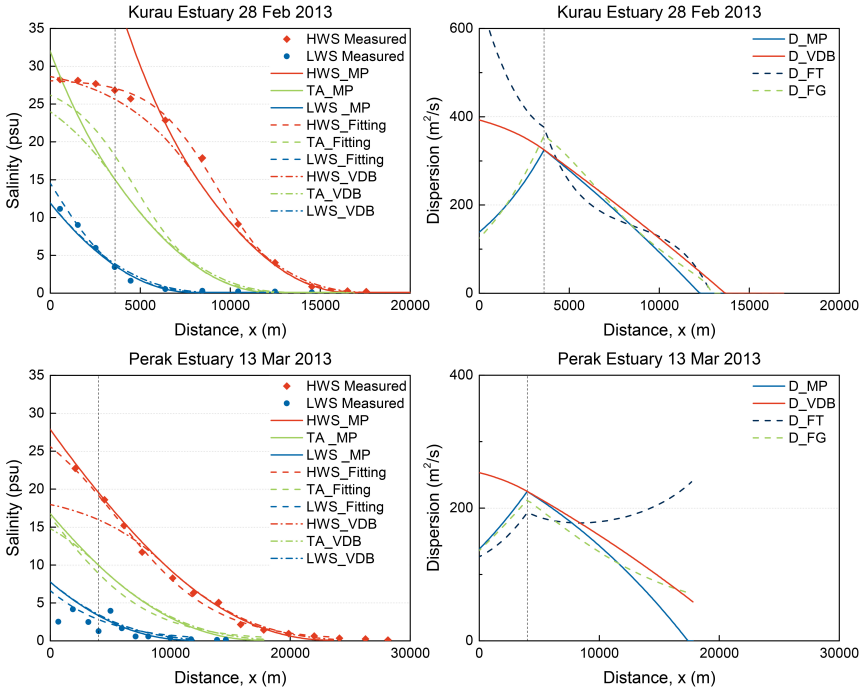

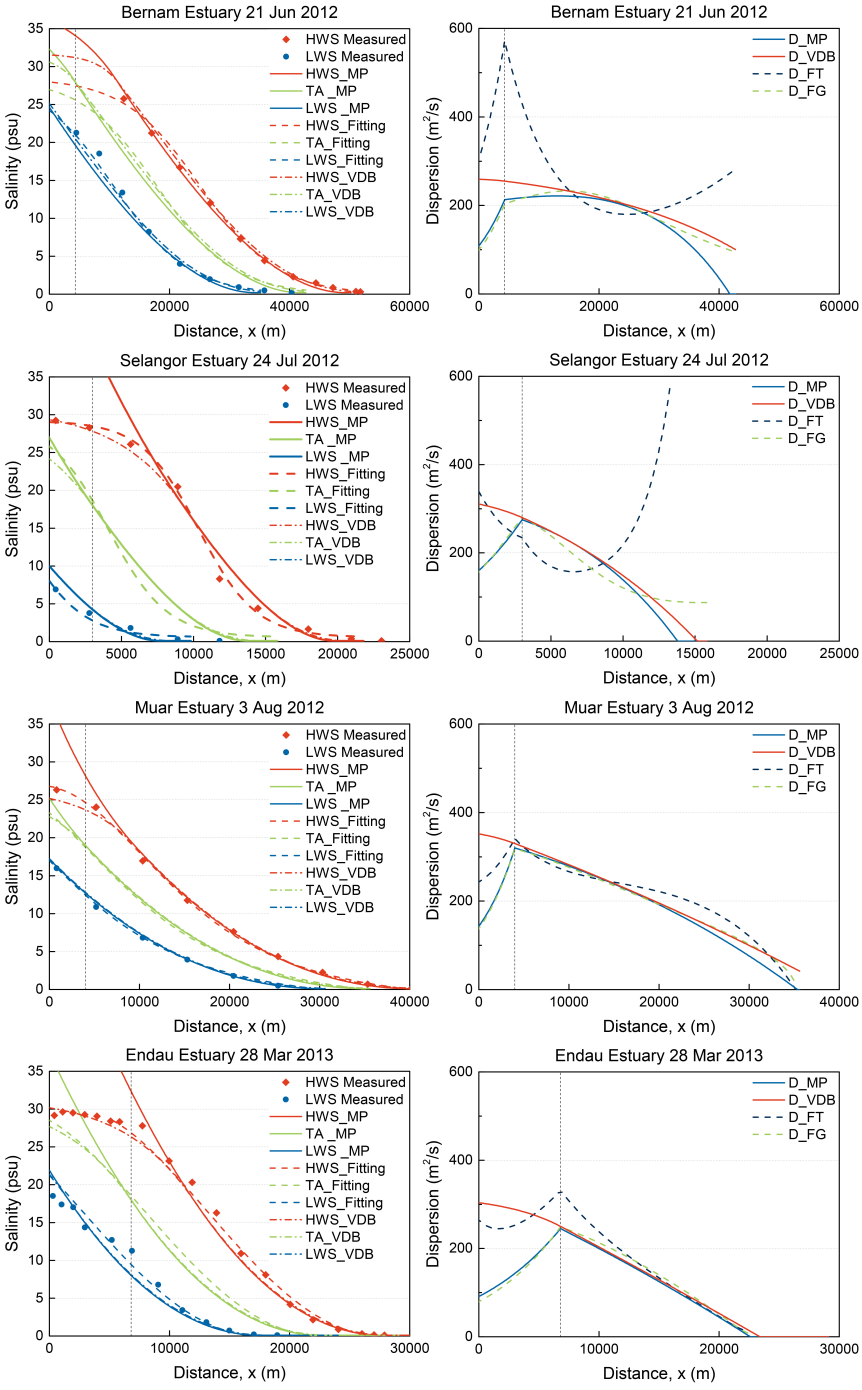
Bernam Estuary 21 Jun 2012
Salinity (psu)
Distance, x (m)
HWS Measured
LWS Measured
HWS_MP
TA _MP
LWS _MP
HWS_Fitting
TA_Fitting
LWS_Fitting
HWS_VDB
TA_VDB
LWS_VDB
Bernam Estuary 21 Jun 2012
Dispersion (m²/s)
Distance, x (m)
D_MP
D_VDB
D_FT
D_FG
Selangor Estuary 24 Jul 2012
Salinity (psu)
Distance, x (m)
Selangor Estuary 24 Jul 2012
Dispersion (m²/s)
Distance, x (m)
Muar Estuary 3 Aug 2012
Salinity (psu)
Distance, x (m)
Muar Estuary 3 Aug 2012
Dispersion (m²/s)
Distance, x (m)
Endau Estuary 28 Mar 2013
Salinity (psu)
Distance, x (m)
Endau Estuary 28 Mar 2013
Dispersion (m²/s)
Distance, x (m)

A

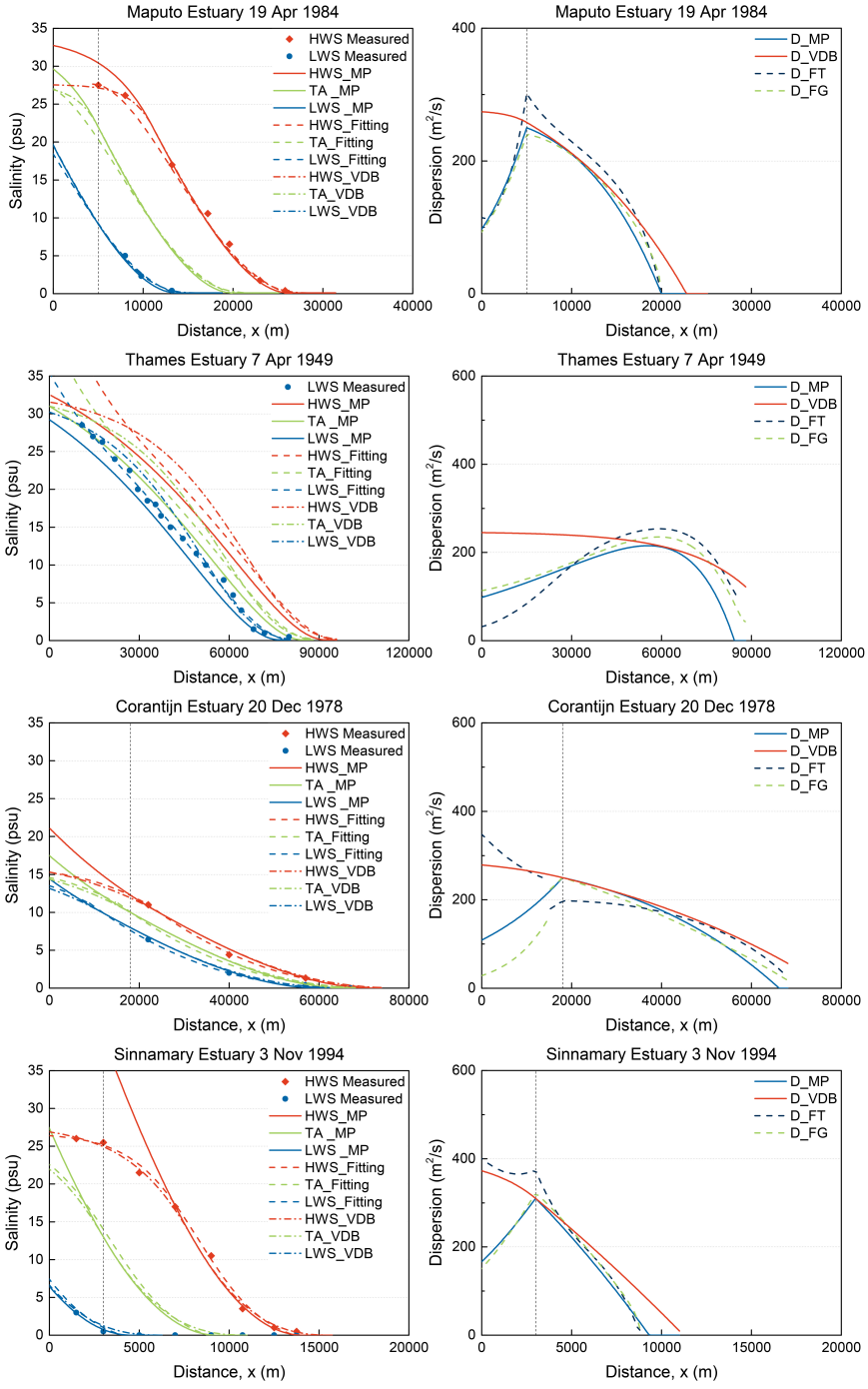
Maputo Estuary 19 Apr 1984
Salinity (psu)
Distance, x (m)
HWS Measured
LWS Measured
HWS_MP
TA _MP
LWS _MP
HWS_Fitting
TA_Fitting
LWS_Fitting
HWS_VDB
TA_VDB
LWS_VDB
Maputo Estuary 19 Apr 1984
Dispersion (m²/s)
Distance, x (m)
D_MP
D_VDB
D_FT
D_FG
Thames Estuary 7 Apr 1949
Salinity (psu)
Distance, x (m)
LWS Measured
HWS_MP
TA _MP
LWS _MP
HWS_Fitting
TA_Fitting
LWS_Fitting
HWS_VDB
TA_VDB
LWS_VDB
Thames Estuary 7 Apr 1949
Dispersion (m²/s)
Distance, x (m)
D_MP
D_VDB
D_FT
D_FG
Corantijn Estuary 20 Dec 1978
Salinity (psu)
Distance, x (m)
HWS Measured
LWS Measured
HWS_MP
TA _MP
LWS _MP
HWS_Fitting
TA_Fitting
LWS_Fitting
HWS_VDB
TA_VDB
LWS_VDB
Corantijn Estuary 20 Dec 1978
Dispersion (m²/s)
Distance, x (m)
D_MP
D_VDB
D_FT
D_FG
Sinnamary Estuary 3 Nov 1994
Salinity (psu)
Distance, x (m)
HWS Measured
LWS Measured
HWS_MP
TA _MP
LWS _MP
HWS_Fitting
TA_Fitting
LWS_Fitting
HWS_VDB
TA_VDB
LWS_VDB
Sinnamary Estuary 3 Nov 1994
Dispersion (m²/s)
Distance, x (m)
D_MP
D_VDB
D_FT
D_FG

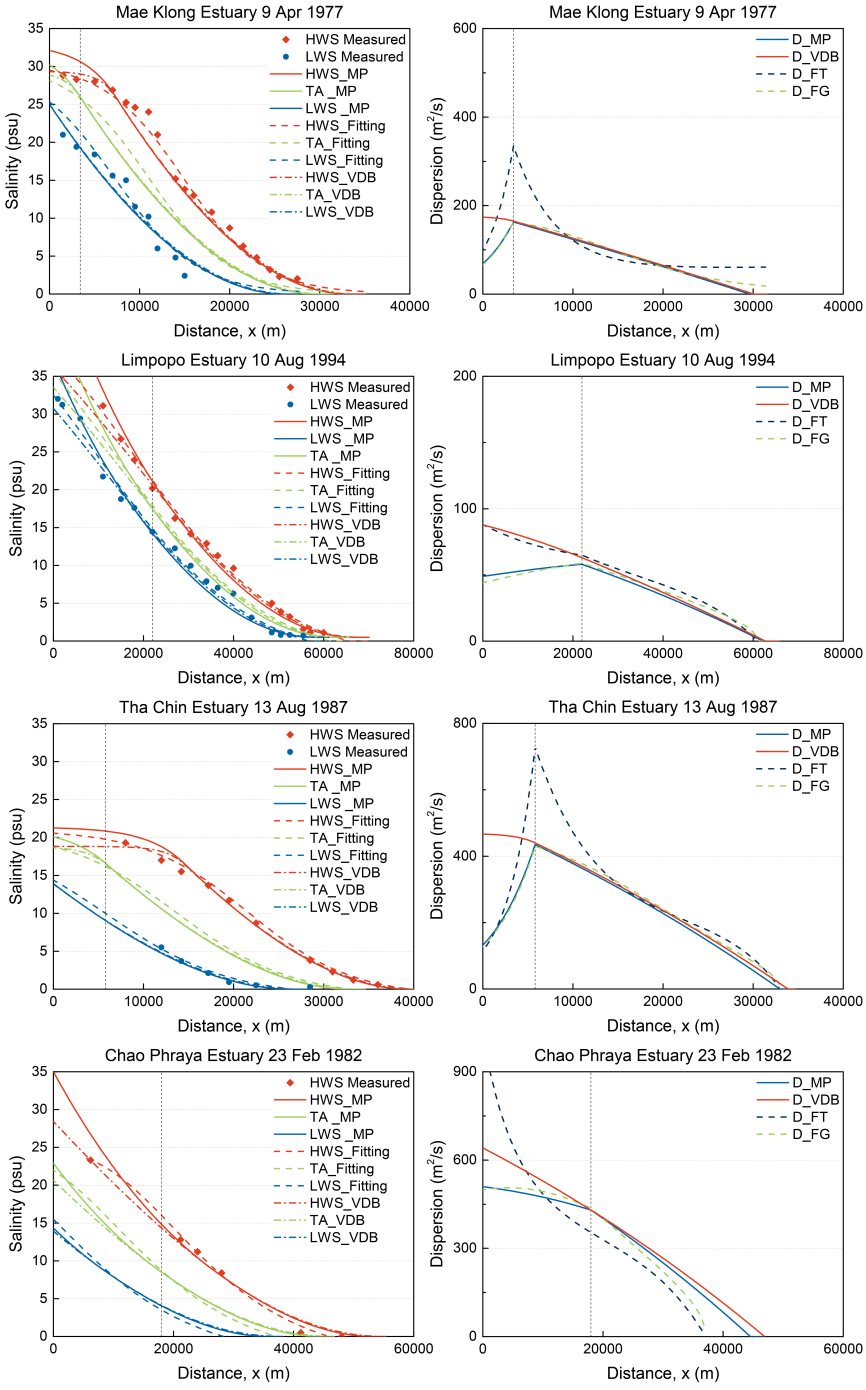
Mae Klong Estuary 9 Apr 1977
Salinity (psu)
Distance, x (m)
HWS Measured
LWS Measured
HWS_MP
TA _MP
LWS _MP
HWS_Fitting
TA_Fitting
LWS_Fitting
HWS_VDB
TA_VDB
LWS_VDB
Mae Klong Estuary 9 Apr 1977
Dispersion (m²/s)
Distance, x (m)
D_MP
D_VDB
D_FT
D_FG
Limpopo Estuary 10 Aug 1994
Salinity (psu)
Distance, x (m)
HWS Measured
LWS Measured
HWS_MP
LWS _MP
TA _MP
HWS_Fitting
TA_Fitting
LWS_Fitting
HWS_VDB
TA_VDB
LWS_VDB
Limpopo Estuary 10 Aug 1994
Dispersion (m²/s)
Distance, x (m)
D_MP
D_VDB
D_FT
D_FG
Tha Chin Estuary 13 Aug 1987
Salinity (psu)
Distance, x (m)
HWS Measured
LWS Measured
HWS_MP
TA _MP
LWS _MP
HWS_Fitting
TA_Fitting
LWS_Fitting
HWS_VDB
TA_VDB
LWS_VDB
Tha Chin Estuary 13 Aug 1987
Dispersion (m²/s)
Distance, x (m)
D_MP
D_VDB
D_FT
D_FG
Chao Phraya Estuary 23 Feb 1982
Salinity (psu)
Distance, x (m)
HWS Measured
HWS_MP
TA _MP
LWS _MP
HWS_Fitting
TA_Fitting
LWS_Fitting
HWS_VDB
TA_VDB
LWS_VDB
Chao Phraya Estuary 23 Feb 1982
Dispersion (m²/s)
Distance, x (m)
D_MP
D_VDB
D_FT
D_FG

A

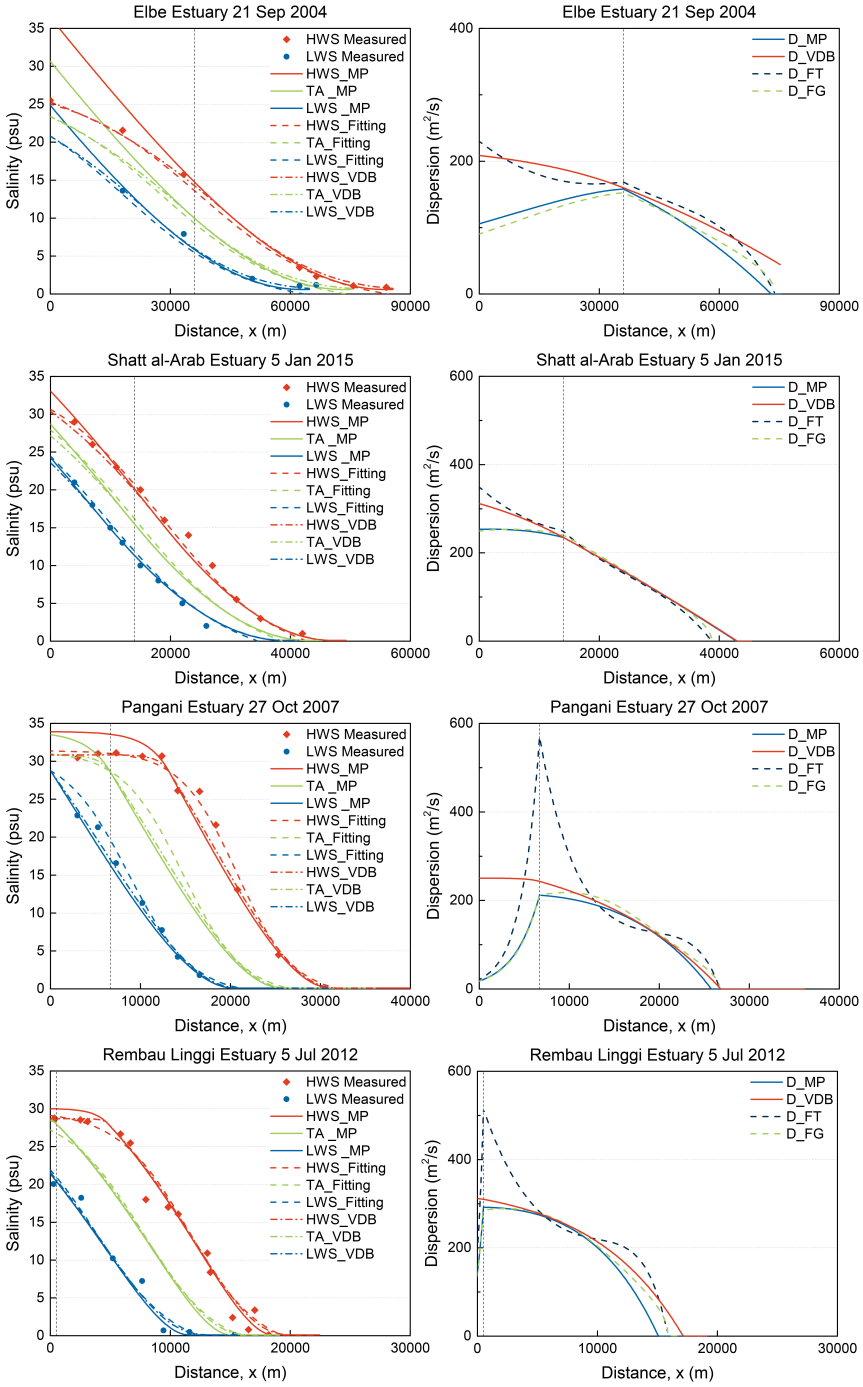
Elbe Estuary 21 Sep 2004
Salinity (psu)
Distance, x (m)
HWS Measured
LWS Measured
HWS_MP
TA _MP
LWS _MP
HWS_Fitting
TA_Fitting
LWS_Fitting
HWS_VDB
TA_VDB
LWS_VDB
Elbe Estuary 21 Sep 2004
Dispersion (m²/s)
Distance, x (m)
D_MP
D_VDB
D_FT
D_FG
Shatt al-Arab Estuary 5 Jan 2015
Salinity (psu)
Distance, x (m)
Shatt al-Arab Estuary 5 Jan 2015
Dispersion (m²/s)
Distance, x (m)
Pangani Estuary 27 Oct 2007
Salinity (psu)
Distance, x (m)
Pangani Estuary 27 Oct 2007
Dispersion (m²/s)
Distance, x (m)
Rembau Linggi Estuary 5 Jul 2012
Salinity (psu)
Distance, x (m)
Rembau Linggi Estuary 5 Jul 2012
Dispersion (m²/s)
Distance, x (m)

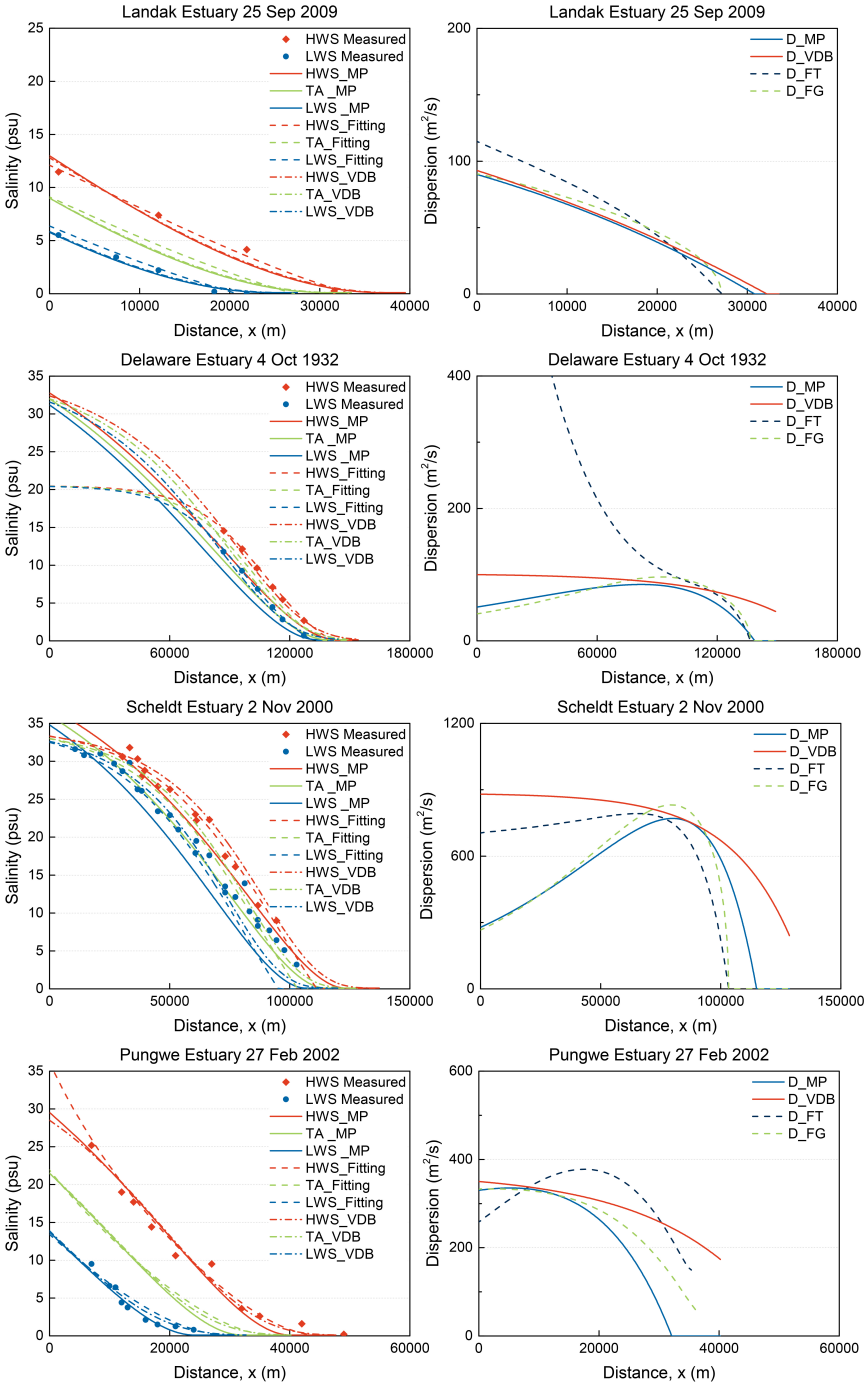
Landak Estuary 25 Sep 2009
Salinity (psu)
Distance, x (m)
HWS Measured
LWS Measured
HWS_MP
TA _MP
LWS _MP
HWS_Fitting
TA_Fitting
LWS_Fitting
HWS_VDB
TA_VDB
LWS_VDB
Landak Estuary 25 Sep 2009
Dispersion (m²/s)
Distance, x (m)
D_MP
D_VDB
D_FT
D_FG
Delaware Estuary 4 Oct 1932
Salinity (psu)
Distance, x (m)
Delaware Estuary 4 Oct 1932
Dispersion (m²/s)
Distance, x (m)
Scheldt Estuary 2 Nov 2000
Salinity (psu)
Distance, x (m)
Scheldt Estuary 2 Nov 2000
Dispersion (m²/s)
Distance, x (m)
Pungwe Estuary 27 Feb 2002
Salinity (psu)
Distance, x (m)
Pungwe Estuary 27 Feb 2002
Dispersion (m²/s)
Distance, x (m)

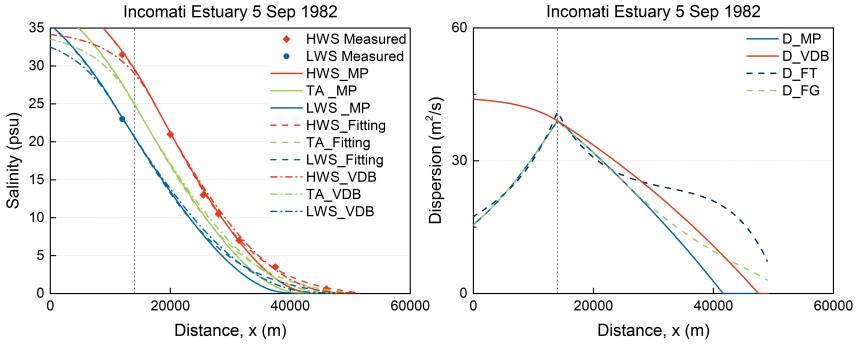

Figure A.6 Left: Application of the analytical solution from the maximum power (MP) method (solid lines) to observations (symbols) for high water slack (in red) and low water slack (in blue). The green line shows the tidal average condition. Dash lines reflect the curve fitting to the observations. Dash dot lines reflect the application of the Van der Burgh (VDB) method. Right: Simulated dispersion coefficient using different methods. Total dispersion (D_{FT}) and dispersion due to gravitational circulation (D_{FG}) from curve fitting are shown in dash lines for reference.

A.13. Summary of application by two methods

The application results using the maximum power (MP) concept and the pure Van der Bergh (VDB) approach are summarized in Table A.7. The data chosen from each estuary with star-marked label is used in Appendix A.12.

Following mathematic functions are used for curve fitting: Dose Response (Dose Resp), Slogistic1, Rational5, and Polynomial4 (Poly4).

Table A.8: Summary of boundary conditions by two methods.

Label	S_0	MP		VDB		Fitting function
		D_0 (m^2/s)	C_3 (psu^{-1}ms^{-2})	D_0 (m^2/s)	K (-)	
1*	15	325	0.0064	325	0.4	Dose Resp
2*	10	225	0.0082	225	0.3	Slogistic1
3*	28	213	0.0089	255	0.18	Slogistic1
4*	18	275	0.0066	280	0.35	Dose Resp
5*	19	320	0.0093	330	0.35	Rational5
6*	18	245	0.0059	250	0.45	Poly4
7a	29	66	0.0035	68	0.25	Slogistic1
7b	32.5	37	0.0043	42	0.2	Dose Resp
7c*	22	250	0.0069	258	0.3	Poly4
7d	25	115	0.0046	118	0.25	Slogistic1
7e	26	120	0.0055	125	0.23	Dose Resp
8*	31	98	0.0093	245	0.12	Poly4
9a	14	170	0.0114	170	0.3	Slogistic1
9b	12	150	0.0100	150	0.25	Dose Resp
9c*	10	250	0.0141	250	0.3	Poly4
10a	8	250	0.0063	250	0.35	Dose Resp
10b	6.5	220	0.0058	220	0.4	Slogistic1
10c*	13	310	0.0070	310	0.35	Dose Resp
11a	24	510	0.0090	520	0.5	Dose Resp
11b*	26	163	0.0069	165	0.5	Slogistic1
12a	23	46	0.0044	51	0.5	Slogistic1
12b	13	66	0.0056	70	0.5	Slogistic1
12c	16	78	0.0056	92	0.55	Dose Resp
12d*	17.5	58	0.0051	63	0.5	Dose Resp
13a	23	490	0.0094	490	0.45	Slogistic1
13b	25.5	590	0.0087	600	0.45	Slogistic1
13c*	16.5	435	0.0099	440	0.48	Dose Resp

continued on next page

continued from previous page

Label	S_0	MP		VDB		Fitting function
		D_0 (m²/s)	C_3 (psu^{-1}ms^{-2})	D_0 (m²/s)	K (-)	
14a	11	295	0.0051	305	0.5	Poly4
14b	1	160	0.0071	165	0.43	Poly4
14c*	8.5	430	0.0076	430	0.45	Rational5
14d	12	495	0.0066	510	0.5	Dose Resp
15a	10	145	0.0055	150	0.35	Slogistic1
15b*	10	158	0.0063	160	0.3	Dose Resp
16a	11.5	280	0.0088	280	0.45	Slogistic1
16b	16	340	0.0099	340	0.45	Rational5
16c	27	400	0.0092	400	0.48	Dose Resp
16d*	15.5	235	0.0086	235	0.5	Dose Resp
17a*	28.5	212	0.0070	243	0.38	Dose Resp
17b	28	130	0.0054	145	0.38	Dose Resp
18*	28	292	0.0090	310	0.3	Dose Resp
19*	9	90	0.0040	93	0.45	Dose Resp
20a	11	95	0.0269	200	0.12	Dose Resp
20b*	32	51	0.0103	100	0.13	Dose Resp
21a	31	88	0.0097	225	0.12	Slogistic1
21b*	33	278	0.0173	800	0.12	Dose Resp
22a*	21.5	330	0.0124	350	0.1	Poly4
22b	20	415	0.0165	500	0.1	Dose Resp
23a*	25	39	0.0058	39	0.4	Dose Resp
23b	17	46	0.0052	46	0.38	Dose Resp
23c	16	50	0.0056	50	0.42	Dose Resp

References

Abdullah, A. D., Gisen, J. I. A., van der Zaag, P., Savenije, H. H. G., Karim, U. F. A., Masih, I., and Popescu, I.: Predicting the salt water intrusion in the Shatt al-Arab estuary using an analytical approach, Hydrology and Earth System Sciences, 20, 4031–4042, 2016.

Banas, N. S., Hickey, B. M., MacCready, P., and Newton, J. A.: Dynamics of Willapa Bay, Washington: A highly unsteady, partially mixed estuary, Journal of Physical Oceanography, 34, 2413–2427, 2004.

Bowden, K. F. and Gilligan, R. M.: Characteristic features of estuarine circulation as represented in the Mersey estuary, Limnology and Oceanography, 16, 490–502, 1971.

Burchard, H. and Schuttelaars, H. M.: Analysis of tidal straining as driver for estuarine circulation in well-mixed estuaries, Journal of Physical Oceanography, 42, 261–271, 2012.

Cai, H. and Savenije, H. H. G.: Asymptotic behavior of tidal damping in alluvial estuaries, Journal of Geophysical Research: Oceans, 118, 6107–6122, 2013.

Cai, H., Savenije, H. H. G., and Toffolon, M.: A new analytical framework for assessing the effect of sea-level rise and dredging on tidal damping in estuaries, Journal of Geophysical Research: Oceans, 117, 2012.

Cai, H., Savenije, H. H. G., Zuo, S., Jiang, C., and Chua, V. P.: A predictive model for salt intrusion in estuaries applied to the Yangtze estuary, Journal of Hydrology, 529, 1336–1349, 2015.

Chatwin, P. C.: Some remarks on the maintenance of the salinity distribution in estuaries, Estuarine and Coastal Marine Science, 4, 555–566, 1976.

Davies, G. and Woodroffe, C. D.: Tidal estuary width convergence: Theory and form in North Australian estuaries, Earth Surface Processes and Landforms, 35, 737–749, 2010.

Dyer, K. R.: Estuaries: a physical introduction, John Wiley & Sons, 1973.

Dyer, K. R.: The salt balance in stratified estuaries, Estuarine and coastal marine science, 2, 273–281, 1974.

Fischer, H. B.: Mass transport mechanisms in partially stratified estuaries, Journal of fluid mechanics, 53, 671–687, 1972.

Fischer, H. B.: Longitudinal dispersion and turbulent mixing in open-channel flow, Annual Review of Fluid Mechanics, 5, 59–78, 1973.

Fischer, H. B.: Mixing and dispersion in estuaries, Annual review of fluid mechanics, 8, 107–133, 1976.

Fischer, H. B., List, E. J., Koh, R. C. Y., Imberger, J., and Brooks, N. H.: Mixing in inland and coastal waters, Academic Press, New York, 1979.

Friedrichs, C. T., Armbrust, B. D., and De Swart, H. E.: Hydrodynamics and equilibrium sediment dynamics of shallow, funnel-shaped tidal estuaries, in: Physics of Estuaries and Coastal Seas, Balkema Rotterdam, 1998.

Gisen, J. I. A.: Prediction in ungauged estuaries, Ph.D. thesis, Delft University of Technology, 2015.

Gisen, J. I. A., Savenije, H. H. G., and Nijzink, R. C.: Revised predictive equations for salt intrusion modelling in estuaries, Hydrology and Earth System Sciences, 19, 2791–2803, 2015a.

Gisen, J. I. A., Savenije, H. H. G., Nijzink, R. C., and Abd. Wahab, A. K.: Testing a 1-D analytical salt intrusion model and its predictive equations in Malaysian estuaries, Hydrological Sciences Journal, 60, 156–172, 2015b.

Guo, L., van der Wegen, M., Roelvink, D. J. A., Wang, Z. B., and He, Q.: Long-term, process-based morphodynamic modeling of a fluvio-deltaic system, part I: The role of river discharge, Continental Shelf Research, 109, 95–111, 2015.

Hansen, D. V. and Rattray, M.: Gravitational circulation in straits and estuaries, Tech. rep., Dept. of Oceanography, Univ. of Washington, 1966.

Hunkins, K.: Salt dispersion in the Hudson Estuary, Journal of Physical Oceanography, 11, 729–738, 1981.

Kleidon, A.: Thermodynamic foundations of the Earth system, Cambridge University Press, 2016.

Kuijper, K. and Van Rijn, L. C.: Analytical and numerical analysis of tides and salinities in estuaries; part II: salinity distributions in prismatic and convergent tidal channels, Ocean Dynamics, 61, 1743–1765, 2011.

Langbein, W. B.: The hydraulic geometry of a shallow estuary, Hydrological Sciences Journal, 8, 84–94, 1963.

Lerczak, J. A., Geyer, W. R., and Chant, R. J.: Mechanisms driving the time-dependent salt flux in a partially stratified estuary, Journal of Physical Oceanography, 36, 2296–2311, 2006.

MacCready, P.: Toward a unified theory of tidally-averaged estuarine salinity structure, Estuaries, 27, 561–570, 2004.

MacCready, P.: Estuarine adjustment, Journal of Physical Oceanography, 37, 2133–2145, 2007.

MacCready, P.: Calculating estuarine exchange flow using isohaline coordinates, Journal of Physical Oceanography, 41, 1116–1124, 2011.

MacCready, P. and Geyer, W. R.: Advances in estuarine physics, Annual Review of Marine Science, 2, 35–58, 2010.

McCarthy, R. K.: Residual currents in tidally dominated, well-mixed estuaries, Tellus A: Dynamic Meteorology and Oceanography, 45, 325–340, 1993.

Nguyen, A. D. and Savenije, H. H. G.: Salt intrusion in multi-channel estuaries: a case study in the Mekong Delta, Vietnam, Hydrology and Earth System Sciences, 10, 743–754, 2006.

Nguyen, A. D., Savenije, H. H. G., van der Wegen, M., and Roelvink, D.: New analytical equation for dispersion in estuaries with a distinct ebb-flood channel system, Estuarine, coastal and shelf science, 79, 7–16, 2008.

Park, J. K. and James, A.: Mass flux estimation and mass transport mechanism in estuaries, Limnology and Oceanography, 35, 1301–1313, 1990.

Pein, J. U., Stanev, E. V., and Zhang, Y. J.: The tidal asymmetries and residual flows in Ems Estuary, Ocean Dynamics, 64, 1719–1741, 2014.

Pethick, J. S.: An introduction to coastal geomorphology, Tech. rep., Dept. of Geography, Univ. of Hull, 1984.

Prandle, D.: Salinity intrusion in estuaries, Journal of Physical Oceanography, 11, 1311–1324, 1981.

Prandle, D.: On salinity regimes and the vertical structure of residual flows in narrow tidal estuaries, Estuarine, Coastal and Shelf Science, 20, 615–635, 1985.

Pritchard, D. W.: Salinity distribution and circulation in the Chesapeake Bay estuarine system, Journal of Marine Research, 11, 106–123, 1952.

Pu, X., Shi, J. Z., Hu, G., and Xiong, L.: Circulation and mixing along the North Passage in the Changjiang River estuary, China, Journal of Marine Systems, 148, 213–235, 2015.

Ralston, D. K. and Stacey, M. T.: Longitudinal dispersion and lateral circulation in the intertidal zone, Journal of Geophysical Research: Oceans, 110, 2005.

Rijkswaterstaat: Water management in the Netherlands, Tech. rep., Rijkswaterstaat, Centre for Water Management, 2011.

Savenije, H. H. G.: A one-dimensional model for salinity intrusion in alluvial estuaries, Journal of Hydrology, 85, 87–109, 1986.

Savenije, H. H. G.: Salt intrusion model for high-water slack, low-water slack, and mean tide on spread sheet, Journal of Hydrology, 107, 9–18, 1989.

Savenije, H. H. G.: Determination of estuary parameters on basis of Lagrangian analysis, Journal of Hydraulic Engineering, 119, 628–642, 1993a.

Savenije, H. H. G.: Predictive model for salt intrusion in estuaries, Journal of Hydrology, 148, 203–218, 1993b.

Savenije, H. H. G.: Salinity and tides in alluvial estuaries, Elsevier, 2005.

Savenije, H. H. G.: Salinity and tides in alluvial estuaries, 2ndEdn, http://salinityandtides.com/, Elsevier, 2012.

Savenije, H. H. G.: Prediction in ungauged estuaries: An integrated theory, Water Resources Research, 51, 2464–2476, 2015.

Shaha, D. C. and Cho, Y.-K.: Determination of spatially varying Van der Burgh's coefficient from estuarine parameter to describe salt transport in an estuary, Hydrology and Earth System Sciences, 15, 1369–1377, 2011.

Simpson, J. H., Brown, J., Matthews, J., and Allen, G.: Tidal straining, density currents, and stirring in the control of estuarine stratification, Estuaries, 13, 125–132, 1990.

Smith, R.: Buoyancy effects upon longitudinal dispersion in wide well-mixed estuaries, Philosophical Transactions of the Royal Society of London A: Mathematical, Physical and Engineering Sciences, 296, 467–496, 1980.

Stacey, M. T. and Ralston, D. K.: The scaling and structure of the estuarine bottom boundary layer, Journal of Physical Oceanography, 35, 55–71, 2005.

Stacey, M. T., Burau, J. R., and Monismith, S. G.: Creation of residual flows in a partially stratified estuary, Journal of Geophysical Research: Oceans, 106, 17 013–17 037, 2001.

Stigter, C. and Siemons, J.: Calculation of longitudinal salt-distribution in estuaries as function of time, Waterloopkundig Laboratorium, 1967.

Svendsen, I. A. and Putrevu, U.: Nearshore mixing and dispersion, Proceedings of the Royal Society of London A: Mathematical, Physical and Engineering Sciences, 445, 561–576, 1994.

Taylor, G. I.: The dispersion of matter in turbulent flow through a pipe, Proceedings of the Royal Society of London A: Mathematical, Physical and Engineering Sciences, 223, 446–468, 1954.

Thatcher, M. L. and Najarian, T. O.: Transient hydrodynamic and salinity simulations in the Chesapeake Bay network, Estuaries and Coasts, 6, 356–363, 1983.

Van der Burgh, P.: Ontwikkeling van een methode voor het voorspellen van zoutverdelingen in estuaria, kanalen en zeeen, 1972.

Van Veen, J.: Ebb and flood-channel systems in the Netherlands tidal waters (in Dutch English summary) KNAG 2ed Series Part 67, Republished translated and annotated by Delft University of Technology, 2001.

Verlaan, P. A. J. and Spanhoff, R.: Massive sedimentation events at the mouth of the Rotterdam waterway, Journal of Coastal Research, 16, 458–469, 2000.

Wang, T., Geyer, W. R., and MacCready, P.: Total exchange flow, entrainment, and diffusive salt flux in estuaries, Journal of Physical Oceanography, 47, 1205–1220, 2017.

Wang, Z. B., Stive, M. J. F., Winterwerp, J. C., Arends, A. P., Jeuken, C., and Kuijper, C.: A new morphological schematization of the Western Scheldt estuary, The Netherlands, in: Proceedings of the 2nd IAHR Symposium on River, Coastal and Estuarine Morphodynamics, IAHR, 2001.

Winterwerp, J. C., Wang, Z. B., van Braeckel, A., van Holland, G., and Kösters, F.: Man-induced regime shifts in small estuaries—II: a comparison of rivers, Ocean Dynamics, 63, 1293–1306, 2013.

Xu, Y., Zhang, W., Zhu, Y., and Zheng, J.: Analytical solution for salt intrusion in multiple-freshwater-source estuaries: application to Humen Estuary, Environmental Earth Sciences, 76, 661, 2017.

Zhang, E., Savenije, H. H. G., Wu, H., Kong, Y., and Zhu, J.: Analytical solution for salt intrusion in the Yangtze Estuary, China, Estuarine, Coastal and Shelf Science, 91, 492–501, 2011.

Curriculum Vitæ

Zhilin ZHANG

Zhilin Zhang was born on 3 August 1991 in Pingxiang, China. She got her Bachelor degree in environmental engineering in June, 2012, and her thesis is about water supply to buildings. In the following September, she started pursuing her Master degree in the same major at South China University of Technology in Guangzhou, Guangdong. Her supervisor was Prof. Chunde Wu and the project regards water purification and water pollution control. She then got the honor of outstanding graduate student of Guangdong Province. With the China Scholarship Council Ph.D. fellowship, she moved to the Netherlands in 2015. She worked under the supervision of Prof. Hubert Savenije and Prof. Zheng Bing Wang at Delft University of Technology. The research topic is about saltwater intrusion in estuaries. With all these study experiments, she calls herself "a watery researcher".

List of Publications

Journal papers

3. **Z. Zhang** and H. H. G. Savenije, *Maximum power concept towards saline and fresh water mixing in open estuarine systems*, Earth Syst. Dynam. (under review).

2. **Z. Zhang** and H. H. G. Savenije, *Thermodynamics of saline and fresh water mixing in estuaries*, Earth Syst. Dynam. **9**, 241-247 (2018).

1. **Z. Zhang** and H. H. G. Savenije, *The physics behind Van der Burgh's empirical equation, providing a new predictive equation for salinity intrusion in estuaries*, Hydrol. Earth Syst. Sci. **21**, 3287-3305 (2017).

Conference abstract

4. **Z. Zhang** and H. H. G. Savenije, *Testing thermodynamics of saline and fresh water mixing in estuaries*, Physics of Estuaries and Coastal Seas Meeting 2018, Galveston, USA.

3. **Z. Zhang** and H. H. G. Savenije, *The influence of tidal strength on salinity distributions in estuaries*, European Geosciences Union General Assembly 2018. Vienna, Austria.

2. **Z. Zhang** and H. H. G. Savenije, *The influence of neap and spring tide on stratification and salt intrusion in alluvial estuaries*, European Geosciences Union General Assembly 2017-1906. Vienna, Austria.

1. **Z. Zhang** and H. H. G. Savenije, *Dispersion in alluvial convergent estuaries*, European Geosciences Union General Assembly 2016-9393. Vienna, Austria.

Acknowledgements

In the first twenty-three years of my life, I have never thought about pursuing a Ph.D. degree. It is amazing that an occasion had changed the trajectory of my whole life, which to a wonderland I enjoy and grow up. I always feel lucky with the help and company of a group of trustful friends and colleagues.

First of all, I would like to express my deepest gratitude to my promoter Prof. Hubert Savenije. Hubert (since I can't pronounce "Huub" well) offered me the opportunity of doing research in Delft. He is always generous in supporting and encouraging me. Not only he taught me everything about the estuaries, but also every tiny English grammar. I always got fast and valuable feedback from him, and he inspired me to attend international conferences to broaden my horizon. It is a real pleasure to work with him. I also want to thank him for the Dutch summary of this dissertation.

I am grateful to my promoter Prof. Zheng Bing Wang. He helped me to find a position in Delft. He is professional in estuaries and I can always learn knowledge after talking with him. Thanks for putting faith in my topic.

I feel so warm working in the water management group. Every one is friendly and connected. Thanks to my former and current officemates, Joanna, Zongji, Lingna, Yoshi, Hendy, Rosa, Afia, Win Min, Sha, Themis, Shima, Siamak, Amir, and Juan Carlo, for creating a cozy office with interesting chats. I appreciate our secretaries Lydia and Betty for patient help.

I appreciate Xin, Chunyan, Jiangliang, and Yu; they not only accompany but help me with ideas about estuaries. I need to thank Yinrong and Sixue for sharing life experiments. Thank all my friends including without limitation: Mengshi Yang, Dan Cheng, Jun Nie, Yang Zhou, Sien Liu, Runxiang Li, Rong Zhang, Riming Wang, Hao Yu, Ding Ding, Yan Song, Xun Sun, Zhanxiong Liu. They are trip partners, food sharers, and lovely chatters, making my life entertaining. Thank the Chinese colleagues Jianzhi Dong, Wei Shao, Yang Lyu, Zhengwu Wang, Xinyu Liu, Changrang Zhou, Yuchen Tang, Yuxue Guo, Haoyang Lyu. We have enjoyable memory. Thank my former and current roommates.

I thank my supervisor Prof. Chunde Wu when I was a master student. Without his support and encouragement, I would not be able to pursue a doctoral degree in the Netherlands. You are remembered by all friends.

My warmest thanks to my best friends and beloved family. Their love and support remind me I AM a "precious" as my Chinese name means.

Zhilin Zhang
Delft, August 2018